Fracture Properties Analysis of Rotationally Moulded Plastics for Their Application in Skin-Foam-Skin Sandwich Structure

The thesis is submitted in partial fulfilment of the requirements of Bournemouth University for the degree of Doctor of Philosophy by

ABU NASER MUHAMMAD SAIFULLAH

January 2017

Bournemouth University, UK

In Collaboration with Longitude Consulting Engineers Ltd.

Copyright Statement

This copy of the thesis has been supplied on condition that anyone who consults it is understood to recognise that its copyright rests with its author and is subject to BU-Longitude Consulting Engineers Ltd commercialisation and confidentiality agreement. It is also emphasised here that no quotation from the thesis and no information derived from it may be published without the author's consent and reference to above-mentioned agreement.

Abstract

Rotational moulding is a low pressure, high temperature manufacturing method and is considered to be the best for making large hollow shape plastic parts. Due to its long heating cycle, mould rotation during heating and slow cooling rate, it is completely different from injection or other moulding processes. The mechanical properties of rotationally moulded plastics are totally dependent on unique heating or cooling cycles. With the growing demand for rotationally moulded plastics in load bearing and other applications, a better understanding of their fracture properties is essential. In the rotational moulding process, multilayer plastic products such as skin-foam-skin three layered sandwich structures can be manufactured in a single manufacturing step without any joints. It exhibits relatively high stiffness, strength-to-weight ratios and is used increasingly in various applications such as automotive and marine. During the lifetime of the sandwich material, it may face multiple or repeated impact events.

Therefore, the aim of this work is to develop a better understanding of the fracture behaviour of rotationally moulded plastics in order to use them in skin-foam-skin sandwich structure and reduce in-service failures due to impact. Here, rotationally moulded two different commercially available Polyethylene (PE) and Polypropylene (PP) plastics are tested. Microstructural details of the plastics are investigated here. Fracture properties, particularly fracture toughness properties are studied using J-integral elastic-plastic fracture mechanics approach to identify the fracture initiation point. Impact properties are also investigated at a wide range of temperatures. PE materials are found to have better fracture properties. It is observed that with the fracture toughness plastic's microstructure particularly crystal and amorphous region thickness are related. The understanding from these works is followed by the manufacture of rotationally moulded skin-foam–skin sandwich structure and testing of low velocity impact properties of this structure from 20 J to 100 J energy level with a drop weight impact testing machine. PE is used for both in skin and core layer and sandwich samples are manufactured at four different skin-core thickness combinations. Impact force resistance and bending stiffness are found to be increased with an increase of both skin and core layer thickness. Low velocity repeated impact properties of the rotationally moulded sandwich samples are also investigated from 20 J to 50 J energy level at the end of this project to understand the effect of repeated impact on the sandwich

structure. The samples are subjected to single impact event repeatedly up-to penetration at each energy level. Impact energy-impact number curve obtained from repeated impact test provides an equation for prediction of the number of repeated impacts for the penetration of the sandwich samples at each energy level.

Publications resulting from this thesis

Journal Paper

1. Saifullah A, Thomas B, Tabeshfar K, Cripps B and Wang L, Fracture toughness of rotationally moulded Polyethylene and Polypropylene, Polymer Engineering and Science, Accepted, 5th February, 2017, DOI: 10.1002/pen.24531.

Conference Papers

1. A Saifullah, B Thomas, K Tabeshfar, B Cripps and L Wang, Impact properties analysis of rotationally molded polyethylene and polypropylene for a wide range of temperatures, Society of Plastic Engineers, *SPE ANTEC* Indianapolis, Indiana, P. 1686-89, 2016, USA.
2. A Saifullah, B Thomas, K Tabeshfar and B Cripps, Rotationally moulded thermoplastic sandwich composites in small marine leisure craft: fracture properties and damage analysis of the composite structure, The Royal Institution of Naval Architects (RINA) Conference, *Innovation in Small Craft Technology*, P. 11-16, 13-14th April, 2016, London, UK.
3. A Saifullah, B Thomas and B Cripps, Rotationally moulded plastic materials using in marine leisure craft for better environmental sustainability, *Provocative Plastic Conference*, Museum of Design in Plastics (MoDIP), Arts University Bournemouth September, 2015, UK.

Presentations

1. A Saifullah, B Thomas, K Tabeshfar and B Cripps, Analysis of fracture properties of rotationally moulded plastics for their application in skin-foam sandwich structures to be used in marine leisure craft applications, British Plastic Federation Seminar on Rotational Moulding Industries, 24th November, 2016, Northampton, UK.
2. A Saifullah, B Thomas, K Tabeshfar and B Cripps, The uses of rotationally moulded thermoplastic materials in marine leisure craft applications, The 8th Annual Postgraduate Conference, 9th March, 2016, Bournemouth University, UK.
3. A Saifullah, B Thomas, Khan Z A and B Cripps, The uses of fully recyclable rotationally moulded thermoplastic materials in marine leisure craft for better environmental sustainability, The 7th Annual Postgraduate Conference, 20-21st January, 2015, Bournemouth University, UK.

Table of Contents

List of Figures

List of Tables

List of Equations

Author's Declaration

I hereby declare that except where specific reference is made to the work of others, the contents of this thesis are original and have not been submitted in whole or in part for consideration for any other degree or qualification in this, or any other university. The work shown in this thesis is carried out by me with the guidance of Dr. Ben Thomas, Prof. Kamran Tabeshfar and Prof. Bob Cripps. This thesis contains nothing which is the outcome of work done in collaboration with others, except as specified in the text and acknowledgements.

Abu Naser Muhammad Saifullah

Acknowledgements

Nomenclature

PP	Polypropylene	W_e	Work for crack growth in inner fracture process zone
PE	Polyethylene	W_p	Non-essential work for plastic
PIAT	Peak internal air temperature	W_B	Energy to break
EB	Ethylene-butane copolymer	G_Q	Critical energy release rate
EO	Ethylene-octane copolymer	K_C	Critical stress intensity factor
EoL	End of life disposal	J_{IC}	Fracture toughness at crack initiation
MFI	Melt flow index	J-R curve	A plot of resistance to crack extension
MDPE	Medium density polyethylene	DMTA	Dynamic mechanical thermal Analysis
HDPE	High density polyethylene	W	Test specimen width
LDPE	Low density polyethylene	a	Initial notch
LLDPE	Linear low density polyethylene	B	Test specimen thickness
J-R curve	Crack resistance curve	LEFM	Linear elastic fracture mechanics
J	J-integral	σ_y	Yield stress
L.V.I	Low velocity impact	σ	Stress
$\bar{m}$	Mass ratio	ε	Strain
F_{max}	Peak impact force	λ	Wavelength
NMR	Nuclear Magnetic Resonance	θ	Scattering angle
SAXS	Small angle X-ray scattering	x_{vol}	Volumetric percentage of crystal
WAXS	Wide angle X-ray scattering	x	Weight fractions of crystal
DSC	Differential Scanning Calorimetry	ρ_c	Crystal density
L_C	Lamellar thickness	ρ_a	Amorphous density
ASTM	American Society for Testing and Materials	q	Scattering vector
ESIS	European Structural Integrity Society	D	Lamellar Long period
MAS	Magic angle spinning	CP	Cross polarisation
SPE	Single pulse excitation	SEM	Scanning electron microscope
SENB	Single edge notched bend specimen	E''	Loss modulus
E'	Storage modulus	$\tan \delta$	Damping factor

Chapter 1. Introduction

1.1   Rotational Moulding

Rotational moulding is a low pressure, high temperature and comparatively slow manufacturing method for making hollow, one piece plastic parts, also known as roto-moulding or rotary casting (Cramez, M. et al., 2002; Crawfoard, R. J. K., M.P, 2003; Crawford, R., 1996; Torres, F. and Aragon, C., 2006). The first recognition of this manufacturing process was in the 1940s and the use of this process has been constantly increasing since the 1950s with the introduction of PE in the market. Nowadays it is considered a very competitive alternative to blow forming, injection and compression moulding, particularly for large hollow plastic parts because of the low cost production of relatively stress-free articles, with uniform wall thickness and potentially complex shapes.

The rotational moulding process consists of four different stages (Figure 1.1 Rotational moulding process (Vázquez-Fletes, R. C. et al., 2016). First of all polymer powder, granules or liquids are placed in a mould (stage- 1). The mould is then heated to melt the powder over a period of time dependant on the polymer type with slow rotation over two axes (stage-2). Once it is done, the cooling process starts with
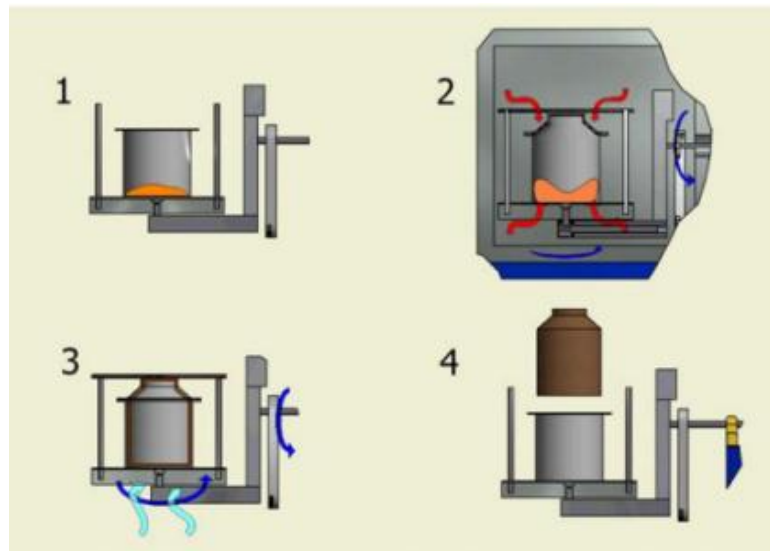
Figure 1.1 Rotational moulding process (Vázquez-Fletes, R. C. et al., 2016).

continued rotation of the mould to solidify the plastic into the desired shape (stage-3). Finally, the mould is opened and the plastic product is removed with or without some small finishing operations (stage-4) (Crawford, R., 1996; Vázquez-Fletes, R. C. et al., 2016).

1.2   Uniqueness of the rotational moulding process

During rotational moulding, the plastic powder is heated at an elevated temperature beyond their melting point for a longer period than with other moulding processes. Normally plastics degrade under prolonged heating at temperatures above their melting point. As a result, rotational mould grade plastic powder must have resistance to this kind of degradation during manufacturing process.

In rotational moulding, product quality depends on the oven temperature and time as well as cooling rate and duration. Lower oven temperature or short oven time lead to less time for the plastic powder to consolidate, resulting in poor strength and stiffness. On the other hand, higher temperatures or oven time can lead to powder degradation that manifests as brittleness in the final product. The internal structure of the plastic product (e.g. crystal structure, crystallinity etc.) forms during the cooling phase. Here, a slow (air cooling) or high (water spray) cooling rate has immense effect on the plastics final properties.

1.3   Comparison of the rotational moulding process with other moulding processes

Rotationally moulding is different from other moulding processes such as injection moulding due to the zero shear (Godinho, J. et al., 2002) with prolonged heating, a long cycle time, very slow cooling rates and the presence of oxygen in contact with the mould's inner surface (Crawfoard, R. J. K., M.P, 2003; Crawford, R., 1996). These processing conditions create a particular morphology and microstructure that uniquely affects the mechanical behaviour of the rotationally moulded products (Oliveira, M. and Cramez, M., 2001; Oliveira, M. et al., 1996).

Insufficient heating can cause voids or bubbles with spherulitic morphology containing very rough topography and deep gaps trapped within the polymers. Overheating induces polymer degradation on the inside surfaces, creating small imperfect spherulites in plastics.

Both the presence of bubbles and imperfect smaller spherulites reduce the strength and increase the brittleness of the materials. Careful monitoring of the Peak Internal Air Temperature (PIAT) during moulding cycles and using antioxidants are normally done to prevent improper heating and degradation of the polymers respectively (Oliveira, M. and Cramez, M., 2001; Oliveira, M. et al., 1996).

The slow cooling rate of this process increases the crystallinity and produces a larger size of spherulites in the materials leading to higher tensile and flexural properties (Godinho, J. et al., 2002), but lower impact strength with sensitivity to crack formation (Friedrich, K., 1979; Oliveira, M. and Cramez, M., 2001). This contrasts with injection moulding where high shear rates and rapid cooling are used to shape a product (Godinho, J. et al., 2002).

A skin-core morphology with a specific orientation is formed due to the thermo-mechanical environment applied in the injection moulding process. Rapid cooling (200-500 K/min) creates smaller size spherulites with lower crystallinity. Smaller crystalline regions and spherulites result in an increase in inter-crystalline tie molecules that improve the toughness properties of the materials (Oliveira, M. and Cramez, M., 2001).

In compression moulding, although thermoset materials are most common, thermoplastics are also moulded and this process exhibits thermo-mechanical conditions between the two extremes roto-moulding and injection moulding process.

1.4   Advantages and limitations of rotational moulding process

The advantages and limitations of rotational moulding processes (Cramez, M. et al., 2002; Crawfoard, R. J. K., M.P, 2003; Torres, F. and Aragon, C., 2006) are briefly listed here.

Table 1.1 List of advantages and limitations of rotational moulding process (Crawfoard, R. J. K., M.P, 2003).

No.	Advantages	Limitations
1.	Mould made of relatively inexpensive materials	Long processing cycle
2.	Product with different thickness can be produced in same mould.	Considered to be uneconomical for large production volume
3.	Uniform thickness distribution of the products.	Limited number of suitable raw material due to the prolong oven time.
4.	Very complex shapes are possible to produce.	Conversion of raw material from pellet to powder form adds more cost.
5.	Hollow plastic parts	Poor understanding of rotationally moulded plastic properties and morphology
6.	Layered structure	
7.	low material wastage	

1.5   Raw materials for rotational moulding

The number of materials in rotational moulding industry is increasing all the time but is currently limited to certain commercial plastic materials. Polyethylene (PE) is currently the most widely used material in the rotational moulding industry. Poly Vinyl Chloride (PVC) plastisol is also used in many applications. Other materials such as Polycarbonate (PC), Nylon , Polypropylene (PP), unsaturated Polyesters, ABS, Acetyl, Acrylics, Cellulosic, thermoset materials such as Epoxies, Fluorocarbons, Phenolic, Polybutylenes, Polystyrenes, Polyurethanes are also available in the rotational moulding industry, though their application is limited (Crawfoard, R. J. K., M.P, 2003). These materials must have certain properties to be suitable for rotational moulding such as high thermal stability, good mechanical properties, low cost and low viscosity. Improper viscosity creates problems in the plastic melt flow during the moulding process (Crawfoard, R. J. K., M.P, 2003; Crawford, R., 1996; Waigaonkar, S. et al., 2008).

1.6 Application of rotational moulding

Applications for rotational moulding are increasing day by day since its inception in the market particularly in one piece large shape products. It has typically been using to make chemical, oil or water tanks, pipe fittings, pump housings, effluent or air ducts, litter or sanitation bins, leisure boats, playground furniture, buoys, life belts, floating decks and road signage. In essence, any large hollow shape is potentially viable for rotational moulding.

(a)

(b)

(c)

(d)

Figure 1.2 Examples of roto-moulded products, container boxes (a), chiller unit tank (b), litter bins (c), road sign (d) (Crawfoard, R. J. K., M.P, 2003).

1.7   Skin-foam-skin three layered sandwich structure in rotational moulding

In rotational moulding it is possible to manufacture double walled or sandwich structures alongside conventional single layer plastic products. Skin-foam-skin sandwich structures made of rotational moulding process have two skins separated by a foam core (Boccaccio, A. et al., 2013; Casavola, C. et al., 2014).

Figure 1.3 Rotationally moulded skin-foam-skin three layer sandwich structure.

The main advantages of these sandwich structures are high specific stiffness and strength, higher strength to weight ratio, better bending stiffness, low weight, excellent thermal insulation and acoustic damping compared to homogenous materials. Most importantly it provides an excellent adhesion between skin and core layer since this composites contains seamless and continuous interface between the distinct skin and foam layers (Boccaccio, A. et al., 2013; Casavola, C. et al., 2014; Pop-Iliev, R. et al., 2006) compared to current fibre reinforced sandwich composites. In rotational moulding, the whole sandwich structure is made in a single manufacturing step which reduces production time and ensures better interfacial adhesion between the core and skin layer compared to traditional sandwich structure making processes. In traditional techniques for manufacturing fibre reinforced skin-foam sandwich composites, skin and core layers are produced separately, then attached in a successive step (Boccaccio, A. et al., 2013).

a)   b)

Figure 1.4 Rotationally moulded boats with skin-foam-skin three layered structures (a, b) (Pioner, 2017).

Currently rotationally moulded skin-foam-skin three layered sandwich structures are used in automotive and marine applications such as floating buoys. Moreover, these materials are increasingly used in small marine leisure craft such as small kayaks, canoes and boats (up-to 10 metres long) because the whole hull can be made of this skin-foam-skin structure in a single manufacturing step without any joints; this means lower cost and higher production rate. Moreover these materials are fully recyclable as both skin and foam materials of this structure are normally the same thermoplastic material.

Figure 1.5 Rotationally moulded skin-foam boat hull is being made inside the mould in a single manufacturing step (Crawfoard, R. J. K., M.P, 2003).

1.7.1 Skin materials

In a sandwich structure, the face sheets can be made of many different materials for example from isotropic, anisotropic or composite materials. Generally polyethylene (PE) or polypropylenes (PP) are used for the skin layers of rotationally moulded sandwich structures.

1.7.2 Core Materials

The other main component of a sandwich structure is the core material. The core has a relatively low density, giving it high flexural strength and stiffness properties relative to the overall panel density. To maintain the effectiveness of the sandwich structure the core must be strong enough to withstand the compressive or crushing loads placed on the panel. The core also must resist the shear forces involved when subjected to deformation. If the core collapses, the mechanical stiffness advantage is lost and the material is considered to have failed. In rotationally moulded sandwich structures PE or PP polymeric foam is used. Foam is normally manufactured through generating gas with a blowing agent within the main polymer matrix (Liu, S. J. and Tsai, C. H., 1999). Using the same material for skin and foam ensures better adhesion between foam and skin layers as well as other mechanical properties.

1.7.3 End-of-life disposal (EoL)

Rotationally moulded skin-foam-skin three layered sandwich structure are generally made of same type of material for the skin and core layers. It offers a better end-of-life disposal opportunity since this mono-material thermoplastic sandwich structure can be recycled easily (in contrast to current GRP hulls which provide a significant waste issue). For the thermoplastic materials the mechanical recycling process is carried out so that they are grounded down, reprocessed, blended or compounded to be used in many second-life applications (Hamad, K. et al., 2013). In this process, materials are cleaned and separated for maintaining purity and reducing contamination that deteriorates the quality of the

material in the recycling process. From this point of view, this rotationally moulded sandwich structure does not need to be separated from other materials as it is made of mono-material thermoplastic materials. Therefore it offers a far easier recycling process without any contamination compared to others such as composite skin-foam sandwich structures and allows this to be recycled to a material with similar properties to the original.

1.8 Fracture properties of rotationally moulded plastics

There have been few research works carried out on rotationally mould grade materials and hence, research is not as extensive as other moulding processes such as injection or compression moulding (Torres, F. and Aragon, C., 2006). Materials mould-ability, manufacturing condition optimisation and mechanical properties such as tensile and flexural properties analysis have been done previously however (Cramez, M. et al., 2002; Crawfoard, R. J. K., M.P, 2003; Godinho, J. et al., 2002; Waigaonkar, S. et al., 2008). Also, some understanding has been achieved of the impact properties of rotationally moulded plastics (Pick, L. T. and Harkin-Jones, E., 2003). Fracture behaviour analysis at slow and dynamic loading rates, and crack initiation and propagation analysis which help to ensure plastic material's durability and performance under static and dynamic loading conditions have not been performed on rotationally moulded plastic materials. Moreover, our understanding of the materials microstructure arrangements, morphology and their relation with the fracture behaviour are still absent.

1.9 Skin-foam-skin sandwich structure in real life environment

Rotationally moulded three layered skin-foam-skin sandwich structures are currently being used in boat hulls, kayaks, canoes and automotive applications due to their higher stiffness and strength-to-weight ratios compared to homogenous rotationally moulded plastic grades. In these applications mechanical properties, particularly impact properties and damage by foreign objects are one of the major concerns since sandwich structures are known to be susceptible to impact damage, and this damage may severely reduce stiffness and load carrying capacity of the structure over time (Abrate, S., 1997; Casavola, C. et al., 2014; Chai, G. B. and Zhu, S., 2011). During the lifetime of the sandwich material, it may face multiple repeated impact events (e.g during mooring for a dinghy). Damage created by one

impact event can grow rapidly with multiple local impact events and this can build to create failure (Çoban, O. et al., 2009). This failure is common in real world products such as canoes and boat hulls and has been observed by the manufacturers.

1.10 Major contribution of the thesis

From the above discussion it is clear that the unique heating and cooling cycles and lower cooling rates in the rotationally moulding process compared to other moulding processes are responsible for the materials quality, particularly the mechanical properties of the products manufactured from this process. An understanding of fracture properties of rotationally moulded plastics is essential for the further expansion of their use in various load bearing applications. Skin-foam-skin three-layered sandwich structures can be manufactured using this moulding process and during the service life of the sandwich composite structures impact damage caused by sudden impact forces affect the stability and mechanical performance of the structure.

Therefore, the aim of this work is to investigate the fracture properties of the rotationally moulded plastics and their application in rotationally moulded three layered skin-foam-skin sandwich structure. Material properties particularly fracture properties of the rotationally moulded plastics are studied here using a fracture mechanics approach to identify the fracture toughness properties. Microstructural details are also studied to analyse their toughness mechanisms. Moreover, impact properties are also investigated at a wide range of temperatures and analysed in terms of microstructure of this plastic materials. Following this, an understanding of these fracture properties is used to select suitable design criteria for the manufacture of the rotationally moulded three layered skin-foam-skin sandwich structure in order to resist real-world impacts. The rotationally moulded sandwich structure is manufactured at different core and skin thickness combinations and the effect of skin and core thickness on the low velocity impact properties of rotationally moulded sandwich composite are investigated. In the literature review (Chapter 2), details of low velocity impact testing of sandwich structures are reviewed and the findings are used to inform our own low velocity impact testing of rotationally moulded sandwich materials and the damage characterisation at both core and skin layers . Repeated impact tests of rotationally

moulded sandwich structures are also studied in the final part of this work at different impact energies to understand the effect of repeated or multiple impact events on the fatigue-impact lifetime of this structure.

1.11 Aim and objectives

The aim of this research work is to develop a better understanding of the fracture behaviour of rotationally moulded plastics in order to use them in skin-foam-skin sandwich structure and reduce in-service failures due to impact load.

To achieve the above aim, the following objectives have been investigated in this work-

1. To investigate the microstructure of the plastics such as crystal structure, crystal and amorphous region thickness, melting temperature and behaviour, polymer structure and dynamic mechanical analysis using wide angle x-ray scattering (WAXS), small angle x-ray scattering (SAXS), differential scanning calorimetry (DSC), solid-state NMR and dynamic mechanical thermal analysis (DMTA) respectively.

2. To investigate the fracture toughness property at slow loading rate of rotationally moulded plastics by following a fracture mechanics approach and its relation with the microstructure of the plastics.

3. To investigate the fracture properties of rotationally moulded plastics at dynamic loading rates with drop weight impact test conditions and their relation with the microstructure of the tested plastics.

4. To investigate the low velocity impact properties of rotationally moulded skin-foam-skin sandwich structures at different skin and core layer thickness combinations.

5. To investigate the low velocity repeated impact properties of the sandwich structures to identify the effect of repeated impact on these structures.

1.12 Organisations of thesis

This thesis consists of eight chapters, described as follows-

- Chapter 1 gives a brief description of the rotational moulding process, its applications and differences with other moulding processes, highlights the major contribution of the thesis and aim and objectives of this research.

- Chapter 2 presents a literature survey on the current research on the properties analysis of rotationally moulded plastics, impact properties analysis of the rotationally moulded plastics, fracture toughness analysis, manufacturing processes of skin-foam-skin sandwich structure in rotational moulding process, low velocity impact and repeated impact properties of sandwich structure.

- Chapter 3 describes the material details, moulding process of the plastics, microstructural characterisations of the moulded plastics, rotational moulding of skin-foam-skin sandwich structures and experimental work performed in this study.

- Chapter 4 contains the microstructural analysis of the rotationally moulded plastics.

- Chapter 5 gives the analysis of fracture toughness and drop weight impact properties and their relation with the microstructure of the plastics.

- Chapter 6 presents the low velocity impact properties analysis of rotationally moulded skin-foam-skin sandwich structures.

- Chapter 7 describes the low velocity repeated impact properties of the sandwich structures.

- Chapter 8 presents the conclusions and recommendations for future work.

Chapter 2. Literature Review

In this chapter, firstly recent research on rotationally moulded plastic materials properties particularly impact and fracture toughness properties are presented with focussing on polyethylene and polypropylene as these are mostly used materials in rotational moulding process. Topics of impact properties and related parameters, theories related to fracture toughness analysis and measuring fracture toughness of polyethylene and polypropylene are discussed. Following this, the literature review is focussed on application of rotationally moulded materials in three layered skin-foam-skin sandwich structure, manufacturing processes of this sandwich structure, low velocity impact and repeated impact properties of sandwich structure.

2.1   Rotationally moulded plastic materials properties analysis

Rotational moulding is one of the fastest growing moulding processes in plastic industry. To cope with this growth, research work on rotational moulding process parameters as well as rotationally moulded plastic properties has also been conducted in recent times. From previous research findings, it is known that rotational moulding plastic properties are very dependent on the manufacturing process. It has a unique manufacturing process that is described earlier of this thesis. The internal air temperature inside the mould is related to process conditions. Therefore, precise measurement and control of internal air temperature helps to optimise the process parameters for ensuring better product quality. Based on this theory and findings, the ROTOLOG system has been developed that gives the moulders better control of their manufacturing process in this industry (Crawford, R., 1996). To improve thermal and oxidative degradation resistance of the powder during long oven cycles an antioxidant is normally mixed with them. Oxidative degradation happens when the amount of the antioxidant reaches zero, this is known as the oxidation induction time (OIT). Cramez et al. (Cramez, M. et al., 2002) developed a methodology to predict and identify this OIT point for the elimination of degradation in the heating cycle. The presence of bubbles inside the products is considered to be harmful for the product quality; this is also related to the process parameters. Efficient ways were identified by researchers to solve this problem by optimising cycle times of the manufacturing process. The selection of the right kind of resin for the particular application has always been a concern for the

moulders. Multiple Attribute-based Decision Making (MADM) was used to select the right kind of resin, based on the technique of order preference by similarity to the ideal solution (TOPSIS) (Waigaonkar, S. et al., 2008).

Mechanical properties such as tensile, flexural and impact strengths of rotationally moulded plastics were measured and compared with compression and injection moulded plastics to identify the differences in ultimate product properties for inherent manufacturing processing variations (Godinho, J. et al., 2002; Pick, L. T. and Harkin-Jones, E., 2003).

Rotationally moulded plastic showed higher stiffness and strength than that of injection moulded plastics because of the higher crystallinity and spherulitic sizes created by the slow cooling rate used in the manufacturing process. Finally, Godinho et al. (Godinho, J. et al., 2002) proposed a unified theory based on laminate and thermo-mechanical indices concept for the prediction of the mechanical properties of the rotationally moulded plastics. Though flexural and tensile properties were predicted well following these theories, impact properties were not investigated. The effect of the cooling rate on the growth of spherulite size and impact properties was also investigated [42]. Structural characterisation using X-rays, micro-hardness testers and tensile properties were measured for rotationally moulded PE where these properties were found to be related to spherulitic levels rather than small scale or microstructural arrangements [43]. Drop weight impact performance of rotationally moulded PE was studied at different temperatures between -60 to 20°C and its relationship to the Dynamic Mechanical Thermal properties was sought (DMTA) (Pick, L. T. and Harkin-Jones, E., 2003). Normally DMTA examines the thermal transitions of semi-crystalline materials in terms of temperature and frequency. The β transition is for the motion changes in the amorphous part; this has some correlation with impact properties and was identified qualitatively for the lowest and highest impact strength. Analysis of impact response of roto-moulded skin-core-skin sandwich panels (PE-foam-PE) was carried out with extensive lab work and finite element method (Casavola, C. et al., 2014). For the

improvement of the mechanical properties of the roto-moulded plastics, natural fibre reinforcement was also reported recently (Torres, F. and Aragon, C., 2006).

The use of rotational moulding plastic materials in static load bearing applications is increasing with time. Understanding of crack initiation and propagation behaviour in the rotationally moulded materials is very necessary for the full characterisation of fracture behaviour. Fracture toughness analysis under fracture mechanics approaches which provides the information on crack initiation and propagation mechanism has not been done yet for rotationally moulded materials. Moreover, impact properties analysis is only limited to certain rotationally moulded grade materials in the literature.

Therefore, in this research work, fracture toughness analysis and impact properties analysis are carried out for rotationally moulded plastic materials. Rotationally moulded polypropylene and polyethylene materials are used for the investigation. PE is used about 90% of all polymers that are rotationally moulded and has excellent rotational moulding ability, hydrolytic stability, water absorption resistance, excellent recyclability, lower cost, and moderate strength (Crawfoard, R. J. K., M.P, 2003). PP offers some advantageous properties compared to PE such as higher stiffness and resistance to higher service temperature. Besides, PP also has good rotational mould ability, higher water absorption resistance and hydrolytic stability etc. As a result there is an increasing interest for using PP in rotationally moulded plastic products. Here a comprehensive literature review is presented for the impact properties and fracture toughness analysis of rotationally moulded grade materials in the following section focusing on Polyethylene (PE) and Polypropylene (PP).

2.2 Impact and fracture toughness analysis of rotationally moulded PP and PE

2.2.1 Basic structure of Polypropylene (PP)

PP has been used extensively in many applications such as household, automotive, fibre, pipes and fittings, furniture since its first production by G. Natta in 1954. In the general carbon chain arrangement of PP, CH_3 (methyl) group is attached to the second carbon atom. Based on the methyl group arrangement in the PP chain, it is divided into three categories.

If all the methyl groups are attached on the same side of the chain, the PP is called Isotactic PP (i-PP). In syndio-tactic (s-PP) and atactic PP (a-PP), pendant methyl groups are arranged in alternating and random manner respectively (Tripathi, D., 2002).

a)

$$CH_2 = CH$$
$$|$$
$$CH_3$$

b)

isotactic polypropylene

syndiotactic polypropylene

atactic polypropylene
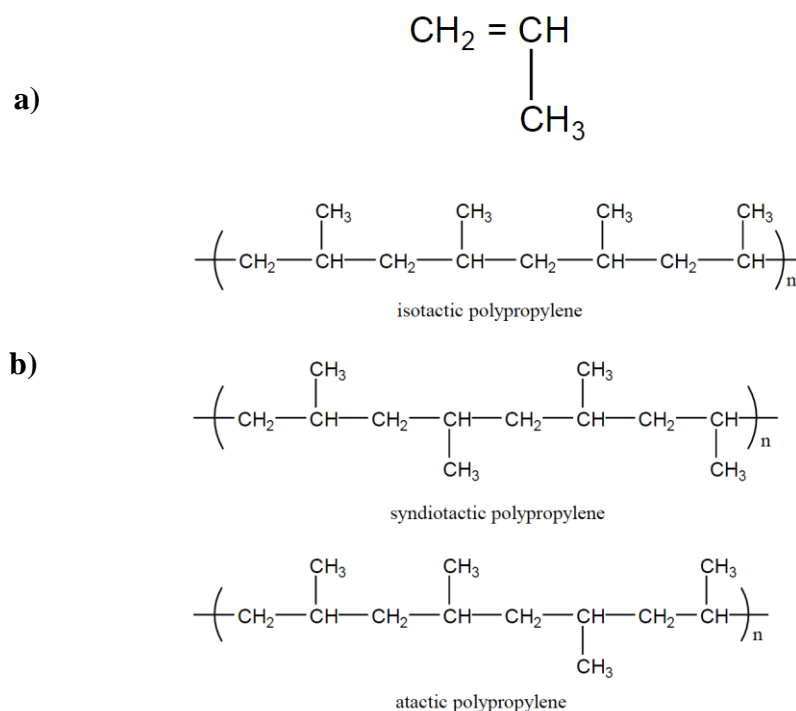
Figure 2.1 (a) Basic structure of PP, (b) isotactic, syndiotactic and atactic PP (Tripathi, D., 2002).

—P—P—P—P—E—P—P—P—E—P—P—P—P—P—E—P—P—P—P—P—P—E—P—P—
random copolymer

—P—P—E—E—P—P—P—P—E—E—E—P—P—P—P—P—E—E—E—E—E—P—P—P—
block copolymer
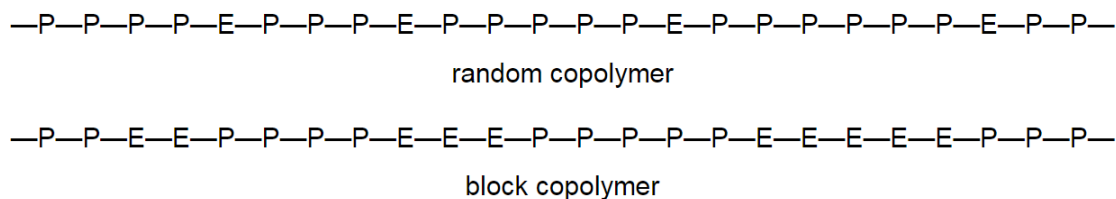
Figure 2.2 Typical chain arrangement of random and block PP co-polymer (Tripathi, D., 2002).

In order to change the properties of the homo-polymer PP, other phases or co-monomers such as ethylene or other materials are added to produce co-polymers. PP co-polymers are of two types; these differ in the percentage of co-monomers and their arrangement in the chain. Random co-polymers have a lower content of co-monomers (typ. between 2-7%) whereas hetero-phasic or block co-polymers contain higher percentages of co-monomers. Both of their chain structures are shown in figure 2.2.

2.2.2 Basic structure of Polyethylene (PE)
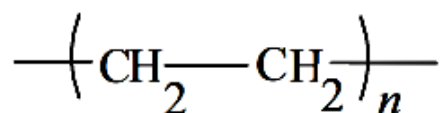
$$-\left(CH_2-CH_2\right)_n-$$

Figure 2.3 Structure of Polyethylene (Kyu, T. a. N., Domasius, 2008).

PE was discovered in 1933 by Gibson and Fawcett of Imperial Chemical Industry, UK. It is formed from the polymerisation of ethylene ($CH_2=CH_2$) and is the most popular polymer consumed in the world (Vasile, C. and Pascu, M., 2005). PE is divided into three categories based on density; this is controlled by the amount of branching in the PE chain during the polymerisation process. Low, medium and high densities PE have densities of 0.915-0.925, 0.092-0.940 and 0.940-.960 g/cm^3 respectively which control their ultimate properties and thermal behaviour. Co-monomers such as 1- butene, 1- hexene, 1-octene are also used to polymerise polyethylene co-polymers for bringing changes in their ultimate properties.

2.2.3 Impact properties

In the rotational moulding industry, generally impact properties are measured to check the quality of the products and to test the effects of blend and processing modifications (Pick, L. T. and Harkin-Jones, E., 2003). Instrumented falling weight tests with a hemispherical dart are used to test the impact properties according to the ASTM drop weight impact testing standard. In this research work, a force transducer is attached to the dart of the test

rig for recording additional force data during the impact event but this is not rotational moulding industry standard approach.

Impact properties of rotationally moulded samples vary with the polymer type. Polymer properties such as molecular weight and distribution, crystallinity, polymer chain length and the degree of branching of the polymer chains can also affect the impact properties. A higher molecular weight favours a higher number of entanglements among the tie chains connecting lamellar blocks leading to greater plastic deformation with higher fracture energy absorption. Molecular weight does not have a direct effect on the microstructure, though it has an effect on the density of the tie molecules that is beneficial to the impact strength. MFI (melt flow index) is the amount of the materials that flow at a standard temperature in 10 minutes, an indication of the viscosity of the molten polymer at a certain temperature and shear rate. It is used in rotational moulding to predict the behaviour of the molten polymer during processing since MFI testing is done under low shear rate conditions which are similar to those in the rotational moulding process. MFI has an inverse relation with molecular weight and the MFI value increases with the decrease of molecular weight of the material. Therefore, impact properties also decrease with the increase in MFI value. Low MFI values are one of the key differences between an injection mould and a rotational mould plastic blend. A higher number of side branches in the polymer chain increases the amount of tie molecules between the crystallites as does a higher molecular weight, leading to higher impact resistance. In addition, the length of alkyl side chains in the polymer chain of polyethylene also affects the impact strength. It was found (Kalyon, D. M. and Moy, F. H., 1988) that linear low density polyethylene with octene side groups showed better impact strength than with the hexene side groups because of the higher number of tie molecules and entanglement. Processing parameters of rotational moulding also influence the impact properties. During the melting of powder in the oven, air is trapped between the polymer particles and creates bubbles in the plastic part that reduces the impact strength (Oliveira, M. and Cramez, M., 2001; Oliveira, M. et al., 1996). Bubbles formed in this way prevent the stresses that are imposed on the part from being distributed properly (Kalyon, D. M. and Moy, F. H., 1988; Kelly, P., 1981) which results in lower energy to initiate a crack and for further crack propagation.

When processing of rotationally moulded components is carried out it is seen that a short oven time in the rotational moulding cycle creates under-fused components with lots of bubbles whereas a long oven time reduces the amount of bubbles, but risks degrading the product due to oxidation (Crawford, R. and Nugent, P., 1992). The use of an internal mould pressure during the moulding process after the melting of powder in the mould was reported as an effective way to reduce the bubbles as well as to improve the impact strength (Kontopoulou, M. and Vlachopoulos, J., 1999; Spence, A. and Crawford, R., 1996). The cooling rate of the moulding process develops the spherulitic morphology that is directly related to impact properties. A slow cooling rate creates larger spherulites and induces lower impact strength (Way, J. et al., 1974). For polypropylene, rapid quenching in water was found to increase the impact strength compared to a slow cooling rate (Ismail, Y. et al., 2001) as quenching creates smaller spherulites .
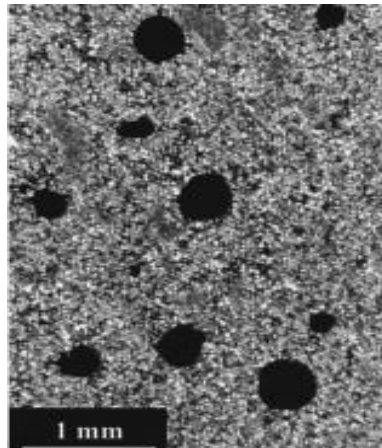
Figure 2.4 Morphology of PE sample with air bubbles (Oliveira, M. and Cramez, M., 2001).

Testing conditions such as testing velocity has an effect on the impact properties of rotationally moulded plastics. When the polymer deforms, the chains of molecules rearrange themselves in the direction of the applied force. In high velocity the molecular chains have only a very short time to rearrange themselves compared to lower velocity and they consequently break in a more brittle manner. Therefore, with increasing testing velocity, the elongation decreases and the Young's modulus and maximum stress increase.

Temperature has a direct effect on fracture behaviour under impact and can change the fracture mode significantly (T, P. L., 2004). Polymers behave in a more brittle manner at lower temperatures and at higher temperatures they fail in a ductile manner. Therefore researchers tried to find out the relationship between the thermal transitions of rotationally moulded plastics and their impact properties (Pick, L. and Harkin-Jones, E., 2005; Pick, L. T. and Harkin-Jones, E., 2003).

Dynamic mechanical thermal analysis (DMTA) is generally used to characterize the thermal transitions of the materials that are created by chain movements in the materials. It can identify the storage (E') and loss modulus (E") for the elastic and viscous responses of a viscoelastic materials respectively. tanδ is the ratio of the loss modulus to storage modulus.

There are three transitions for semi-crystalline polymers particularly in PP and PE. α, β, γ transition peaks normally represent the chain motion in the crystalline portion, glass transition and amorphous region respectively (Sirotkin, R. and Brooks, N., 2001). Different transitions of rotationally moulded PP were investigated before and impact behaviour was described based on these transitions (T, P. L., 2004). PP is a brittle material because of its high glass transition or β transition temperature. To reduce this brittleness co-polymerization was carried out with ethylene to lower the β transition temperature (Feng, Y. et al., 1998). The β transition has a correlation with high impact strength of PE and was found in the region between the high impact strengths obtained at low temperatures and the lower impact strengths obtained at high temperatures (Pick, L. T. and Harkin-Jones, E., 2003). A numerical relation was also developed between peak impact strength, tanδ and the β transition region of polyethylene (Pick, L. and Harkin-Jones, E., 2005). The density of the materials is directly related to the height of β peak in loss modulus curve. Previous work generally showed that higher height of β peak (loss modulus) results in better impact resistance for PE, however a recent research by Pick et al (Pick, L. T. and Harkin-Jones, E., 2003) showed a correlation between lower height of β peak and increased impact strength for higher density rotationally moulded PE and this warrants further investigation.

2.3 Fracture Toughness Analysis

Every material contains some inherent flaws from where damage can start and final failure can happen at the largest of these imperfections. Fracture mechanics were first described by A. A. Griffith (Williams, J. G., 1984). He noticed that the potential energy of a stressed body decreases as inherent flaw size increases because of the energy release that ultimately creates the new surfaces of the growing flaw. Finally he developed a relation between the flaw size and stress at failure based on this observation. In fracture mechanics, notches of a certain length are made in the samples with definite size and shape to simulate the effect of natural flaws in real time fractures. Nowadays fracture mechanics is well established and offers a range of theories for measuring the toughness parameters of plastics. In addition to conventional material properties such as tensile strength (Shao-Yun Fu, B. L., Yiu-Wing Mai, 2009) fracture toughness parameter is necessary as it helps to predict the progress of damage of the material subjected to external loads.

2.3.1 Fracture toughness measurement theories in fracture mechanics

2.3.1.1 Linear Elastic Fracture Mechanics (LEFM)

Generally for brittle polymers such Polymethyl methacrylate and Polystyrene, LEFM can be applied successfully (Williams, J. G., 1984). In this fracture mechanics theory, a load is applied to pre-notched single-edge-notch bending (SENB) or a compact tensile (CT) sample to deform it, the crack initiation or K_c – critical stress intensity factor is measured from this test. This characterises the elastic field around the crack tip from the following equation for SENB sample (Hashemi, S. and Williams, J., 1986; Iso, B., 2000) –

$$K_C = f_{(a/w)} \frac{F_Q}{h\sqrt{w}}$$ (2.1)

Where F_Q the load at crack growth initiation, h is the thickness of test sample, w is the test specimen width, $f(a/w)$ is the geometry calibration factor.

From K_C the critical energy release rate G_C at crack growth initiation can be calculated

$$G_C = \frac{W_B}{h \times w \times \emptyset(^a/_w)} \tag{2.2}$$

Where W_B is the energy to break, $\emptyset(^a/_w)$ is the energy calibration factor.

In LEFM, for measuring K_C under plane strain conditions, the test specimen must meet some stringent size criteria according to following equations-

$$a, B, W - a > 2.5 \left(\frac{K_C}{\sigma_y}\right)^2 \tag{2.3}$$

$$W > 2B \tag{2.4}$$

Where, σ_y is the uniaxial yield stress.

Brittle materials can meet this size limits whereas for tough materials it is difficult to maintain this requirements due to the need for much larger specimen sizes and higher plastic deformation, this is considered a severe limitation of LEFM and hence, necessitates the use of inelastic or elastic-plastic fracture mechanics for measuring fracture toughness (Hashemi, S. and Williams, J., 1986; Wang, M.-D. et al., 1992).

2.3.1.2 The elastic-plastic fracture mechanics, J-integral method

Rice introduced the J-integral (Jc) as an elastic-plastic fracture parameter for materials which have non-linear crack growth (Hale, G. E. and Ramsteiner, F., 2001). He mentioned that the energy dissipation (the difference between the external work and the change in the internal potential energy within an area) is possible to calculate using the line integral of the integration line surrounding that area (Astm-D6068-96, 2002; Hale, G. E. and Ramsteiner, F., 2001; Wang, M.-D. et al., 1992).

$$J = \int_\Gamma \left(W dy - T \frac{du}{dx} ds\right) \tag{2.5}$$

Where, Γ is surrounding line, W is the strain-energy, T is the stress acting on the line, u is the displacement, s is the arc length along the integration line. When the material is loaded,

crack propagation happens and the J-value should be equal to the work done per unit are for that crack growth which can be expressed by following equation –

$$J = \left(\tfrac{1}{B}\right) \; dU\big/ da \tag{2.6}$$

Where, B is the specimen thickness, U is the total external work and a is the crack length. For measuring the onset of crack instability or certain critical values of J_c, multiple specimen resistance R-curves were developed by Landes and Begley based on the equation 2.5. In the J-crack growth resistance (J-R) curve, crack growth maintains a power law relation $J = A\,(\Delta a)^N$ and Jc is typically measured at $J_{0.2}$ which refers to the crack resistance at 0.2mm of the total crack growth.
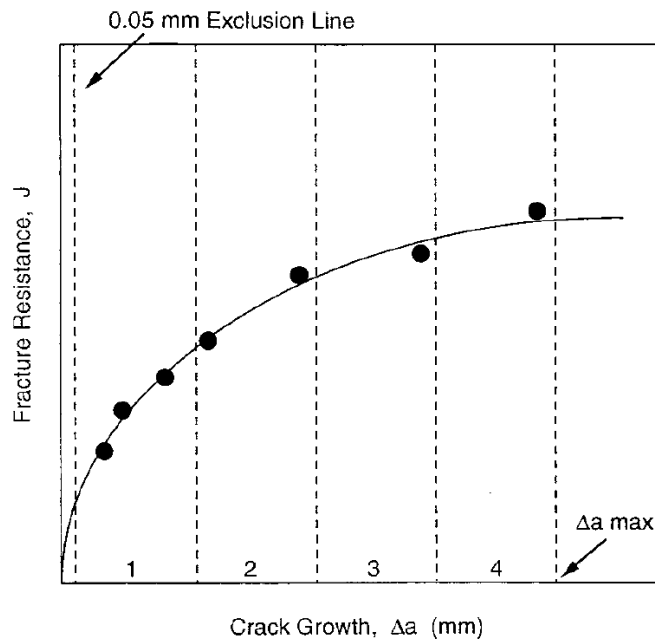
Figure 2.5 Typical J-R curve [21].

To maintain the plane strain condition in J-integral test methods the test samples must maintain the following size criteria (Hashemi, S. and Williams, J., 1986).

$$a, B, (W - a) > 25 \left(\tfrac{J_c}{\sigma_y}\right) \tag{2.7}$$

24

2.3.1.3 Essential Work of Fracture (EWF)

Mai and co-workers extended EWF theory to polymer from the metals which was developed by Broberg (Bárány, T. et al., 2010). It measures the plane stress fracture toughness parameters for thin sheet of ductile polymers by using double edge notched tension samples.

(a)   (b)

(c)
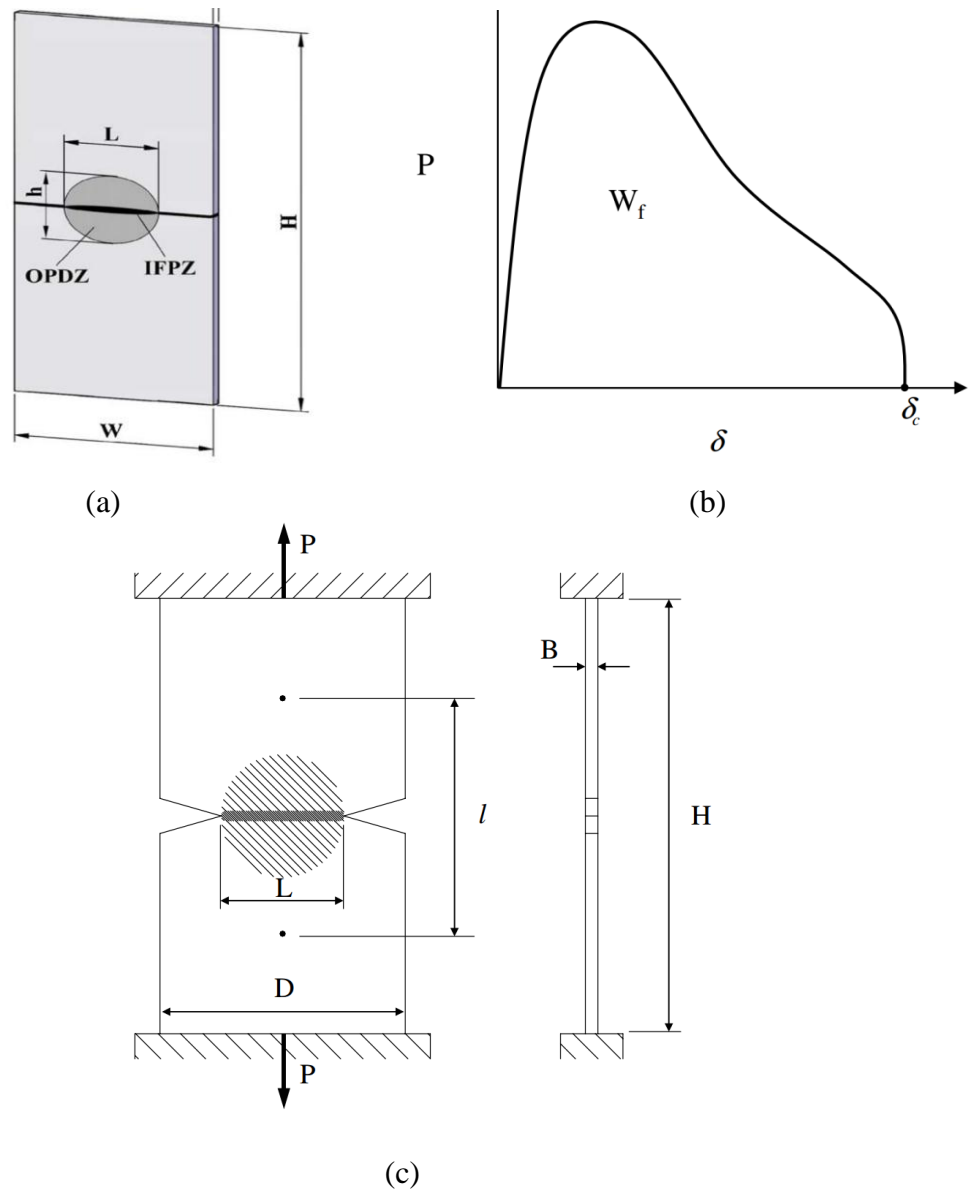
Figure 2.6 The fracture process zone in (a) sample, (b) load-displacement curve, (c) double edge notch tension specimen (Williams, J. and Rink, M., 2007).

Samples with different ligament lengths are tested under load and for every sample a load-displacement curve is achieved wherein W_f is the total work to fracture the specimen (Wang, M.-D. et al., 1992) . Ligament length is equal to the rest of the width after putting notch and initial crack in the test samples.

W_f can be divided into two main components (Bárány, T. et al., 2010; Wang, M.-D. et al., 1992; Williams, J. and Rink, M., 2007) : (1) W_e , the work for crack growth in the inner fracture process zone (IFPZ) and (2) W_p, non-essential work for plastic deformation in the outer plastic deformation zone (OPDZ). The equation for W_f is as follows-

$$W_f = W_e + W_p \tag{2.8}$$

This equation can be written as follows by considering both of the zones within the ligament of the specimen-

$$W_f = W_e Lt + \beta W_p L^2 t \tag{2.9}$$

$$W_f = W_e + \beta W_p L \tag{2.10}$$

Where, L is the ligament length, t is the thickness, β is the shape factor for OPDZ zone.
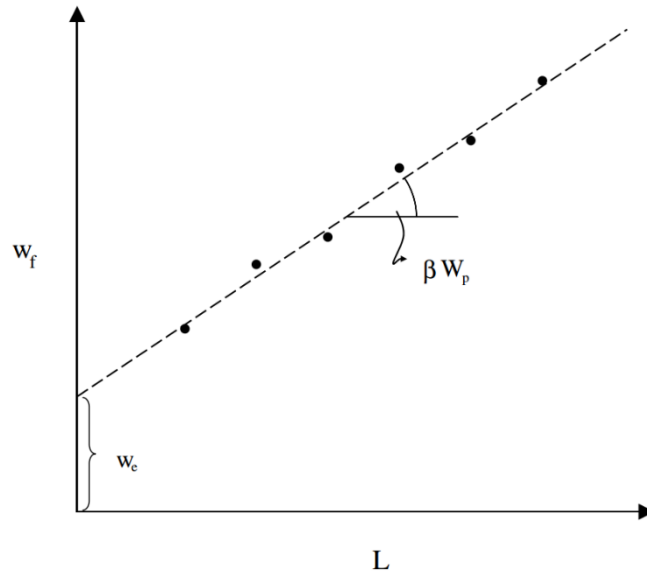
Figure 2.7 Determination of $\boldsymbol{W_e}$ and $\boldsymbol{W_p}$ (Williams, J. and Rink, M., 2007).

In real world tests, W_f is measured at different ligament lengths for the samples and can be plotted as a function of ligament length. From this plot W_e and W_p can be calculated using the intercept of the W_f axis and the slope of the line respectively as shown in Figure 2.7.

EWF has similarity with the J-integral method as both of the methods build resistance curves from multiple specimen testing (Bárány, T. et al., 2010). Moreover, in many papers (Fasce, L. et al., 1999) it was shown that $W_e \equiv J_c$. Although EWF is gaining in popularity

over the J-integral method due to the simpler sample size requirements and no need for crack front determination from fracture surfaces (Bárány, T. et al., 2010; Williams, J. and Rink, M., 2007), there is not yet an internationally accepted standard available.

2.3.2   Measuring Fracture toughness of Polyethylene and Polypropylene

Fracture toughness measurements using different fracture mechanics approaches and the identification of crack propagation mechanisms have been investigated by previous researchers (Benhamena, A. et al., 2011; Chan, M. and Williams, J., 1981, 1983, 1993; El-Bagory, T. M. et al., 2014; Fasce, L. et al., 1999; Fasce, L. A. et al., 2004; Fernando, P. and Williams, J., 1980; Ferrer-Balas, D. et al., 2002; Hashemi, S. and Williams, J., 1986; Mai, Y.-W. and Cotterell, B., 1986; Morhain, C. and Velasco, J., 2001; Pegoretti, A. et al., 2009; Salazar, A. et al., 2014; Salazar, A. et al., 2013; Santarelli, E. and Frontini, P., 2001; Swei, H. et al., 1991), both for PP and PE, with the research focussing on injection or other moulding processes. This type of detailed material analysis is still absent for the rotationally moulded PE and PP however. Here a comprehensive review is presented on fracture toughness analysis of PP and PE based on other moulding processes such as injection, compression or extrusion grade materials.

From the fracture toughness analysis of injection and compression mould grade PP it was found that the toughness is related to the initial notch depth, sample dimensions, temperature and deformation rate (Salazar, A. et al., 2014).The application of Linear Elastic Fracture Mechanics (LEFM) to measure the fracture toughness of PP homo-polymer is restricted to -60°C (Fernando, P. and Williams, J., 1980) because of the excessive non-

linearity at higher temperatures (Fernando, P. and Williams, J., 1980; Salazar, A. et al., 2014; Santarelli, E. and Frontini, P., 2001). Therefore, the elastic-plastic fracture mechanics J-integral method including multiple (Salazar, A. et al., 2013) or single specimen normalisation methods (Morhain, C. and Velasco, J., 2001) and the three parameter Weibull process were used at room temperature for PP homo and co-polymers [12]. Alongside the J-integral method, essential work of fracture theory was applied to analyse fracture behaviour of polypropylene films at plane stress conditions (Ferrer-Balas, D. et al., 2002). It is noteworthy that the essential work for crack growth, W_e in EWF theory is equivalent to J_c as long as the sample geometry is maintained (Fasce, L. et al., 1999; Mai, Y.-W. and Cotterell, B., 1986).

(a)   (b)
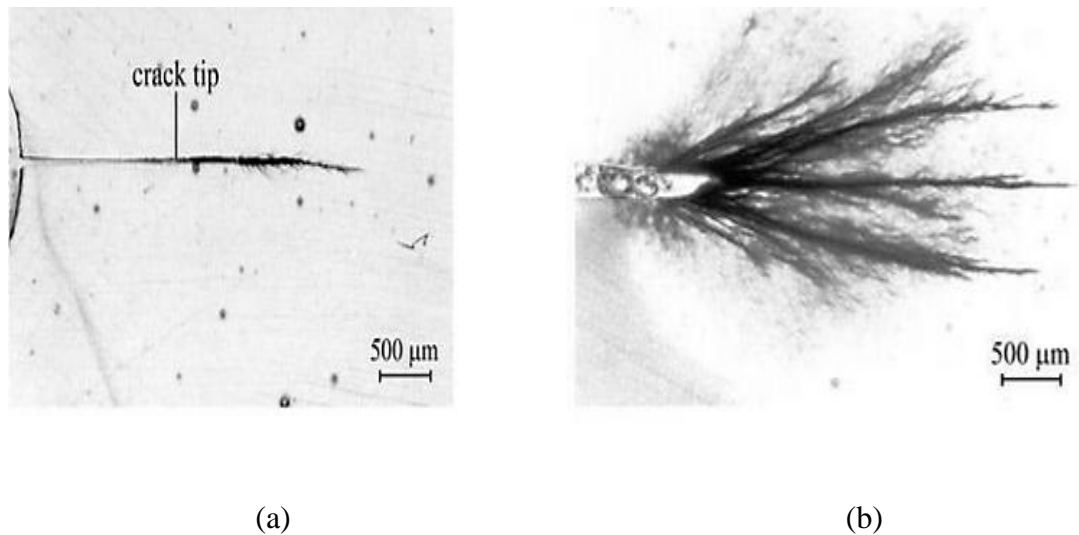
Figure 2.8 Crack tip deformation (crazing) of PP (a) homo-polymer, (b) co-polymer (**Fasce, L. A. et al., 2004**).

The fracture behaviour and deformation mechanisms of different grades of PP (homo and copolymer) were identified (Fasce, L. A. et al., 2004). The main deformation mechanism for homo-polymer was crazing. For co-polymers, cavitation was found to be happened initially inside the co-polymer granules, transferring to the PP matrix to create shear

yielding with void creation that acts as a craze initiation site in PP, leading to an increase of crazing of the material (Figure 2.8- b). The damage zone (Figure 2.8- b) in the crack tip surrounding area was larger for co-polymers than with homo-polymers (Figure 2.8a), that increase the toughness values. The effect of temperature on fracture toughness values was also investigated for PP (Salazar, A. et al., 2014). Random and block ethylene-propylene co-polymer were tested between -20 to 60°C and -80 to 23°C respectively. Fracture toughness values were seen to increase with temperature for random co-polymers. For block co-polymers, temperature didn't have that much effect on toughness.
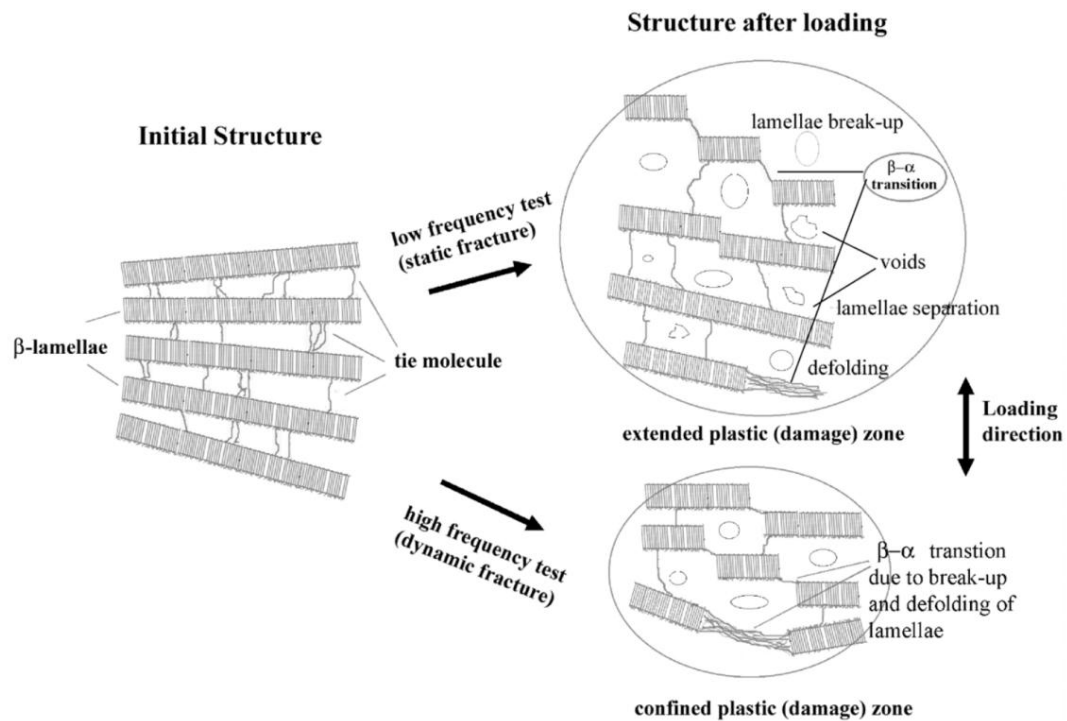
Figure 2.9 Failure process of β crystal structure of PP at low and high strain rates (Chen, H. et al., 2002).

Investigation on the effects of morphological parameters on fracture behaviour and toughness properties of PP have also been conducted in the literature (Doshev, P. et al., 2005; Fasce, L. et al., 1999; Jancar, J. et al., 1993; Sun, Z. and Yu, F., 1991). During the

manufacturing process, PP can be crystallized into different isomorphic modifications such as α- PP, β -PP, Υ-PP (Nedkov, E. and Dobreva, T., 2004). Fracture toughness is closely related to these crystal forms. The β crystal structure has been found to be more tough compared to the α crystal form (Chen, H. et al., 2002; Du H, Z. Y., Liu H, Liu K, Jin M, Li X, Zhang J, 2014) since it contains more tie molecules in its bundle like structure compared to the hatched like structure in the α crystal and absorbs more energy during the fracture event. Failure mechanism of β crystal structure is shown here in

Figure **2.9**. Elastomeric content present in the co-polymer, molecular weight etc. are also believed to have an effect on the fracture toughness properties of PP (Chen, H. et al., 2002; Du H, Z. Y., Liu H, Liu K, Jin M, Li X, Zhang J, 2014; Fasce, L. et al., 1999; Fasce, L. A. et al., 2004; Nedkov, E. and Dobreva, T., 2004; Salazar, A. et al., 2014; Sun, Z. and Yu, F., 1991). The effects of annealing to achieve higher toughness in PP were investigated by previous researchers (Geng, C. et al., 2014) .

For PE, the fracture toughness (K_{IC}) in plane strain condition measured by following the LEFM method requires high sample size requirements especially for the high toughness grade PE (Chan, M. and Williams, J., 1981). Due to this limitation of LEFM, the J-integral with multiple specimen method was applied to study the fracture behaviour of high toughness grade HDPE in the range -80° C to +23° C (Chan, M. and Williams, J., 1993). The J-integral method was also used for LDPE and LLDPE (Hashemi, S. and Williams, J., 1986). Similarly, fracture behaviour analysis of HDPE pipes was also measured using J-integral methods in previous works (Benhamena, A. et al., 2011; El-Bagory, T. M. et al., 2014) . For measuring fracture toughness values of LDPE at room temperature , the essential work of fracture was applied successfully in previous research work (Pegoretti, A. et al., 2009).

Swei et al. (Swei, H. et al., 1991) compared the fracture toughness of three different types of PE and analysed the damage zones and fracture surfaces to identify the crack growth mechanism of PE. They observed four different zones in the fracture surface (Figure 2.10).

(a)   (b)

(c)
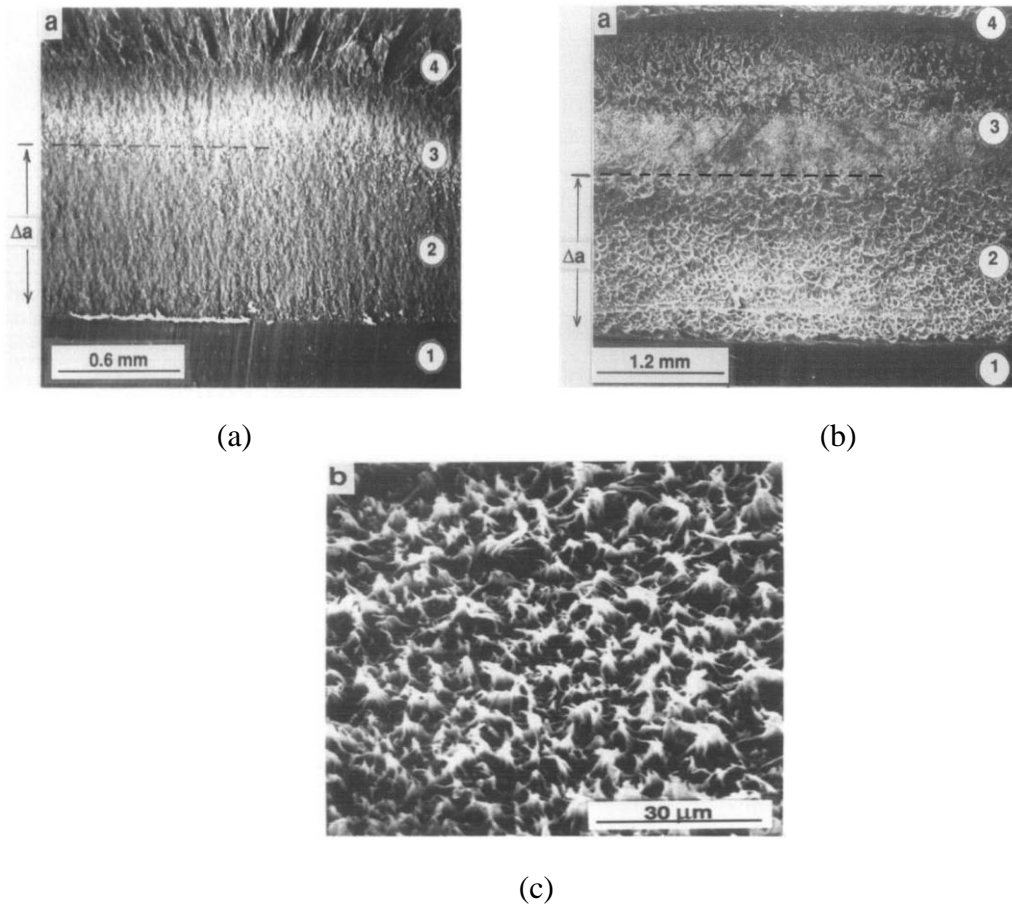
Figure 2.10 Fracture surface of (a) HDPE, (b) PE co-polymer and (c) region-2 at high magnification. Regions 1, 2, 3, 4 are for the notch, stable crack growth, larger fibril un-fractured craze and brittle fracture zone respectively **(Swei, H. et al., 1991)**.

Voids or micro-cracks beyond the notch region are formed during the application of load to the samples; the coalescence of these voids later creates a craze ahead of the initial razor notch at $J \geq Jic$. In this case the crack initiation mechanism is considered the same for both of the HDPE and PE copolymer. The presence of coarser fibrils in region-2 that were needed to be broken for crack propagation, as well as a higher number of multiple local plastic zones (craze and shear bands) in the polyethylene copolymer compared to HDPE were the reasons behind the higher fracture toughness observed for the polyethylene

co-polymer. The same mechanism for slow stable crack growth was also noticed in the water medium for the polyethylene as well (Chan, M. and Williams, J., 1983).Mechanical properties of polymers generally depend on their molecular structure as well as its morphological features such as molecular weight, density, crystallinity, crystal structure etc. In addition, for PE side chain branches also believed to have an effect on its ultimate fracture properties.
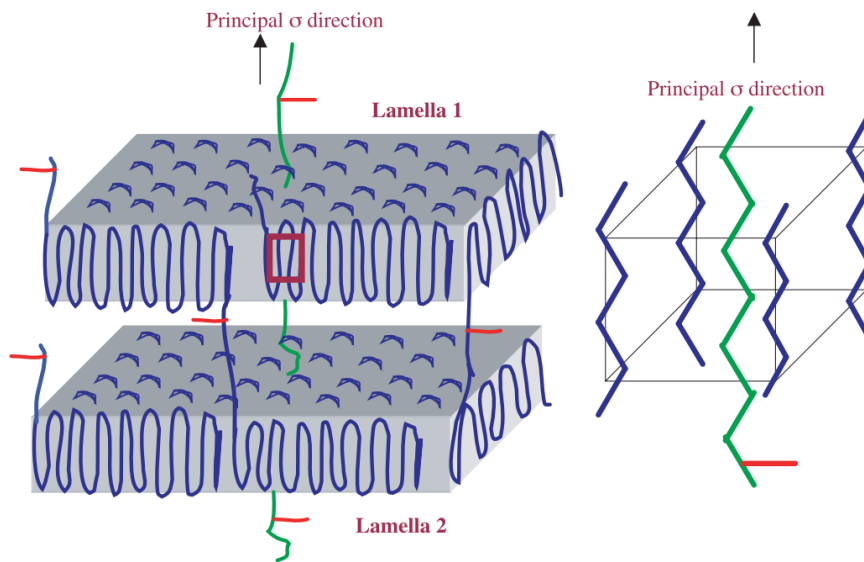
Figure 2.11 A schematic diagram of side chains and lamellae during fracture (**Gupta, P. et al., 2005**).

The effects of molecular weight on HDPE were investigated by Wang et al.(Wang, M.-D. et al., 1993) and found a linear relationship between fracture energy and molecular weight for PE. High molecular weight favours the higher number of entanglements among the tie chains connecting lamellar blocks leading to greater plastic deformation with higher fracture energy absorption. For slow crack growth, crystallinity doesn't determine the time to failure(Lu, X. et al., 1995), though it has a linear relation with yield point of materials (Crist, B. et al., 1989). The cooling rate of the plastic manufacturing process also changes the molecular arrangement of the polymers and this has an effect on the fracture behaviour. Fracture stress was found to be higher for quenched (quick cooling) PE samples over slow

cooled samples. Quenching brings some changes to the molecule arrangement, giving them less time to form crystals; this increases chain branching density and entanglements and decreases crystallinity resulting in higher fracture toughness. The co-monomer type as well as the length of the side chain also has an effect on the fracture behaviour of polyethylene. Longer side chain increases the resistance to crack growth. Fracture analysis of 1-hexene and 1-butene co-monomers HDPE was conducted and hexene was found to have failed after a long time (400 hours) compared to butene co-polymers (30 hours) (Wolfe, A. R., 1998). The same kind of investigation was also conducted by Gupta et al. (Gupta, P. et al., 2005).

2.4 Application of rotationally moulded materials in three layered skin-foam-skin sandwich structure

Rotationally moulded three layered skin-foam-skin sandwich structure can be manufactured in a single manufacturing step without any joint and are currently being increasingly used to make small boats, kayaks, canoes and automotive components. During their service life, damage can be caused due to impact force which is a major concern for the durability of this structure. In the following section the manufacturing process of this structure is described. Intensive literature review is also presented on the impact properties analysis of the skin-core-skin sandwich structure.

2.4.1 Manufacturing Process of rotationally moulded three layered sandwich structure

For the manufacturing of three layered skin-foam-skin sandwich, generally skin and foam layer are produced sequentially (Archer, E. et al., 2007; Pop-Iliev, R. et al., 2006; Vázquez-Fletes, R. C. et al., 2016) . A standard skin powder, e.g. PE is added first, heated in the oven with rotation to melt and spread in the mould, the mould is then removed from the oven, opened and the powder for the foamed core layer is added before returning the mould to the oven to create the foam layer. Once the foam layer is moulded, the mould is removed and opened again to add the third or inner layer and placed it in the oven. This method has some disadvantages such as process interruptions etc. as the mould needs to be opened for

each additional layer. Therefore, a new method was patented in 1990 (Duffy, K., 1990) where drop boxes are used to release the second and third layer. In this sophisticated process, the drop box is filled with foam-able powder. The main mould is charged with the skin material and heated to melt the skin materials to coat the mould surface. When this step is done, the drop box door is opened pneumatically or electronically and releases the second layer foam-able powder to enter the main mould. The second layer powder melts and a foamed layer is produced. After that the second drop box is opened to form the inner skin layer.

For manufacturing of foam in a rotational moulding process, blowing or foaming agents are added with the main materials. Foam is a disperse system of gas and solid polymer matrix (Archer, E. et al., 2003). There are two ways to create the gas phase in the main polymer matrix- physical and chemical foaming. In physical foaming gas phase is injected into the polymer mix and in chemical foaming system solid powder is decomposed to create gas phase. For the rotational moulding, chemical foaming is preferred for producing the skin-foam sandwich structure. Decomposition of blended or mixed blowing agent in the polymer matrix occurs at a certain temperature and creates gas phase in the polymer matrix. Both exothermic and endothermic blowing agents were reported to be blended with Polyethylene. Polypropylene foam is also used in rotational moulding process. Same type of materials are used for the skin and foam layer in skin-foam sandwich structures for achieving better interfacial adhesion. For skin materials polyethylene and polypropylene can only be used as only polyethylene and polypropylene foam are available in the rotational moulding process. Skin materials play vital role in the sandwich structure as they provide the main resistance to the sudden shock or impact force.

2.5   Impact response of rotationally moulded of skin-foam-skin sandwich structure

The impact response of the sandwich structure is crucial in the design, manufacture and maintenance of the sandwich composite. The failure mechanism and damage modes are complex. Different damage modes may be seen at different layers of the sandwich structure. Research works on impact properties analysis with the details of damage modes of glass, carbon and other fibre reinforced honeycomb, aluminium and polymeric foam

sandwich composite structures are found in the literature, however for rotationally moulded skin-foam-skin sandwich the existing published research is very limited with only one published research works found (Casavola, C. et al., 2014). Casavola et al. (Casavola, C. et al., 2014) analysed the impact properties of rotationally moulded sandwich composite from 5 to 70 J energy level. In their investigation they used 44 mm thick sandwich composite. Load-time, damage size and absorbed energy responses were analysed. Effect of related parameters such as skin and core thickness, impact velocity, impactor diameter etc. on impact properties and damage creation were not analysed in their investigation.

Fibre reinforced composite is a polymer which is reinforced by a fibrous phase. The most common fibres are glass, carbon, boron and aramid fibres. In fibre reinforce composite matrix is used to support and protect the fibrous reinforcement. Generally matrix materials are two types - thermoplastic and thermosets resins. For manufacturing of fibre reinforced sandwich composites, the rigid composite skin and core layers are jointed together. Adhesive is used to bond any combination of core and skin layers. The quality of fibre reinforced sandwich panels depends on the adhesive type, efficient application of the adhesive and a surface pre-treatment. Here, details of fibre reinforced sandwich composite and their manufacturing processes are not included as these are out of scope of this thesis. In the following sections an extensive review of impact properties, its classification, important parameters, and damage modes is presented based on fibre reinforced sandwich composite since literature for the impact properties of rotational moulded sandwich composite is unavailable.

2.5.1   Classification of impact response

Impact response can be classified into two categories based on impact velocity- low and high velocity impact. Cantwell and Morton (Cantwell, W. and Morton, J., 1991) suggested less than 10 m/s impact velocity for the low velocity impact whereas Abrate (Abrate, S., 2005) defined less than 100 m/s as low velocity impact event. High and low velocity impact also induce different structural deformation and response (Cantwell, W. and Morton, J., 1989; Sjoblom, P. O. et al., 1988). High velocity impact response is dominated

by the stress wave propagation through the material and creates very localised damage as the structure does not get time to respond. On the other hand low velocity impact is considered as quasi-static and it generates an entire structural response. Delamination and matrix cracking are happened in low velocity impact event whereas fibre breakage and perforation are found in high velocity impact response of composite structure (Liu, D. and Malvern, L. E., 1987).

Alongside of impact velocity, impact mass is a key factor that differentiates the impact response. Olsson (Olsson, R., 2000) stated that the ratio ($\bar{m}$) of the impact mass to the effective plate mass is important for low velocity impact response. He defined that the impact response is quasi static and large mass impact when the mass ratio is greater than eight ($\bar{m}>8$). For the small mass impact, the response is dynamic and the mass ratio should be less than 0.23 and 0.29 for square and circular plate as well.

2.6 Low velocity impact response of sandwich composite

The impact response of sandwich composite subjected to low velocity impact is influenced by both the test and specimen parameters. Test parameters are the impactor diameter and geometry, impact velocity and mass. The test specimen factors including specimen thickness, thickness of facesheet and core. Facesheet is the skin layer of a sandwich composite. The following section will focus on many of these parameters that influence the low velocity impact behaviour of sandwich composite materials.

2.6.1 Geometry of impactor

Impactor geometry is an important factor that dominates the low velocity impact response and has been investigated extensively both for flat and hemispherical shaped impactors (Bernard, M. L. and Lagace, P. A., 1989; Raju, K. et al., 2008; Zhou, G. et al., 2007). Larger contact force was found for the increased radius of the impactor, though less effect was observed for the displacement of whole structure. Raju (Raju, K. et al., 2008; Raju, K. and Tomblin, J., 2001) found that the smaller radius indentor induced matrix cracking and fibre fracture leading to face-sheet damage of the sandwich structure whereas larger radius indentor created core crushing. Between the flat-ended and spherical-end impactor, Zhou

(Zhou, G. et al., 2007) observed higher threshold and ultimate load for flat-ended indentor than that of hemispherical indentor because of the greater stress concentration around the edge of the impactor of flat-ended indentor. Flat-ended impactor also creates larger deflections with greater degree of membrane stretching of the skins. It was found that the hemispherical shaped indentor has been used in most of the research works.

2.6.2   Impactor mass

Impact mass has a great influence on the impact event as it influences the structural response to the applied impact force. Low velocity impact is a quasi-static method which relates to the large impactor mass and when mass ration is $\bar{m} > 8$. Impact mass also influences impact duration as larger impact mass leads to longer impact duration and larger deflection (Olsson, R., 2000). For small mass impact, the impact response duration is very low and therefore it transfer a higher impact energy to the sandwich composite that causes earlier damage initiation and larger delamination compared to large mass impact response.

2.6.3   Impact Velocity

The magnitude of the impact velocity is related to the contact force and deflection of the sandwich composite in the low velocity impact event (Bland, P. and Pitakthapanaphong, S., 2005; Olsson, R., 2000; Olsson, R., 2003; Robinson, P. and Davies, G., 1992). Peak force was found to be proportionally related to the impact velocity. It was that found higher impact force for the increase of impact velocity, though impact velocity was not related to the impact duration (Bland, P. and Pitakthapanaphong, S., 2005; Daniel, I. M., 2009).

2.6.4   Thickness of the skin or face-sheet

Facesheet thickness plays a crucial role in impact event. Absorbed energy (Mohan, K. et al., 2007), failure load, deflection at failure (Shuaeib, F. and Soden, P., 1997) were found to be increased with the increase of facesheet thickness of the sandwich structure. Thicker facesheet leads to higher contact force and smaller displacement with the constant impact energy (Chai, G. B. and Zhu, S., 2011). In addition it also reduces the impact duration. Zhou et al. (Zhou, G. et al., 2007) observed changes in flexural stiffness, damage

mechanism and load transfer between top skin/core with the change of facesheet thickness. Because increasing facesheet thickness increased shear and bending stiffness of the structure. The impact response of the sandwich structure depends on the facesheet when the facesheet is tough and the density of core material is low. The failure mechanism shifts from facesheet dependent to foam core dependent behaviour when the facesheet material is less tough and the core density is increased from low to high (Shih, W. and Jang, B., 1989).

2.6.5 Thickness of core

The core layer of a sandwich structure provides support to the facesheet and ensures the better impact resistance by reducing crack propagation in the facesheet. Types of core material (Akay, M. and Hanna, R., 1990), varying core density and thickness have an effect on low velocity impact response of a sandwich structure. The polymer foam sandwich structure showed more elastic behaviour with the increase of foam core thickness (Ozdemir, O. et al., 2015). Therefore maximum contact force was found to be decreased whereas contact time of the impact event and maximum deflection increased. Besides, increase in energy absorption capacity was also determined.

For the increase of foam core density from low to high, higher rigidities were noticed resulting in higher contact force. This behaviour of the stronger core is considered as an advantage for protecting the skin from the impact damage. Damages in polymer foam core were identified and found core indentation with matrix cracking at low energies of impact event while core crushing with composite facesheet fracture were reported at higher energies (Compston, P. et al., 2006).

Environmental conditions such as temperature, moisture and testing condition such as strain rate have also some effect on the low velocity impact response of the sandwich structure. Maximum contact force, energy absorption capacity are related with the temperature. Research works on the effect of strain and moisture effect are still very limited in the literature.

2.6.6   Damage mechanism

For the development of the damage in the sandwich composite during the low velocity impact event facesheet thickness, core thickness and density , indentor shape and diameter are strongly related. Generally damage in the facesheet happens because of the localised impact deformation in the impacted area. In the core the damage is occurred for the transverse contact pressure (Richardson, M. and Wisheart, M., 1996).

From the experimental investigation of the sandwich composite five different failure modes were identified as follows (Abrate, S., 1997, 2005; Daniel, I. M., 2009)-

- Core buckling and debonding
- Core shear and cracking
- Delamination in the top facesheet
- Facesheet matrix cracking and
- Fibre breakage in the facings

Thick and thin honeycomb core sandwich panels were investigated and different damage progression mechanism were identified shown in figure-2.12 (Raju, K. et al., 2008).For thicker core sandwich panels, damage sizes are smaller and facesheet fracture initiation happens earlier compared to thinner core sandwich panels. During the impact event localised bending of facesheet generally happens. As the core crush depth of thicker core is larger, it can accommodates more facesheet bending over a small regions resulting in facesheet fracture initiation earlier or at lower energy level compared to thinner core sandwich panels.

Besides, the crush and damages in the core cells of the thicker core propagates across the width of the sandwich panels over a small region while in the thinner core, the core damage propagation area is also larger. In the figure these two different damage progression mechanism is described based on thick and thin core sandwich panels.
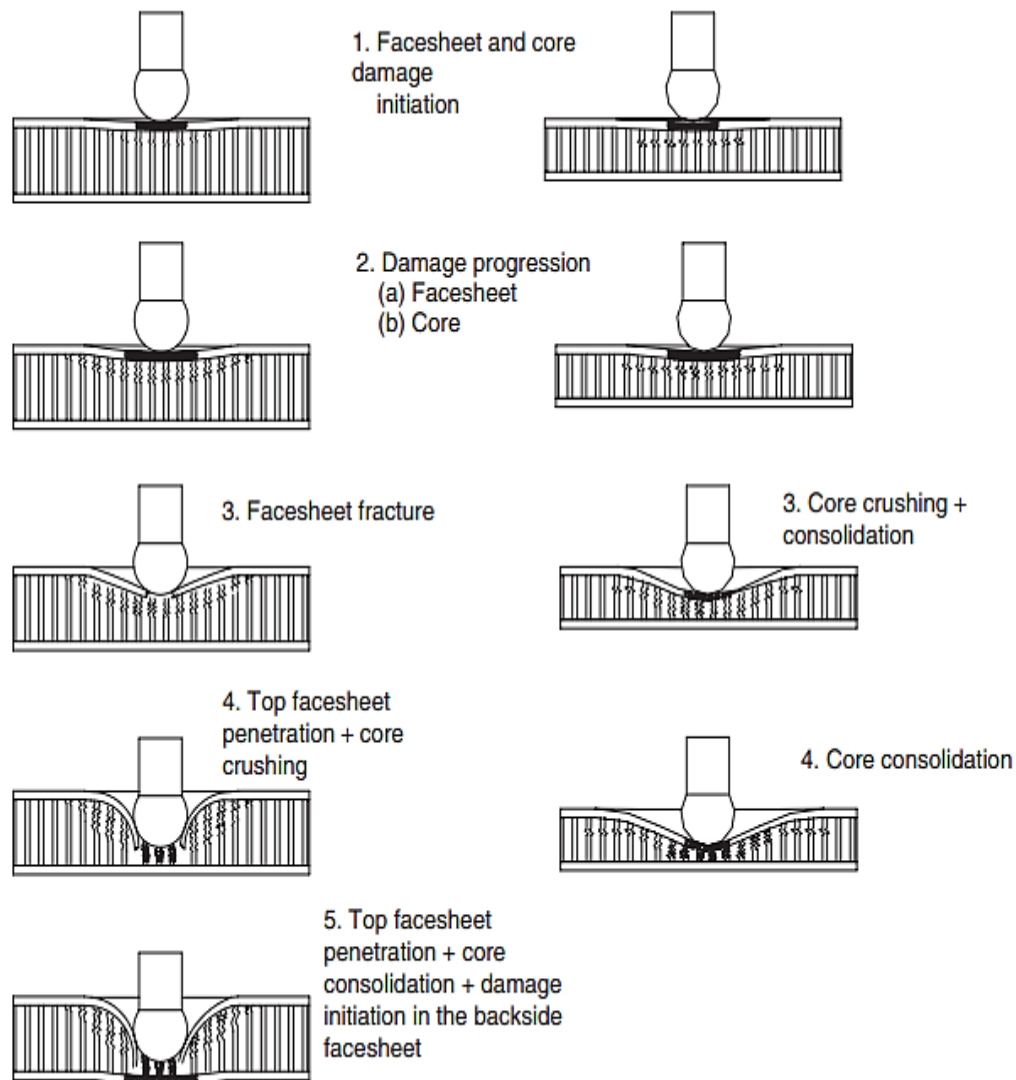
Figure 2.12 Damage progression mechanism for thick and thin core honeycomb sandwich panels (Raju, K. et al., 2008).

Lin et al. (Lim, T. S. and Lee, C. S., 2004) found that the thin face and high density core creates face compressive fracture due to the higher facesheet stress. They also found different failure modes with the changes of the face thickness and core density shown in figure-2.13. It was observed that failure mode changes from core shear failure to face failure with the reduction of facesheet thickness. The same trend was also identified with the increase of core density of the sandwich panels.

40

Face thickness

1.02 mm	Core shear
0.87 mm	
0.72 mm	
0.58 mm	Face failure

(a)

Core density

54 kg/m^3	Core shear
70 kg/m^3	
97 kg/m^3	
117 kg/m^3	Face failure

(b)
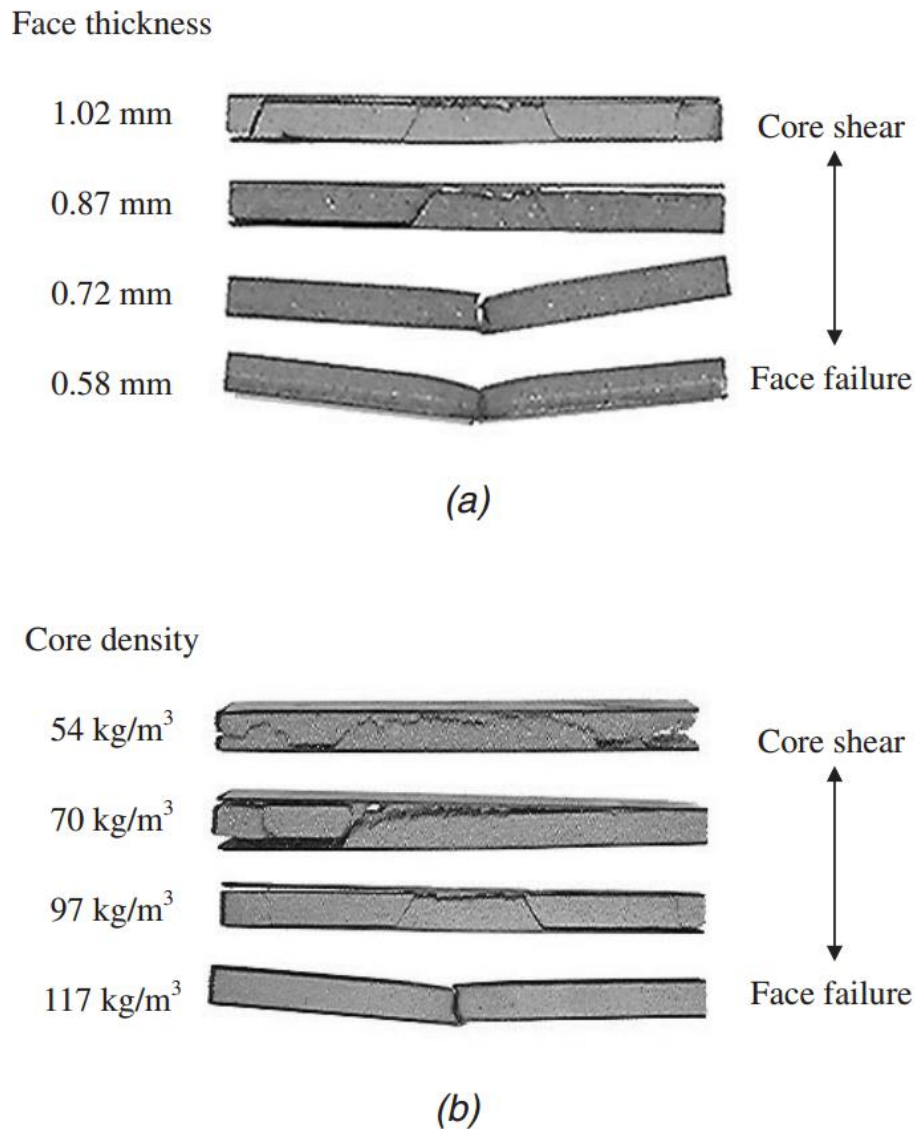
Figure 2.13 Changing of fracture mode with the changes of (a) facesheet thickness and (b) core density of the E-glass/epoxy and PVC foam sandwich panels (Lim, T. S. and Lee, C. S., 2004).

For PVC and alumina foam core sandwich panels, damage modes for the foam core and facesheet were also investigated respectively at quasi-static and impact loading conditions (Lim, T. S. and Lee, C. S., 2004; Yu, J. et al., 2008). With thin facesheet, the sandwich fails in face fracture mode whereas with thick facesheeet core shear failure mode occurs (figure-2.14). De-bonding of facesheet and core layers is seldom observed at static loading

41

condition whereas in impact loading condition de-bonding between facesheet and core is appeared when the deflection of sandwich structure is large .
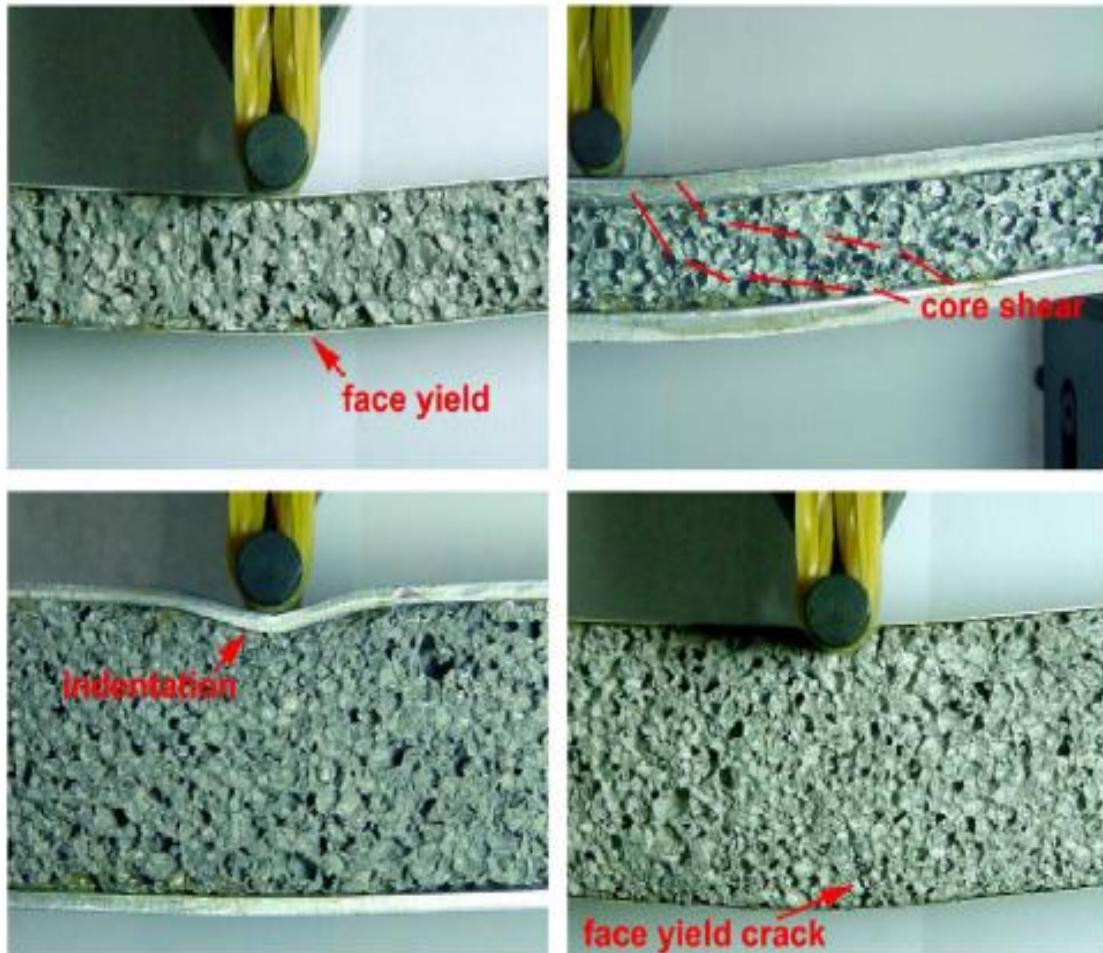
Figure 2.14 Face fracture failure mode for the thin face and core shear failure mode for the thick facesheet of aluminum alloy skins and aluminum-foam core sandwich panel (Yu, J. et al., 2008).

In the force-displacement curve obtained in low velocity impact event for carbon/epoxy-skinned sandwich panels with aluminum honeycomb core (Zhou, G. et al., 2006), three different regions were identified, briefly described here with the figure-2.15.

- Region- I: Elastic region for both core and facesheet without any visible damage.

- Region- II: After region-I, the curves becomes non-linear with a sudden drop indicating the initiation of damage. Beyond this sudden drop the curve again starts to rise sharply.
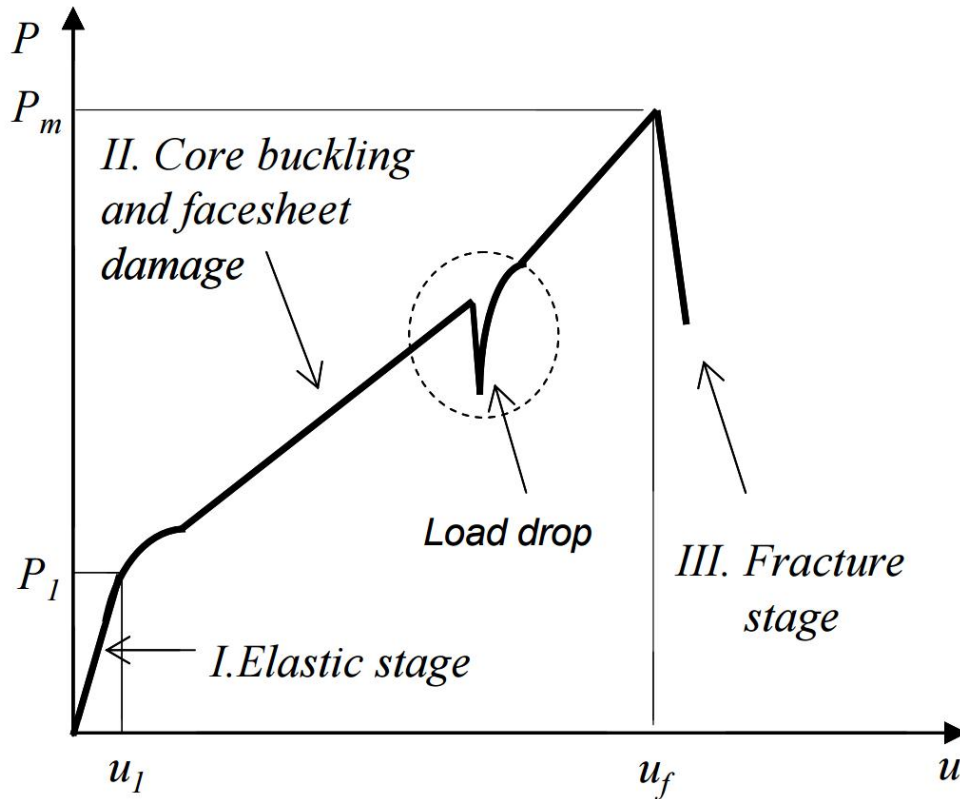
Figure 2.15 Typical load-displacement curve of a carbon-epoxy skinned sandwich panel with aluminum honeycomb core observed in low velocity impact testing (Zhou, G. et al., 2006).

- Region- III: This region is called fracture region. The curve shows dramatic drop for the penetration or complete destruction of the sandwich samples. If the penetration does not happen, the impactor will rebound.

Facesheet transfer the impact force to the core as well as the whole sandwich panel. Therefore it plays a crucial role. For the investigation of failure criteria of the facesheet numerically there are some models are available, though they have got some advantages

and disadvantages as well. Delamination between the facesheet and core layer is one of the main concern in the fibre reinforced sandwich composite panel, as it reduces the strength and stiffness of the sandwich panel drastically.

2.7   Repeated or multiple low velocity impact response

In sandwich composite structures many small damages may be created at various stages of their lifespan such as maintenance, manufacture, assembly or service life caused by many impacts or different repeated impacts (Çoban, O. et al., 2009). These damages are very small and can't be detectable in the naked eye. It is possible that they grow with time and can cause a catastrophic failure. In this circumstance, it is necessary to understand the damages of the sandwich composite under repeated low velocity impact conditions. Besides, repeated low velocity impact test are important for sandwich panel which are using in marine application (Cucinotta, F. et al., 2016) since the stress caused here are similar to water slamming. In most of the experimental investigation, instrumented drop weight impact testing machine is used for the low velocity repeated impact test (Akatay, A. et al., 2015; Cucinotta, F. et al., 2016) . Impact speed and energy is normally managed by the impact heights variation. Pendulum type instrumented impact tester was also reported in the literature (Çoban, O. et al., 2009; Sınmazçelik, T. et al., 2006). For the low velocity repeated impact test there is no international testing standard guidelines at this moment. In this test, generally the sandwich panels are tested under multiple impact shock at the same energy level or at various energy levels until it gets fracture or perforation. Comparison is made between the results of single and repeated low velocity impact shock particularly in terms of peak impact force, deflection of the sandwich panels, time taken for the impact event and impact event number. Damages in the front and rear surface and core layers are investigated at repeated impact event with naked eye or digital camera.

2.8   Low velocity repeated impact response of rotationally moulded skin-foam-skin sandwich structure

Literature on low velocity repeated impact properties is not available for rotationally moulded skin-foam-skin sandwich structures but has been conducted using fibre reinforced sandwich composites as below:
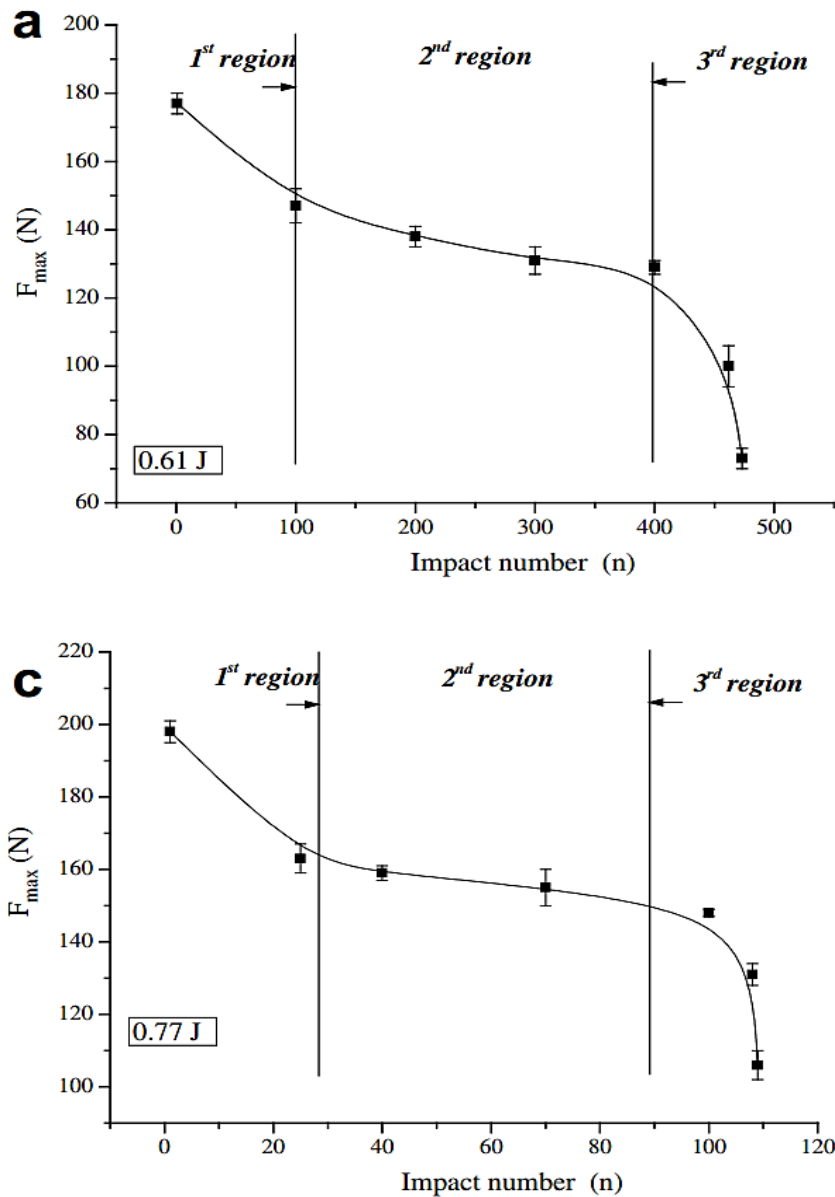
Figure 2.16 Changes of peak force (Fmax) values during repeated impact test of carbon fibre reinforced polyetherimide composites at different energy level (Bora, M. Ö. et al., 2009).

Glass, carbon fibre composites and honeycomb sandwich composites
Low velocity repeated impact properties of glass fibre (Kawaguchi, T. et al., 2004; Sınmazçelik, T. et al., 2006) and carbon fibre composite (Sınmazçelik, T. et al., 2006),thermoplastic matrix composite (Bora, M. Ö. et al., 2009), foam (Atas, C. and Sevim,

C., 2010) and honeycomb core sandwich composite panels were investigated before. Abdullah Akatay et al. (Akatay, A. et al., 2015) investigated repeated impact effect on compressive properties of the honeycomb sandwich panels. They found a catastrophic reduction in compressive strength for the repeatedly impacted samples. It was found that 81, 36, 21, 7 and 4 repeated impact events were able to perforate sandwich samples at 3, 5, 8 20 and 40 J impact energy levels. Therefore it was concluded that the total number of impact event to perforate the sandwich samples was increased when the lower energy level was used. The same observation was also found in other works as well (Atas, C. and Sevim, C., 2010; Cucinotta, F. et al., 2016).
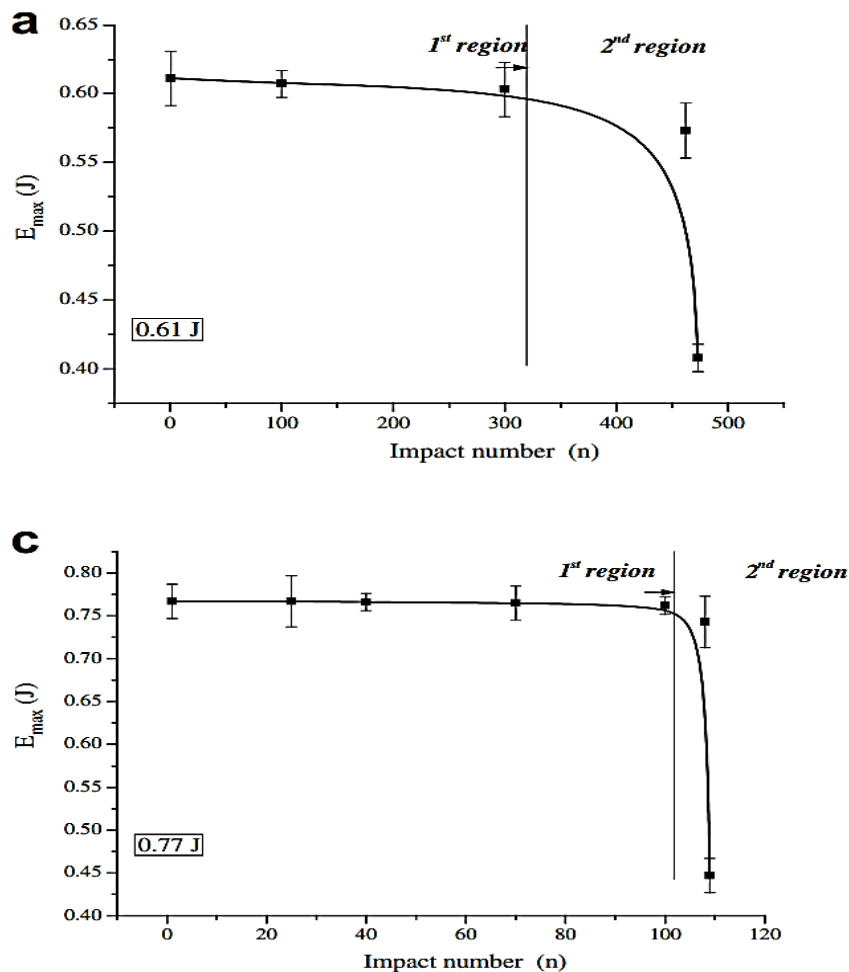
Figure 2.17 Maximum absorbed energy (Emax) values of carbon fibre reinforced polyetherimide composites during repeated impact test at different energy level (Bora, M. Ö. et al., 2009).

PVC foam core sandwich composite

PVC foam core sandwich panels were investigated under low velocity repeated impact test condition (Cucinotta, F. et al., 2016). There was a decay of the stiffness and reduction of the peak impact force that followed the parabolic law with the increase of number of impacts during the testing. Absorbed energy was observed to be increased with the impacts number of the sandwich samples.

Peak impact force curve, absorbed energy curve and impact-fatigue life curve

In the repeated impact test, three regions were identified in peak force versus impact number curve at each energy level until the perforation happens for the repeatedly impacted carbon fibre reinforced polyetherimide composites (Bora, M. Ö. et al., 2009; Çoban, O. et al., 2009; Sınmazçelik, T. et al., 2006) as shown in the figure-2.16. Peak force value reduces sharply in the first region due to the fibre breakage, micro buckling or shear deformations in the compression zone during repeated impact event. The second zone is called "Plateau region" wherein peak force value almost maintains a certain value. Initiation and propagation of matrix deformation and multiplication of delamination happen in this region. After this region, peak force values decreased sharply to the minimum level after a certain impact number. This is because of the fibre fracture in the tensile zone and finally the sandwich samples get full fracture or penetration with a minimum peak force values.

Unlike peak force-impact number curve , two regions were identified in the maximum absorbed energy-impact number curve in the repeated impact event (Bora, M. Ö. et al., 2009) as shown in the figure – 2.17. In the first region, at each energy level, up-to a certain impact number the maximum absorbed energy remains constant. Beyond this region the maximum absorbed energy falls sharply. In the first region, crack initiation and propagation energy balance the energy cumulatively themselves and remain constant up-to a point from where the total fracture or penetration happens into the samples.

From the experimental investigation of low velocity repeated impact test of the honeycomb sandwich composite (Akatay, A. et al., 2015) and thermoplastic matrix composite

(Bora, M. Ö. et al., 2009), it was tried to build a relationship between the energy levels and number of impact. The main purpose of this relation was to predict the impact-fatigue life of a sandwich composite. Figure-2.18 shows the low energy impact-fatigue life of honeycomb structure (Bora, M. Ö. et al., 2009). It was found that up-to a certain energy level the curve shows parabolic variation. Lower than this certain impact energy value, the impact number up-to the fracture or the perforation increased suddenly. From the equation of this curve, impact-fatigue life of the samples can be predicted.
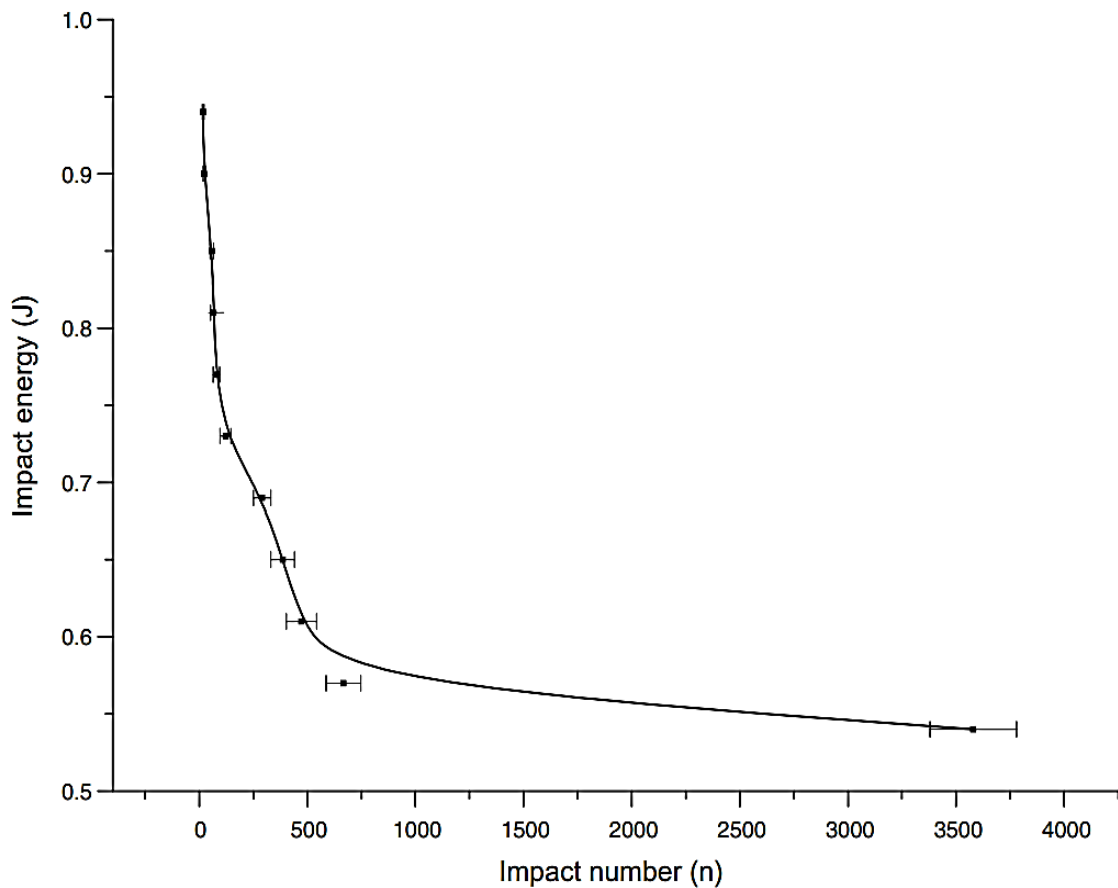
Figure 2.18 Impact fatigue life curve of carbon fibre reinforced polyetherimide composites (Bora, M. Ö. et al., 2009).

2.9 **Summary**

In summary, this chapter is a review of recent research on rotationally moulded plastic materials, fracture toughness and impact properties analysis of polyethylene and polypropylene, manufacturing processes, and impact properties of rotationally moulded skin-foam-skin sandwich structures. Following this literature review the following statements are developed -

1. Analysis of fracture properties, particularly fracture toughness analysis at static loading rate, has been carried out for injection, compression or extrusion moulded plastics, although it is not yet done for rotationally moulded plastics. This represents a research gap that limits the further applications of rotationally moulded materials. This research provides an understanding of crack initiation and propagation mechanisms for rotationally moulded materials under loading conditions, and investigates the influence of material microstructure on the toughness properties which are essential to ensure the durability of rotationally moulded plastics in various applications such as oil and water storage tanks, kayaks, canoes, small boats and automotive applications.

2. Impact properties analysis of rotationally moulded plastics has been performed for certain rotational mould grade materials, though the relation of some morphological parameters such as density, and thermal transitions in materials on the final impact properties are not clear, and this necessitates further investigation. Besides, impact properties analysis gives the information on materials fracture behaviour at high or dynamic loading rate.

3. Rotationally moulded plastics are being used in producing skin-foam-skin sandwich structures which contains higher specific stiffness and strength to weight ratio than the equivalent homogenous structures. Manufacturing processes of this rotationally moulded sandwich structure are reviewed here.

4. Rotationally moulded sandwich structures get damaged due to sudden impact loads. The resulting damage can extend and cause a catastrophic failure by many repeated local impacts during its service life. In the literature only one research work is found

on low velocity impact properties and no work has been done on low velocity repeated impact properties analysis of rotationally moulded sandwich structures. Therefore, extensive research is necessary to investigate the low velocity impact and repeated impact properties of rotationally moulded sandwich structures with identification of damage modes. This work is particularly relevant to the industry as it represents the most common in-service impacts.

These statements in current knowledge from the literature review confirm the aim and objectives of this project (section—1.11) are valid. In the following chapters the experimental methodologies to investigate the fracture behaviour of rotationally moulded plastics, the low velocity, and repeated impact properties of rotationally moulded sandwich structures.

Chapter 3. Experimental Methodology

In this chapter, details are provided on rotationally mould grade materials properties, the manufacturing processes and the testing procedures used in this study. Initially materials details, moulding process, microstructural analysis, mechanical testing procedures for the fracture toughness and impact properties of the rotationally moulded plastics are reported. Details of three layered rotationally moulded skin-foam-skin sandwich structure are then outlined. Following this, procedure of low velocity impact tests and low velocity repeated impact test are presented.

3.1   Material details

Table 3.1 Material details*

No.	Materials Type	Materials Grade	Code	MFI (g/10 mins)	Density (g/cm^3)	Yield Stress (MPa)
1.	Polyethylene-1	Revolve N-307	PE-1	3.50	0.939	17.7
2.	Polyethylene-2	Revolve M-601	PE-2	3.50	0.949	21.5
3.	Polypropylene-1	Revolve PP-25	PP-1	25.00	0.902	25.5
4.	Polypropylene-2	Revolve S-TeQ 35	PP-2	30.00	0.902	23.5

*Data sheets were provided by the materials provider (Matrix Polymers, UK) and attached in Appendix-E in this thesis.

Two different types of rotationally mould grade Polyethylene and Polypropylene were used in this study, supplied by Matrix Polymers Ltd. Of the rotational grade polymers available, PE has been the most popular option for rotationally moulded products (Crawfoard, R. J. K., M.P, 2003; Waigaonkar, S. et al., 2008). Besides, there is also an increasing interest for using PP in this process. Polyethylene and Polypropylene materials are identified by a code starting with PE and PP respectively, followed by a number (1, 2). A limited number of materials data were provided by the manufacturer and are listed in table 3.1. The stress-strain curve of these materials are also provided by the materials provider (Matrix Polymers, UK) and mentioned here in Figure 3.1and Figure 3.2.
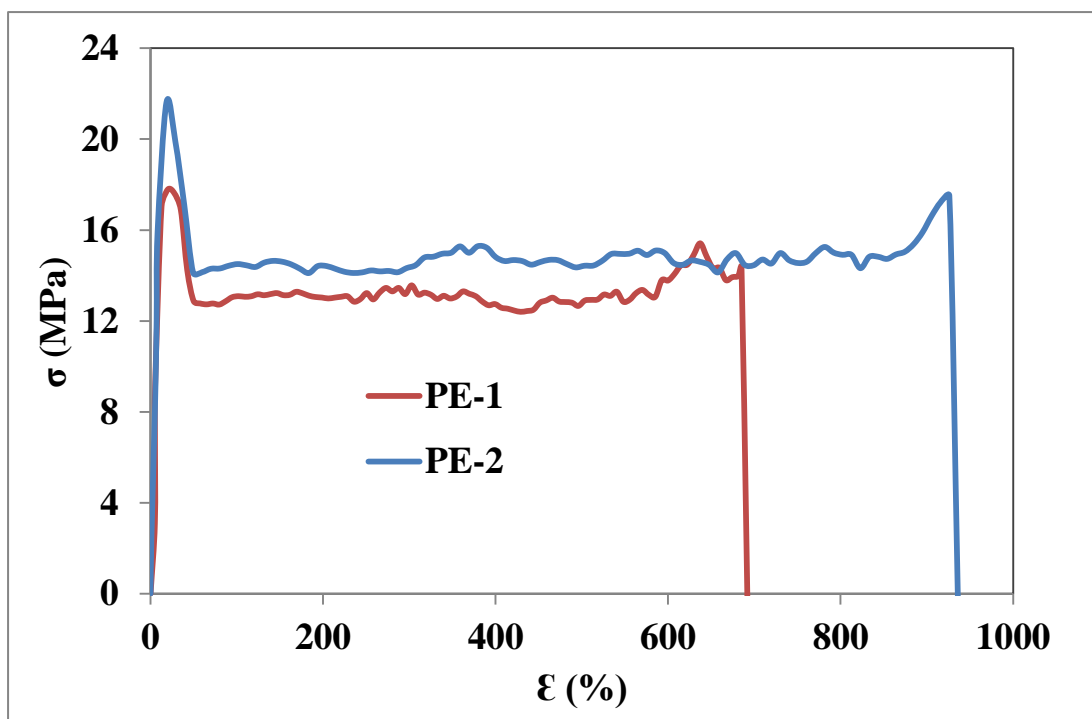
Figure 3.1 Tensile stress-strain curve of PE-1 and PE-2 samples.
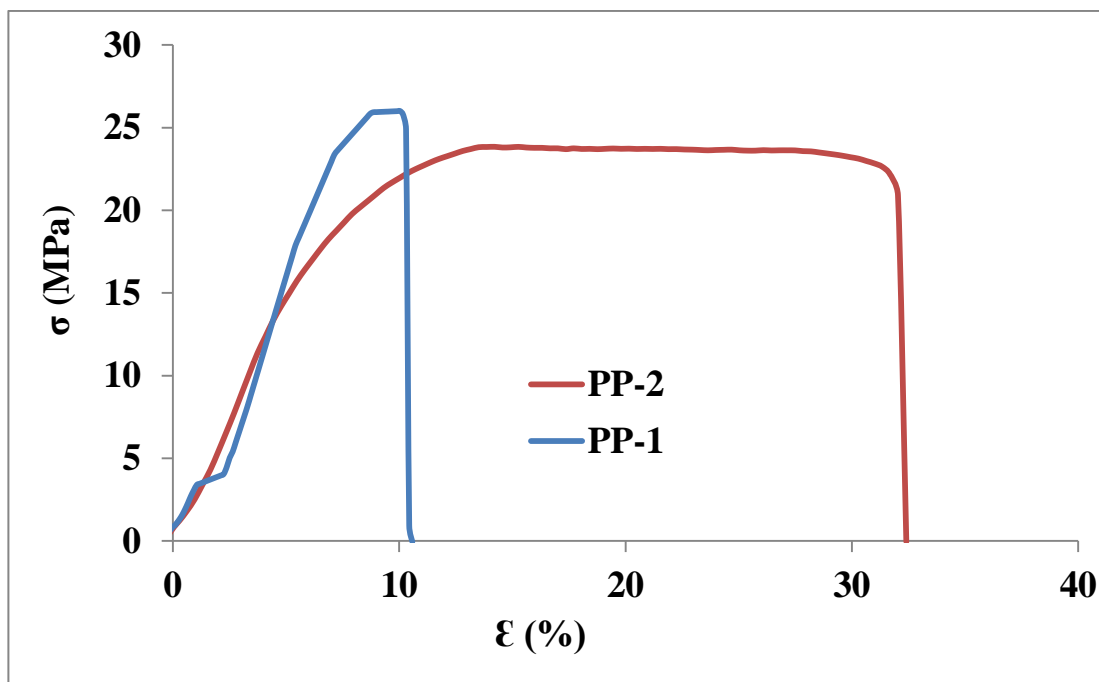
Figure 3.2 Tensile stress-strain curve of PP-1 and PP-2 samples.

3.2   Moulding of the materials

Rotationally moulded plastics were made using a Ferry Roto-speed Carousel type rotational moulding machine at Matrix Polymers Ltd. UK facilities. Mouldings were produced in a 300 mm steel cube mould. A shot weight of 2.5 kg was used in each trial to produce mouldings with a nominal wall thickness of 6 mm. All the mouldings were produced under the following conditions - mouldings were heated up in an oven at 300°C for 16 minutes, then the mould was removed from the oven and cooled with fans for 15 minutes and finally de-moulding was carried out. The actual speed of the major and minor arms of the moulding machine was 12 and 8 rpm respectively. The speed ratio was 2:1 $\left(major\ arm\ speed \middle/ minor\ arm\ speed - major\ arm\ speed \right)$.

Figure 3.3 Rotational moulding facilities in Matrix Polymer UK.

3.3 Microstructural characterisation of the moulded plastics

Details characterisation for the materials microstructure were carried out with solid-state NMR, WAXS, SAXS and DSC analysis in this study and listed in Table 3.2.

Table 3.2 PE and PP materials properties identified by solid state NMR and WAXS in this work.

Material Type	Material (Identified in this work as follows)	PE Content %	Side Branch Type	Side Branch Quantity (C/1000C)	Crystallinity (%)		Melting Temp. (°C)
					WAXS	DSC	
PE-1	Ethylene-1-octene co-polymer	N/A	hexyl	12	63	52.5	132
PE-2	Ethylene-1-octene co-polymer	N/A	hexyl	08	58	51.5	138
PP-1	Propylene-ethylene block copolymer	13.4	N/A	N/A	62	47	167
PP-2	Propylene-ethylene random copolymer	7.3	N/A	N/A	49	29	151

The characterisation processes are described in the following sections.

3.3.1 Differential Scanning Calorimetry (DSC)

The thermal behaviour and degree of crystallinity of the above mentioned materials were investigated by differential scanning calorimetry with METTLER TOLEDO DSC 823e, Ferry FR190S instrument in Matrix Polymer facilities. In DSC, a polymer undergoes a heat treatment which allows the polymer state to be changed in different phase with respect to temperature and time. DSC instrument calculates the difference in heat flow between a sample and an inert reference as a function of time and temperature as both the sample and reference are exposed to a temperature change and measures glass transition, melting point peaks. In this analysis, 5-7 mg samples were placed in an aluminium pan and heated from

40 to 200°C at the rate of 10° C/min under continuous nitrogen purge. The heat required for melting (ΔH) of different materials was measured by integrating the area under melting peak of each material. The degree of crystallinity was calculated by dividing the heat required for melting (ΔH) of different treated materials by the heat required for melting a 100% crystalline sample (ΔH$_C$). For PE, ΔH$_C$ = 293.6 J/g (Kodjie, S. L. et al., 2006) and for PP, ΔH$_C$ = 209 J/g (Cerrada, M. L. et al., 2010) were taken.

3.3.2   Small and Wide Angle X-ray Scattering analysis (WAXS, SAXS)

SAXS measurements were performed on a HECUS SAXS/GISAXS instrument equipped with a XENOCS micro focus CuKα (λ = 1.54 Å) source with Montel optics. The diffracted X-rays were collected with a Dectris Pilatus 100K 2D detector. Thin samples (ca. 0.3mm) were cut and placed into the spectrometer at the collection position and data collected in transmission mode. Silver behenate was used for calibration of the instrument before every collection. Sample collections typically took 4000 seconds. Irena SAS/SANS routines (S1) in Wavemetrics Igor Pro have been used for calibration, data conversion and subsequent analysis (Jemian, J. I. a. P. R., 2009).

WAXS data were collected on a Bruker D8 diffractometer equipment with a sealed tube Cu K-a (λ = 1.5407Å) source running at 1.2 Kilowatts and collected with a lynxeye multi-strip detector. Background scattering was subtracted in order to determine the weight fraction of crystals of each sample using following equation-

$$x = \frac{C}{C+A} \qquad\qquad (3.1)$$

Where C is the area of crystalline profile and A is the area of the amorphous profile.

The crystalline long period, D, which is related to the distance between lamellae, was calculated with following equation from q scattering vector determined in 1-D SAXS data.

$$q = \frac{2\pi}{D} = \frac{4\pi}{\lambda} \sin\theta \qquad\qquad (3.2)$$

Where D is the lamellar long period, λ is the wavelength, and θ is the scattering angle. q is the peak position of 1-D SAXS line graph.

Lamellar thickness was calculated from the following equation-

$$L_C = x_{vol}D \tag{3.3}$$

Where x_{vol} is the volumetric percentage of crystallinity calculated from the crystal weight percentage, x measure from WAXS analysis.

$$x_{vol} = \frac{\frac{x}{\rho_c}}{\frac{x}{\rho_c} + \frac{100-x}{\rho_a}} \times 100\% \tag{3.4}$$

Where ρ_c, ρ_a are the crystal & amorphous density respectively and their values were taken from (Schrauwen, B. A. et al., 2004). (PE- $\rho_c = 1$ g/cm3, $\rho_a = 0.85$ g/cm3 ; PP- $\rho_c = 0.95$ g/cm3, $\rho_a = 0.85$ g/cm3).

3.3.3   Solid-state Nuclear Magnetic Resonance (NMR)

Solid state ^{13}C NMR spectra were acquired using a Varian VNMRS spectrometer operating at 100.56 MHz for ^{13}C, using a 6 mm (rotor outside diameter) magic-angle spinning (MAS) probe for identifying the details of polymer structure of the plastics, side chain branches and quantity of the co-monomers used in PP and PE plastics. Solid state ^{13}C NMR spectra were acquired using a Varian VNMRS spectrometer operating at 100.56 MHz for ^{13}C, using a 6 mm (rotor outside diameter) magic-angle spinning (MAS) probe. Spectra from polyethylene and polypropylene samples were obtained with both cross-polarisation (CP) and single-pulse excitation (SPE) MAS at room temperature with a spinning frequency of 6 KHz. CP spectra were recorded with a recycle delay of 2 s and contact time of 1 ms. Quantitative SPE spectra were acquired using a 90° pulse of 4.5 µs and 60s recycle delay to ensure complete relaxation of the ^{13}C nuclei. The two-pulse phase modulation (TPPM) scheme was used for ^{1}H decoupling for all ^{13}C NMR spectra. These spectra were referenced to tetramethylsilane (Me$_4$Si) by sitting the isotropic high-frequency peak of adamantane to 38.56 ppm.

3.3.4   Dynamic Mechanical Thermal Analysis (DMTA)

A METLER TOLEDO DMTA machine was used to identify the storage and loss modulus, thermal transitions of each material. Samples of 35×10×3 mm were placed in the dual cantilever mode in the DMTA machine. Samples were tested at 0.005 strain from -150 to 100 ℃. The heating rate and frequency were 2 ℃/min and 1 Hz respectively. Generally temperature and frequency dependent behaviour are analysed for the viscoelastic materials particularly for polymer and plastic materials in Dynamic Mechanical Thermal Analysis (DMTA) (Pick, L. and Harkin-Jones, E., 2005). Here, the viscoelastic materials gets a sinusoidal strain over a range of temperatures and the response is consists of two components. One is elastic stress for the phase with strain and the other one is viscous stress for the out of phase with the strain. Dividing these two components by strain, it is possible to get the storage (E') and the loss (E") modulus as follows-

$$E' = \frac{\sigma}{\varepsilon} \sin \delta \qquad\qquad (3.5)$$

$$E" = \frac{\sigma}{\varepsilon} \cos \delta \qquad\qquad (3.6)$$

Storage modulus indicates the elastic and storage potential energy whereas the loss modulus mentions the dissipation of energy during the deformation process. The ratio of the loss modulus to storage modulus is termed as $\tan \delta$.

3.4   Fracture toughness test

3.4.1   Machine and testing arrangements

For the analysis of fracture behaviour at slow loading rates (1mm/min), an Instron operated by servo-hydraulic system is used with a three point bending arrangement. In this work, the three point bending arrangement was designed in-house (Appendix - A) according to the ASTM and ESIS guidelines **(Astm-D6068-96, 2002; Hale, G. E. and Ramsteiner, F., 2001)**. Figure 3.4 shows the testing arrangement in Instron 8872.
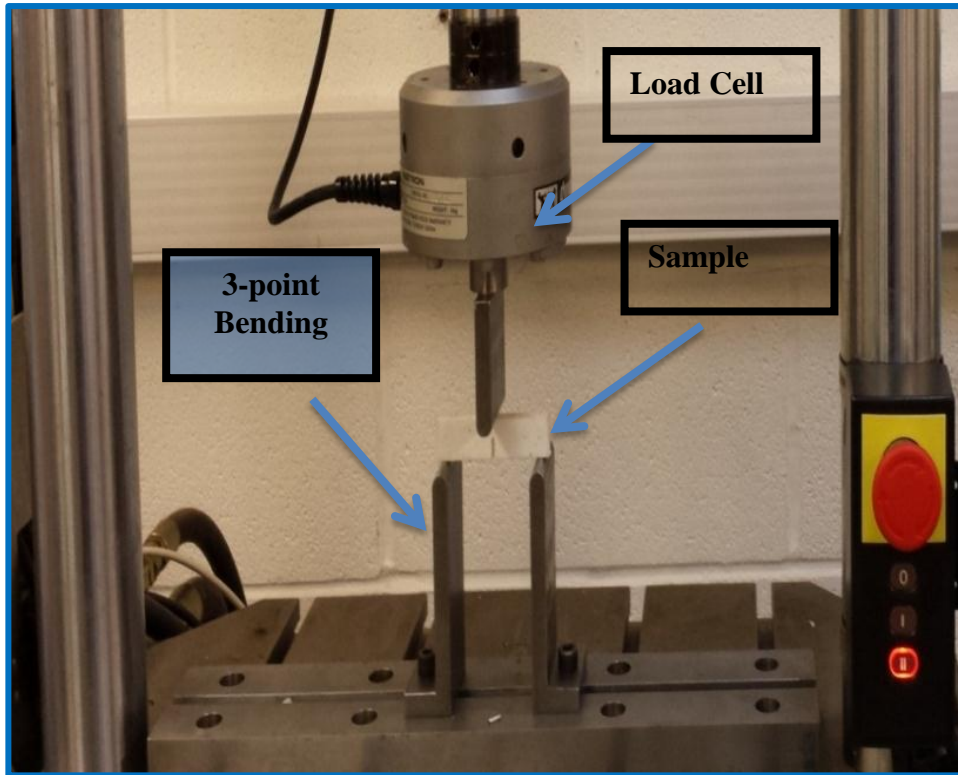
Figure 3.4 Testing arrangement of Instron.

3.4.2   Sample Preparation

Fracture toughness tests were carried out on single edge notched bend specimens (SENB, Figure 3.6.) Specimens with $48 \times 12 \times 6$ mm dimensions (details design in Appendix – B) were cut from the roto-moulded sheet. An initial straight-through slot with a length to width ratio of 0.5 and terminating in a V-notch with 0.1-0.15 mm in root radius was machined. Pre-cracks were inserted into the sample by sliding a fresh steel razor blade for every sample in the root of the machined notch so that the tip radius ≤ 20 μm. To promote a straight crack growth, specimens were equally side-grooved.
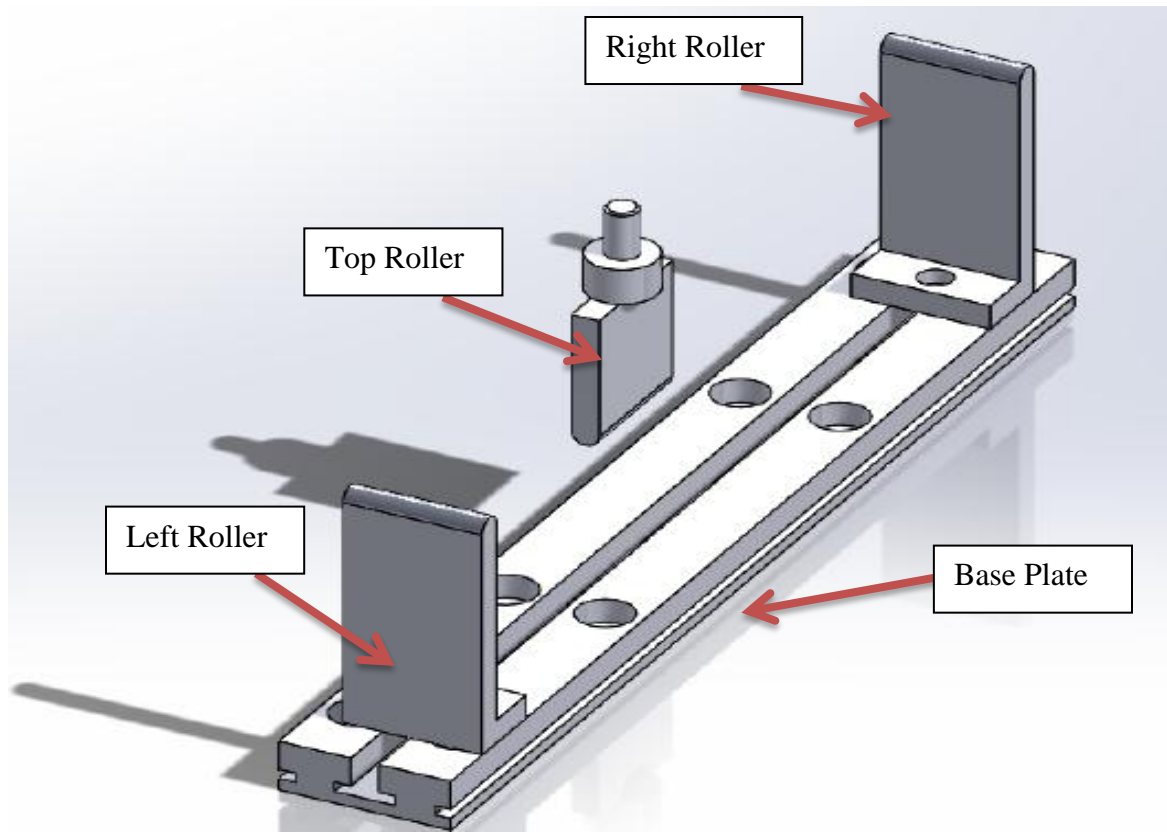
Figure 3.5 Three point bending test arrangement.
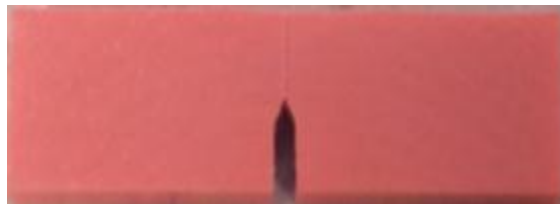
Figure 3.6 Specimen with notch.

3.4.3   Test process

J-integral based on the multiple specimen method was used to find the fracture toughness of the above mentioned plastics by following ESIS (Hale, G. E. and Ramsteiner, F., 2001) and ASTM protocols (Appendix-C) (Astm-D6068-96, 2002). A set of identical specimens of each type of materials were loaded to various displacements in a three point bending

arrangements at 1 mm/min crosshead speed in Instron-8872, unloaded, cooled in liquid nitrogen for 5-10 minutes and finally fractured under impact loading. The initial and final stable crack lengths for every specimen were measured physically from the fracture surfaces, while J was calculated from the total energy require to extend the crack, U, which was determined from the area under the load versus displacement curve obtained from the Instron data acquisition system.

$$J = \frac{2U}{B\,(W-a)} \tag{3.7}$$

where B is the specimen thickness, W is the specimen width and a is the initial crack length.

Crack resistance curve (J-R) was built for each type of plastics where J was plotted versus the crack extension (Δa). J_{IC} was measured at $J_{0.2}$ position of J–R curve.

Table 3.3 Fracture toughness test.

Material Type	Sample Dimensions (length × width × height) mm	Temperature	Test Speed mm/min	V-notch , crack and side groove
PE-1	48×12×6	23ºC	1	Yes
PE-2	48×12×6	23ºC	1	Yes
PP-1	48×12×6	23ºC	1	Yes
PP-2	48×12×6	23ºC	1	Yes

3.4.4   Fractography

An optical microscope (VHX-5000) was used to identify the real crack front and to measure the crack length on the fracture surfaces. SEM (JEOL, JSM-6010 PLUS/LV) images were taken at different magnification scales after applying 50 seconds gold coating for every specimen with an Agar auto sputter-coater gold coating instrument.

3.5 Impact testing of the rotationally moulded plastics

Along with the fracture toughness analysis at slow loading rate, impact test was also conducted to get the behaviour of the rotationally moulded plastic at dynamic loading rate at different temperature. Impact test were carried out with an instrumented falling weight impact testing machine according to ASTM-D 3763 – 02 (Astm-D3763-02) (Appendix-D) standards. In this work impact testing machine was developed in house according to the standard, shown in

Figure 3.7. Impact samples were machined from moulded plastics into 125×125 mm squares and placed on the sample holder with a circular window cut-out of 90 mm diameter in the centre of the holder. The impactor which was used to strike the clamped specimens is a hemispherical indenter with a 12 mm diameter. A piezoelectric impact force sensor of maximum loading capacity of 22.4 kN is used to measure impact force over time for each test. The total falling mass of the impactor for these tests is 9.1 kg (including impactor and crosshead mass).

Figure 3.7 Drop weight impact testing machine.

Table 3.4 Impact test at every 10º C intervals from -40º C to 30º C.

Material Type	Sample Dimensions mm	Diameter of indentor	Mass of falling dart	Impact Speed m/s	Impact height	No. Samples tested at each temp
PE-1	125×125	12 mm	9.1 kg	4.4	1 m	5
PE-2	125×125	12 mm	9.1 kg	4.4	1 m	5
PP-1	125×125	12 mm	9.1 kg	4.4	1 m	5
PP-2	125×125	12 mm	9.1 kg	4.4	1 m	5
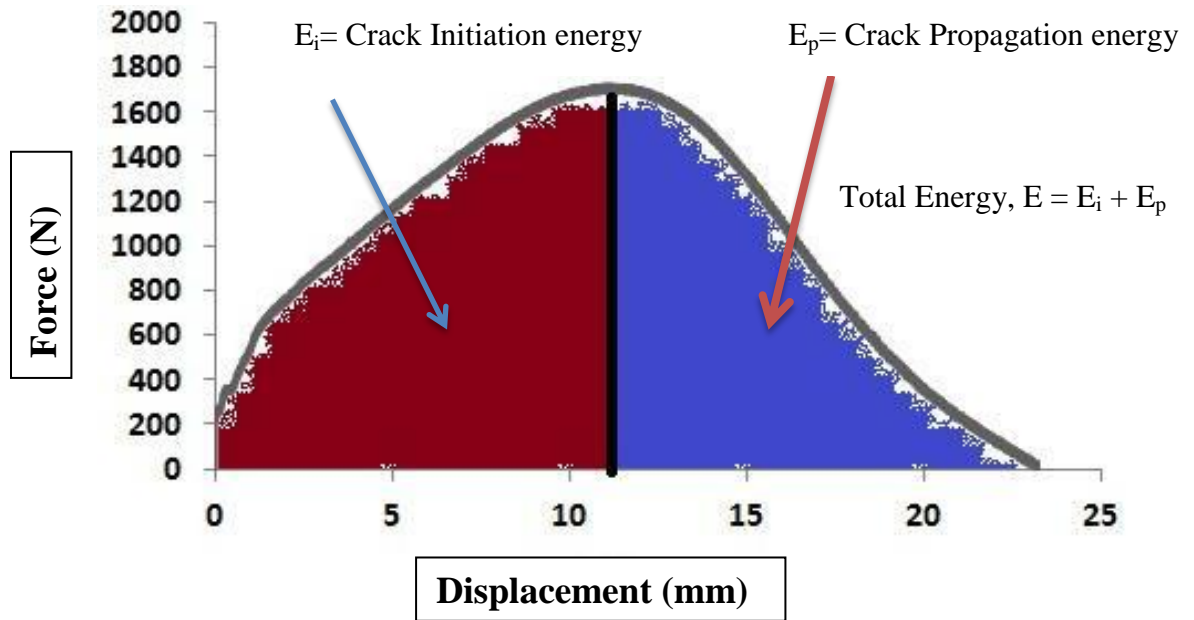
Figure 3.8 Typical force-displacement curve obtained in impact testing.

A high resolution oscilloscope (Picoscope IEPE 4242) was used to acquire the data generated in the impact event. Force- time and force-displacement graph were drawn for each of the test (described in Appendix-D). Peak impact strength was calculated from the area under the curve up-to the highest point in the impact curve while total strength was found from the area under the whole curve of force-displacement curve. Peak impact

strength is also termed as crack initiation energy. For getting the propagation energy, crack initiation energy is deducted from the total energy or strength for all of the samples. An example is given in Figure 3.8. The samples were impacted from a height of 1 m with an approximate 4.4 m/s impact speed. Five impact samples for each material were tested 10 ℃ intervals from -40 to 30 ℃. Samples were conditioned in an environmental chamber (Votsch, VCL 4003) at each temperature for 3 hours before testing.

3.6   Rotational moulding of three layered skin-foam sandwich composite

From the fracture properties analysis of the tested rotationally moulded samples, PE-2 (Revolve M-601 grade) type material was selected for the skin materials of the rotationally moulded three layered skin-foam sandwich structure. For the core layer, M-56 rotationally mould grade foam materials was selected which is also based on PE. Rotationally moulded sandwich composites were made using a Ferry Roto-speed Carousel type rotational moulding machine at Matrix Polymers Ltd. UK facilities. Material used in this sandwich structure are listed in Table 3.5. Four different skin-core thickness combinations were produced and respective shot-weight for each layer is presented in the Table 3.6. Mouldings were produced in a 300 mm steel cube mould. Polymer powder for the outer layer was introduced into the mould at first, heated up-to 140 °C to melt it and form outer layer, then the mould was taken out from the oven and powder was added for foamed core layer and heated up-to 130 °C. At 130°C the foam layer was melted without any expansion. After that polymer powder was added for the inner layer and processed in the oven until the temperature reaches 160 °C. For the inner layer 160°C temperature was used so that the blowing agent in polymer powder for the foam layer can be decomposed and expanded and also the inner layer can be formed. Finally the mould was taken out from the oven to cool down. Air cooling was applied with a five minutes precooling to solidify the products and de-moulding was carried out.

Table 3.5 Material properties used in rotationally moulded sandwich *.

Materials Grade	Material Type	Layer	MFI (g/10 mins)	Density (g/cm^3)	Yield Stress (MPa)
Revolve M-601	PE	Skin	3.50	0.949	21.5
M-56	PE	Core	3	0.310	N/A

*Data provided by the materials provider (Matrix Polymers, UK).

Table 3.6 Shot weights (polymer powder quantity) used in making rotationally moulded sandwich composites.

Sandwich Type	Thickness Combination (Skin + Core + Skin) (mm)	Shot weights (g) (Skin + Core +Skin)
Sandwich-1	1+4+1	450+300+400
Sandwich-2	1+8+1	450+600+400
Sandwich-3	2+4+2	850+300+800
Sandwich-4	2+8+2	850+600+800

3.7 Low velocity impact test of rotational moulded three layered skin-foam sandwich composite

Low velocity Impact test were carried out with an instrumented falling weight impact testing machine according to ASTM-D 3763 – 02 (Astm-D3763-02)standards. Impact sandwich composite samples were machined from moulded sandwich composites sheets into 110×110 mm squares and placed on the sample holder with a circular window cut-out of 90 mm diameter in the centre of the holder. The impactor which was used to strike the clamped specimens is a hemispherical indenter with a 12 mm diameter and attaches to maximum loading capacity of 22.4 kN piezoelectric impact force sensor. The total falling mass of the impactor is 9.1 kg (included impactor and crosshead mass). A high resolution oscilloscope (Picoscope IEPE 4242) was used to acquire the data generated in the impact event. The impact force, time and displacement were obtained for each of the sample from

the force-time and force-displacement (as like as Figure 3.8) curves were found for each of the test. Absorbed energy was calculated from the area under force-displacement curve. Five impact test energy levels 20, 30, 40, 50 and 70 J were used in this test for all of the samples. For finding out the penetration energy level 80 and 100 J were also used for sandwich-3 and sandwich-4 samples. After low velocity impact tests, impact damages were investigated at the front and rear surface and cross-section of the impacted samples with digital optical microscope.

Table 3.7 Low velocity impact test of rotationally moulded skin-foam-skin sandwich samples.

Sandwich Type (Skin+core+skin) mm	Energy Level (J)	Sample Dimensions mm	Diameter of indentor	Mass of falling dart	No. Samples tested at each energy level
Sandwich-1 (1+4+1)	20, 30, 40, 50 & 70	110×110	12 mm	9.1 kg	3
Sandwich-2 (1+8+1)	20, 30, 40, 50 & 70	110×110	12 mm	9.1 kg	3
Sandwich-3 (2+4+2)	20, 30, 40, 50, 70 & 80	110×110	12 mm	9.1 kg	3
Sandwich-4 (2+8+2)	20, 30, 40, 50 70, 80 & 100	110×110	12 mm	9.1 kg	3

3.8   Low velocity repeated impact test

From the result analysis of low velocity impacted sandwich samples, sandwich-3 type sample was selected for the low velocity repeated impact analysis. In this analysis, numbers of impact events were counted until the penetration of the sample occurred. Sandwich-3 type sample got penetration at 80 J and also got prominent scratches at 70 J in the lower skin. As a result of these observations, it was decided to choose the energy range for this experiment from 20 J to 70 J. The impact energies were chosen at 20 J, 30 J, 40 J and 50 J. The samples were subjected to single impact event repeatedly up-to penetration at each energy level.

Table 3.8 Low velocity repeated impact test of rotationally moulded sandwich-3 samples.

Sandwich Type	Energy Level (J)	Sample Dimensions mm	Diameter of indentor	Mass of falling dart	No. Samples tested at each energy level
Sandwich-3 (2+4+2) mm	20, 30, 40 & 50	110×110	12 mm	9.1 kg	3

For the repeated impact test, the same impact testing machine was used. Samples of 110×110 mm squares dimension were cut from the Sandwich-3 type sandwich structures. Samples were clamped and repeatedly impacted with a 12 mm diameter hemispherical indenter. The hemispherical indenter was attached to a 22.4 kN piezoelectric maximum loading capacity impact force sensor. The total falling mass of the impactor was 9.1 kg (included impactor and crosshead mass). A high resolution oscilloscope (Picoscope IEPE 4242) was used to acquire the data generated in the impact event. The impact force, time and displacement were obtained for each of the repeated impact event. Great care was taken during the test so that the every repeated impact event occurred at same point of the samples.

Chapter 4. Analysis of microstructure of rotationally moulded plastics

Microstructural characterisations were carried out to investigate the crystal structure, crystal and amorphous region thickness, melting behaviour, melting point, degree of crystallinity, side chain quantity, storage and loss modulus of the plastics tested in this work with wide and small angle X-ray Scattering , DSC , solid-state NMR and dynamic mechanical thermal analysis. Here the results of the microstructural analysis are presented for the rotationally moulded PP and PE plastics.

4.1   Microstructural Characterisation of PE

4.1.1   WAXS, SAXS, DSC, Solid-state NMR Analysis of PE

Figure 4.1 shows similar groups of peaks in the 20-30 [°2θ] scattering angle regions of the WAXS curve for both of the PE materials. These peaks represent the (110) and (200) crystal planes that confirm the orthorhombic crystal in PE-1 and PE-2 as well (Heeley, E. L. et al., 2014; Pereira, R. et al., 1998). The crystallinity is calculated and listed in Table 3.2 of Chapter 3.
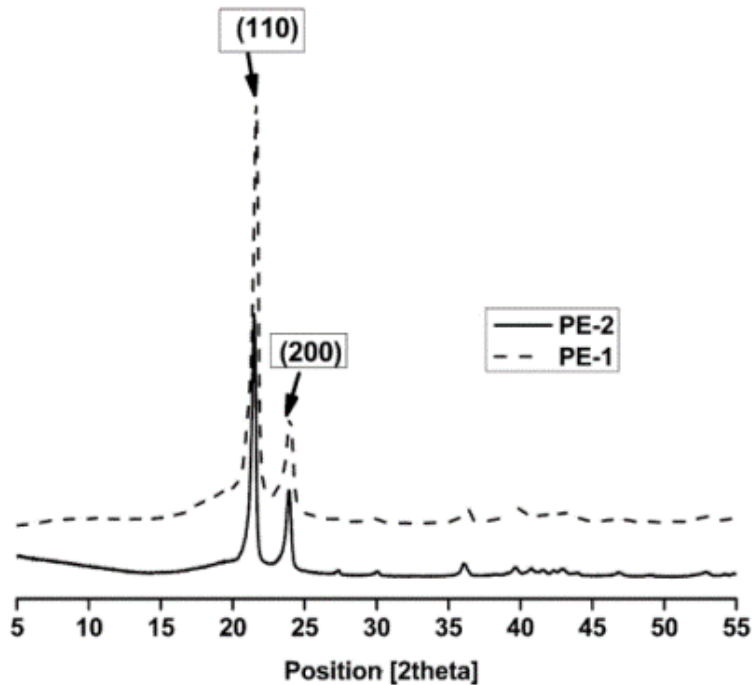

Figure 4.1 Crystal structures of PE-1 and PE-2 from WAXS analysis.

Long period (D), crystal and amorphous thickness (L_C and L_a) of PE materials are measured from the q values shown in Figure 4.2 and shown in Table 4.1. PE-2 is shown to have a higher long period than PE-1. Moreover, higher crystal and amorphous region thickness are also found for PE-2. This matches the higher crystal thickness also found for PE-2 in the DSC analysis due to the increased melting temperature.

The melting point and crystallinity are measured for PE-1 and PE-2 from the DSC curves (Figure 4.3), as per Table 3.2. Only one peak is found in their DSC curves, representing the same type of crystal – orthorhombic phase that is also found in the WAXS analysis.
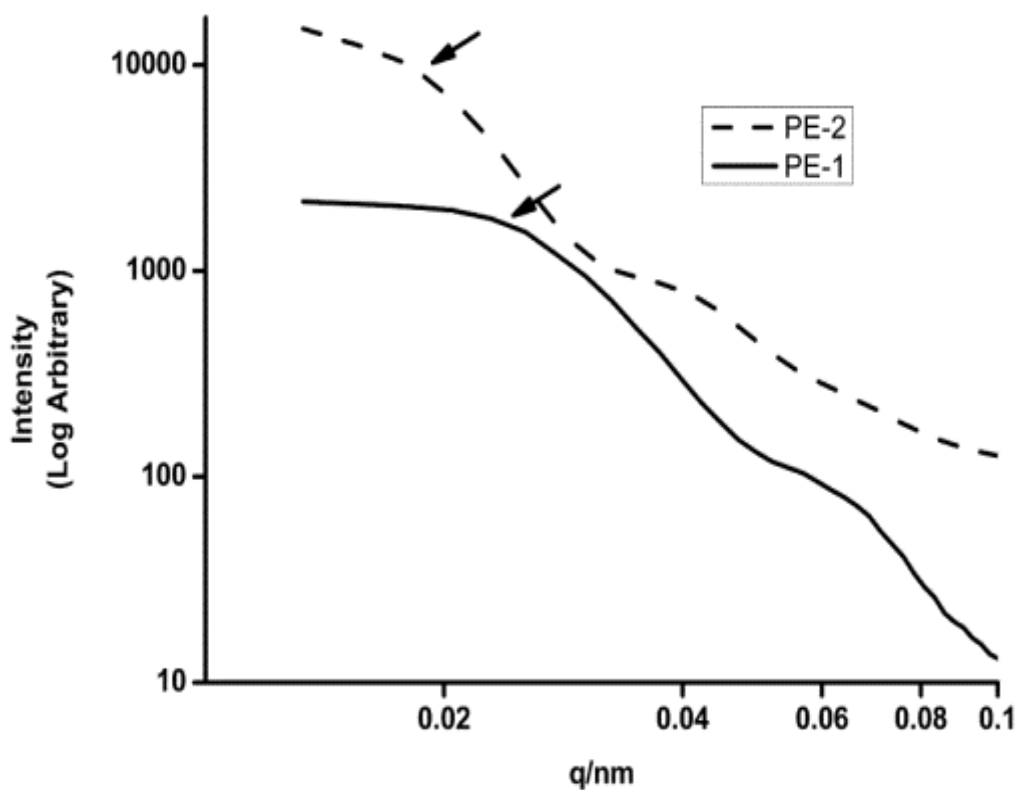

Figure 4.2 1-DSAXS curves of PE-1 and PE-2.

Table 4.1Quantitative SAXS information for microstructure of PE and PP.

Materials	Long period (crystal + amorphous region) (A$^\circ$)	Crystal thickness (A$^\circ$)	Amorphous thickness (A$^\circ$)
PE-1	191.88	113.20	78.67
PE-2	309.27	167.00	142.26
PP-1	181.30	108.05	73.24
PP-2	142.10	54.50	87.60

Crystallinity measured for both PE-1 and PE-2 in DSC analysis shows lower value than that of in WAXS analysis. Lower crystallinity in DSC analysis compared to WAXS analysis was also observed by Isasi et al.(Isasi, J. R. et al., 1999). They concluded that in the DSC analysis only core crystallinity is measured while both the core crystallinity and interfacial region are measured in WAXS analysis. Because of this WAXS analysis always shows higher crystallinity than that of DSC analysis. PE-2 shows very close crystallinity to PE-1, less by only one percent in DSC analysis whereas PE-2 shows five percent less crystallinity compared to PE-1 in WAXS analysis. The observed lower crystallinity of PE-2 might be due to the some rotational moulding processing (heating/cooling) irregularities that is needed to be investigated in future. PE-2 is found to be shown the higher melting point at 137°C due to the higher long period and crystal thickness measured in SAXS analysis and density compared to PE-1.
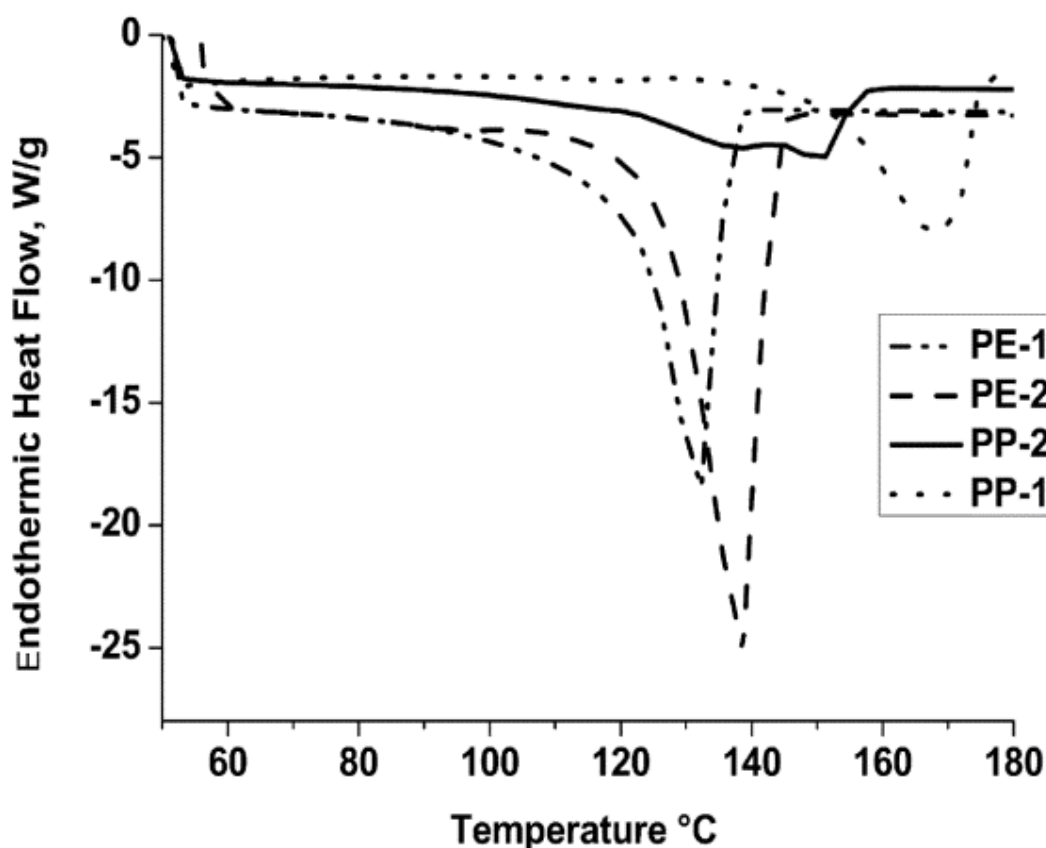
Figure 4.3 DSC curves of melting behaviour for PE and PP.

In Figure 4.4 intense sharp peaks at PPM 32.9 and 31 are clearly seen in solid-state carbon-13 NMR single pulse excitation (SPE) spectra for the orthorhombic crystalline phase and amorphous region respectively (Gao, X. et al., 2010; Pollard, M. et al., 2004; Wang, M. et al., 2007) for the both PE materials. In addition, a second peak was also observed at PPM 14.9 for PE-1 and PE-2. This corresponds to hexyl side branches present in the microstructure (Gao, X. et al., 2010; Pollard, M. et al., 2004). In PE, co-polymerisation is used to improve the density and ultimate material properties. Co-monomer 1-octene introduces hexyl side branches in the PE main chain and this explains the additional peak seen in the NMR analysis. Therefore, it can be said that the rotational grade PE-1 and PE-2 materials tested are ethylene-1-octene copolymers. De-convolution of the SPE spectra provides the quantitative information on side chain branching in PE. The quantity of side branches is listed in Table 3.2. In general, higher branching acts to decrease the density of

PE, this matches our observations here as PE-2 shows the highest density and the lowest number of side branches (8 C/1000C).
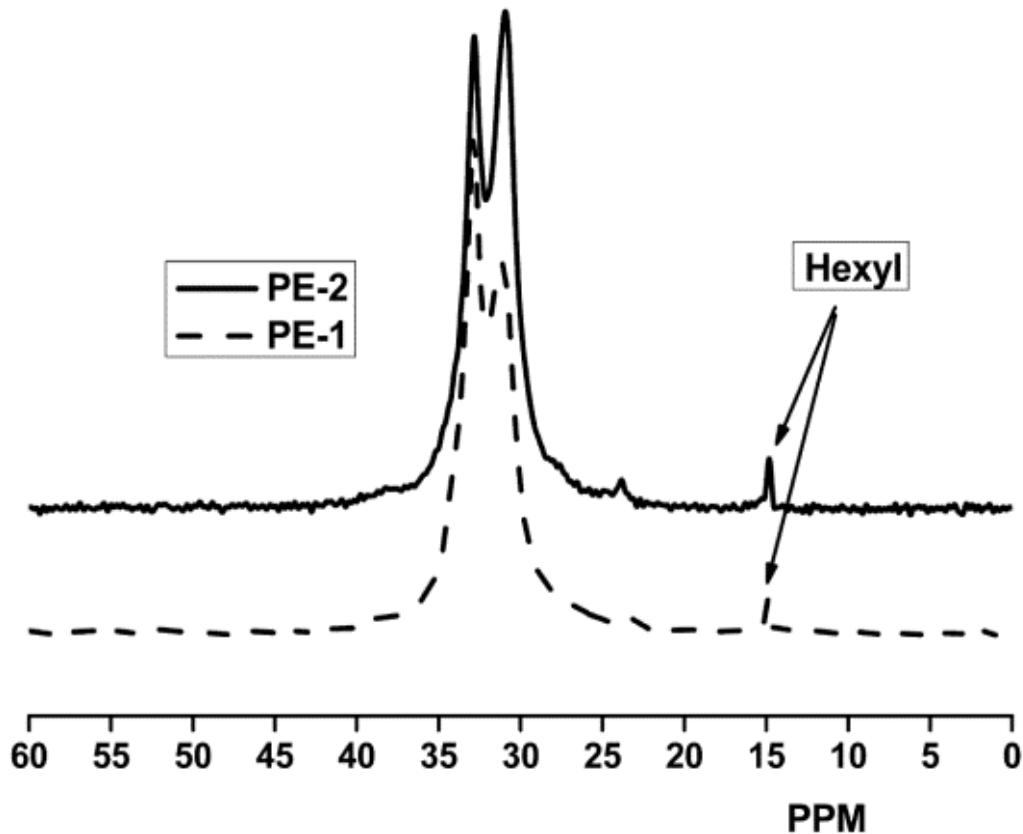

Figure 4.4 Solid State SPE spectra of PE-1 and PE-2

4.1.2   Dynamic mechanical thermal analysis (DMTA) of PE

The storage modulus of PE-1 and PE-2 is presented in Figure **4**.**5**. PE-2 shows the higher storage modulus compared to PE-1. Storage modulus was reported as similar as to the Young or elastic modulus or stiffness and found to be increased primarily with density (Khanna, Y. P. et al., 1985). PE-2 has higher density and crystal thickness and shows better storage modulus. For both of the PE samples, storage modulus deceases with the temperature. This could be due to the enhanced molecular mobility at higher temperatures.

73

In Figure **4.6** the loss modulus of dynamic mechanical analysis of PE-1 and PE-2 is presented. Loss or viscous modulus provides the information of energy absorption during
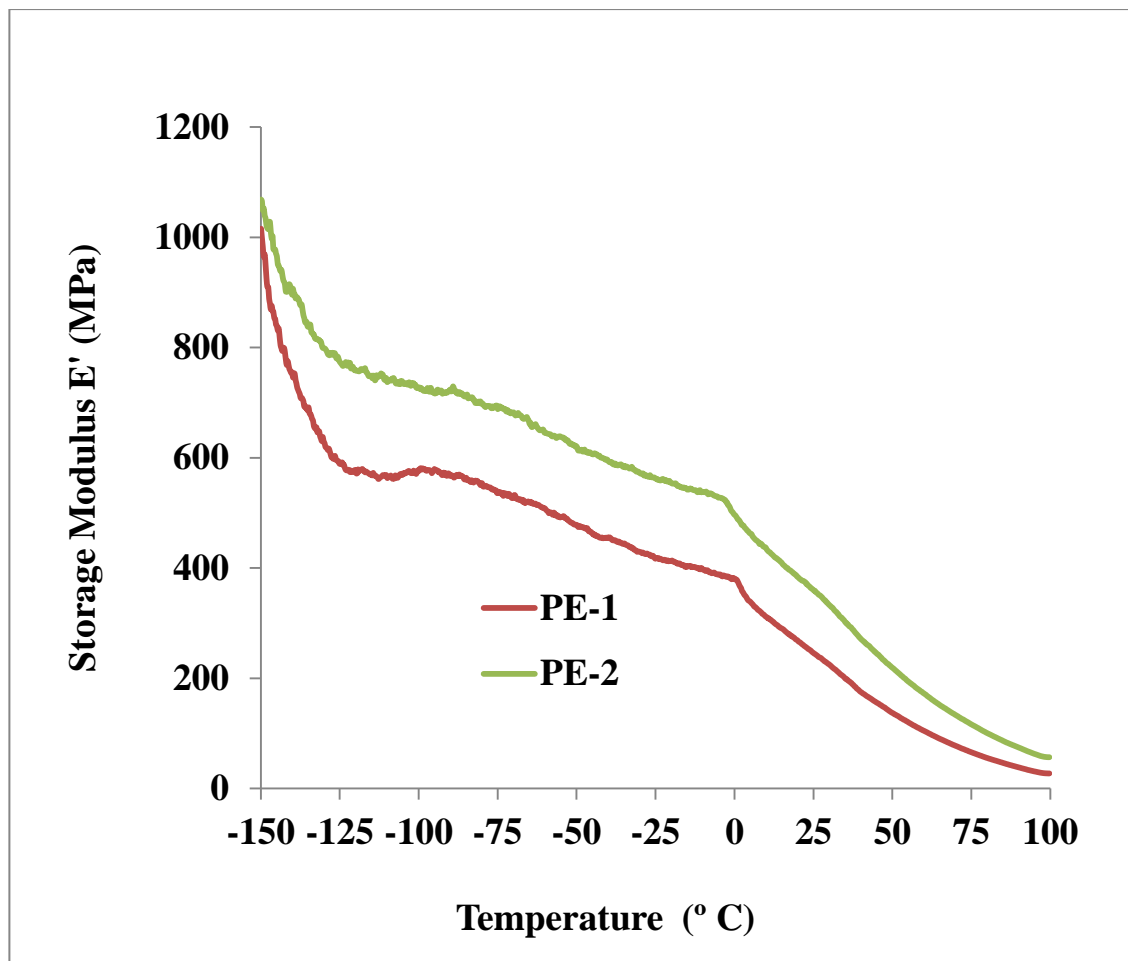

Figure 4.5 Storage modulus of PE-1 and PE-2.

the relaxation of a polymer and mechanism of chain motion. Three different peaks are clearly seen at three different temperatures for both of the PE samples. PE-2 shows α peak at a higher temperature compared to PE-1 with higher intensity. It is generally agreed that the α peak is representative of the crystalline phase and originates from some type of motion in the crystals (Stehling, F. C. and Mandelkern, L., 1970). The high intensity of the α-relaxation peak increases with crystallinity or crystal thickness (Sirotkin, R. and Brooks, N., 2001) which also supports its high density compared to PE-1. PE-1 and PE-2 show the

β relaxation peaks at -48 ℃ and -41 ℃ respectively. It was found that the β relaxation peak is due to the glass transition of PE (Khanna, Y. P. et al., 1985). Molecular motions in more crystalline structure are restricted and needs higher temperature for the relaxations (Pick, L. T. and Harkin-Jones, E., 2003) that is also observed here in PE-2 for the β and α peaks. PE-1 has lower density and shows the β relaxation peaks at lower temperature compared to PE-2. PE-2 shows third peak, the γ transition peak at -125 ℃ while PE-1 shows it at lower than -125 ℃. The γ transition peak involves the movement and relaxation of amorphous region of PE.
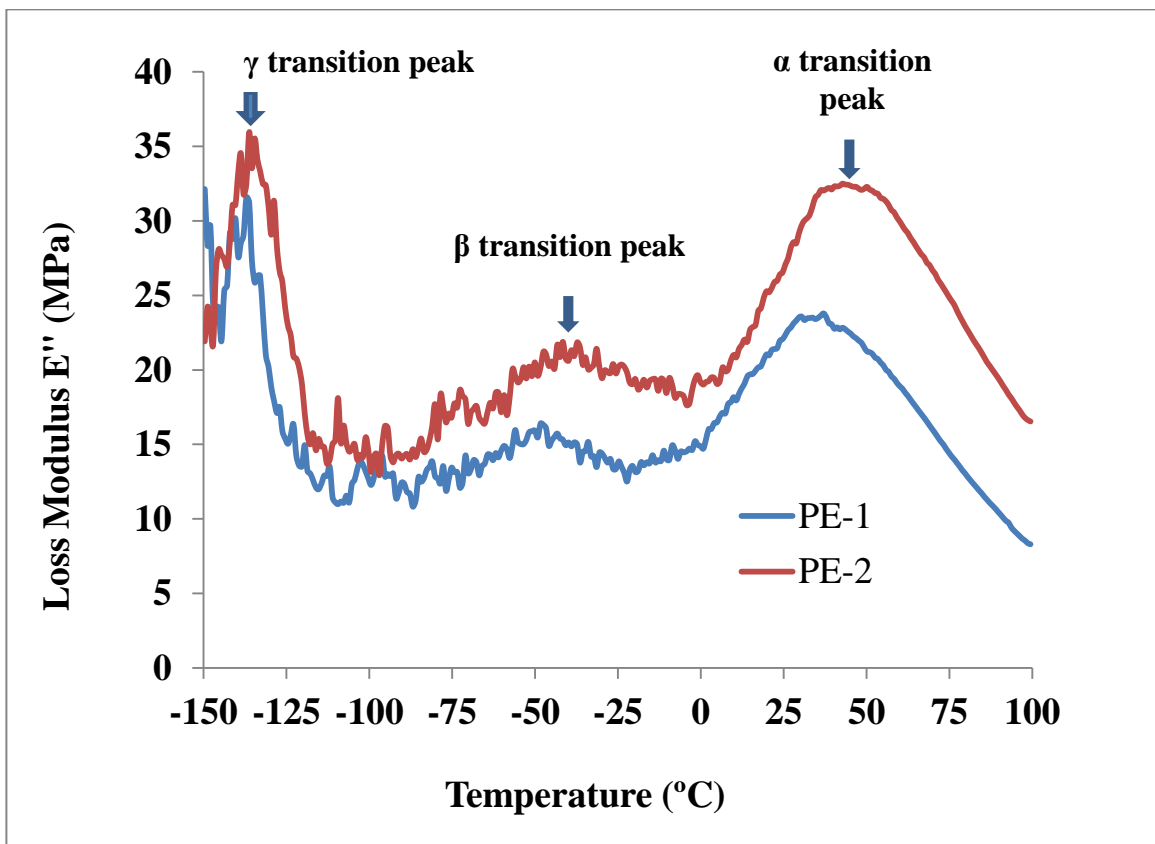

Figure 4.6 Loss modulus of PE-1 and PE-2.

The damping or dissipation factor tanδ is the ratio of loss modulus to storage modulus. tanδ curves of PE-1 and PE-2 are presented in Figure **4.7**. Generally tanδ decreases as the density increases. It is also observed for PE-2 here. PE-2 has higher storage and loss

modulus compared to PE-1 and for PE-2 in the tanδ curve , storage modulus is dominant. Therefore it shows less dissipation in the tanδ curve specially from 0 ºC to 100 ºC.
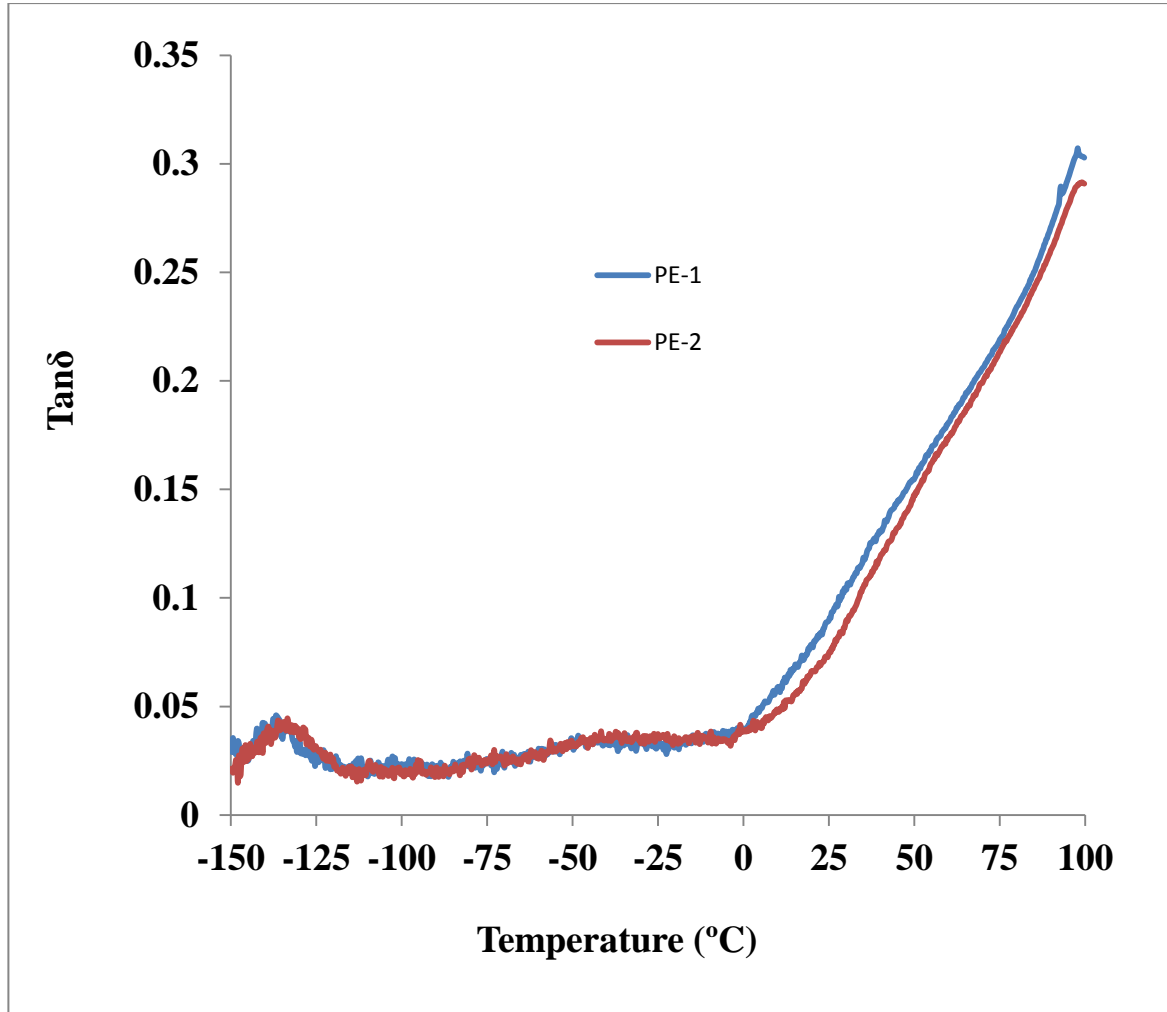

Figure 4.7 Damping factor tanδ of PE-1 and PE-2.

4.2   Microstructural Characterisation of PP

4.2.1   WAXS, SAXS, DSC and Solid-state NMR Analysis of PP

WAXS curves of PP-1 and PP-2 samples show the peaks with some differences in peak intensity and peak position (Figure 4.8). Three main peaks at 2θ scattering angles of

(13.92), (16.74) and (18.42) are observed in PP-1, these represent diffraction from the crystallographic planes of 110, 040 and 030 respectively for the α crystal form of PP (Lezak, E. et al., 2006a; Nedkov, E. and Dobreva, T., 2004; Shao, Y. et al., 2015; Weidinger, A. and Hermans, P., 1961). In PP-2, the intensity of these three peaks is seen to be reduced particularly for the (030) plane peak at 18.42 [°2θ] scattering angle. A Peak at 20 [°2θ] scattering angle was observed for PP-2 for the (117) crystal plane that corresponds to the γ polymorph in the PP (Cerrada, M. L. et al., 2010). The γ form was found for low molecular weight isotactic PP and random copolymers of propylene and α-olefins (Pérez, E. et al., 1999). The crystallinity is calculated and listed in Table 3.2. The crystallinity ratio is found to be lower for PP-2. Figure 4.9 represents the one- dimensional SAXS results for both types of PP tested. PP-2 is seen to have a lower crystal and higher amorphous thickness than that of PP-1(Table 4.1).
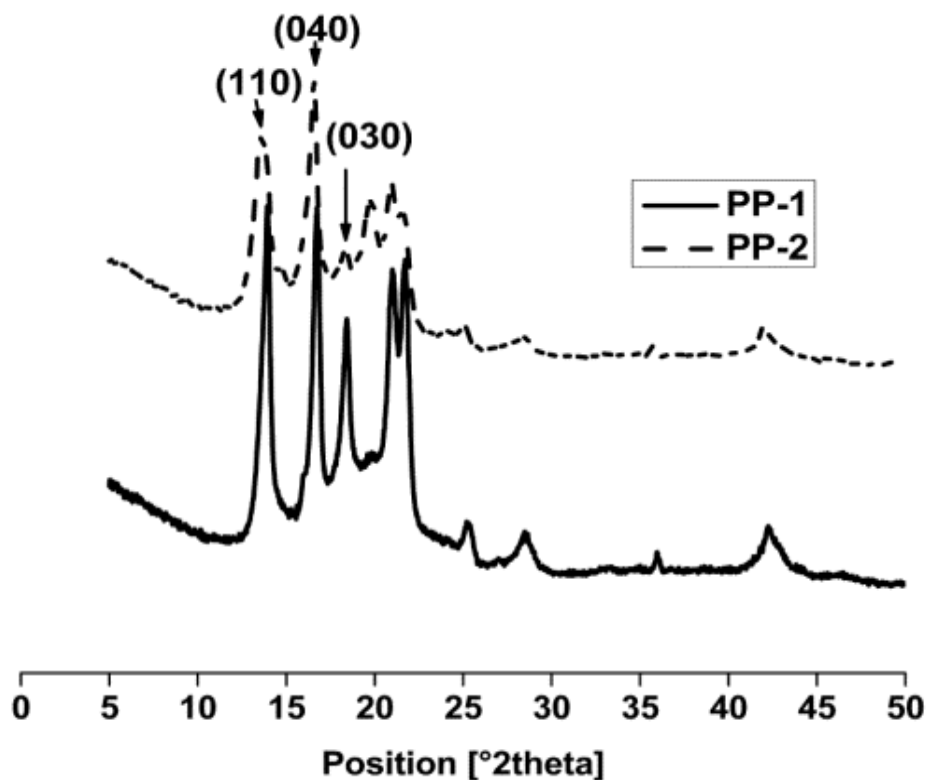

Figure 4.8 Crystal structure of PP-1 and PP-2.
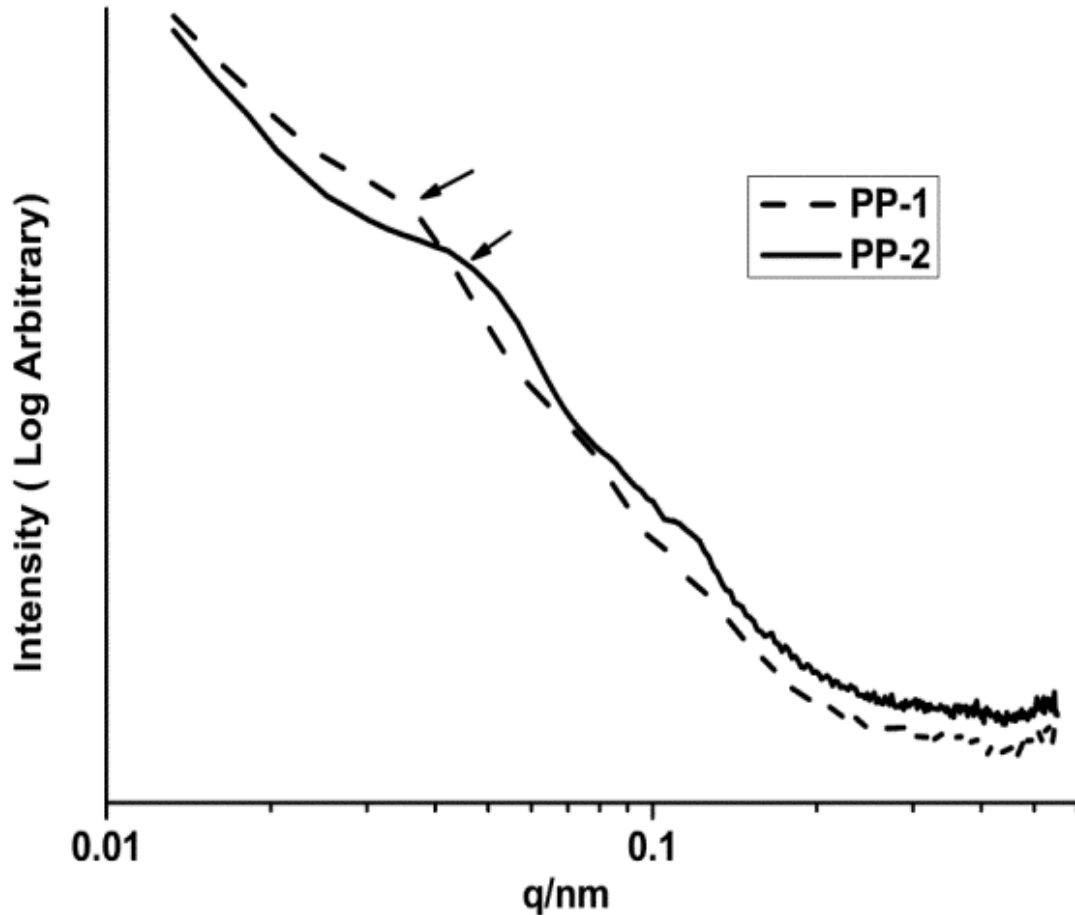
Figure 4.9 SAXS 1-D curves of PP-1 and PP-2 materials

The DSC (Figure 4.3) curves for PP-1 shows the thermal behaviour only for the α-crystal phase. A doubling or shoulder melting peak was observed for the α and γ-crystal phase in the DSC graphs for PP-2 (Cerrada, M. L. et al., 2010) which also supports the WAXS profiles. Crystallinity is also measured in DSC analysis. It is found that both PP-1 and PP-2 show lower crystallinity in DSC analysis compared to WAXS analysis, mentioned in Table- 3.2 of Chapter-3. Because in DSC analysis only core crystallinity is measured whereas in WAXS analysis both core crystallinity and interfacial region are measured (Isasi, J. R. et al., 1999). The melting temperature of PP-2 is found to be lower than that of

PP-1, this could be due to the lower crystallinity observed in DSC and WAXS analysis in this study (Chen, H. et al., 2002; Varga, J., 2002).
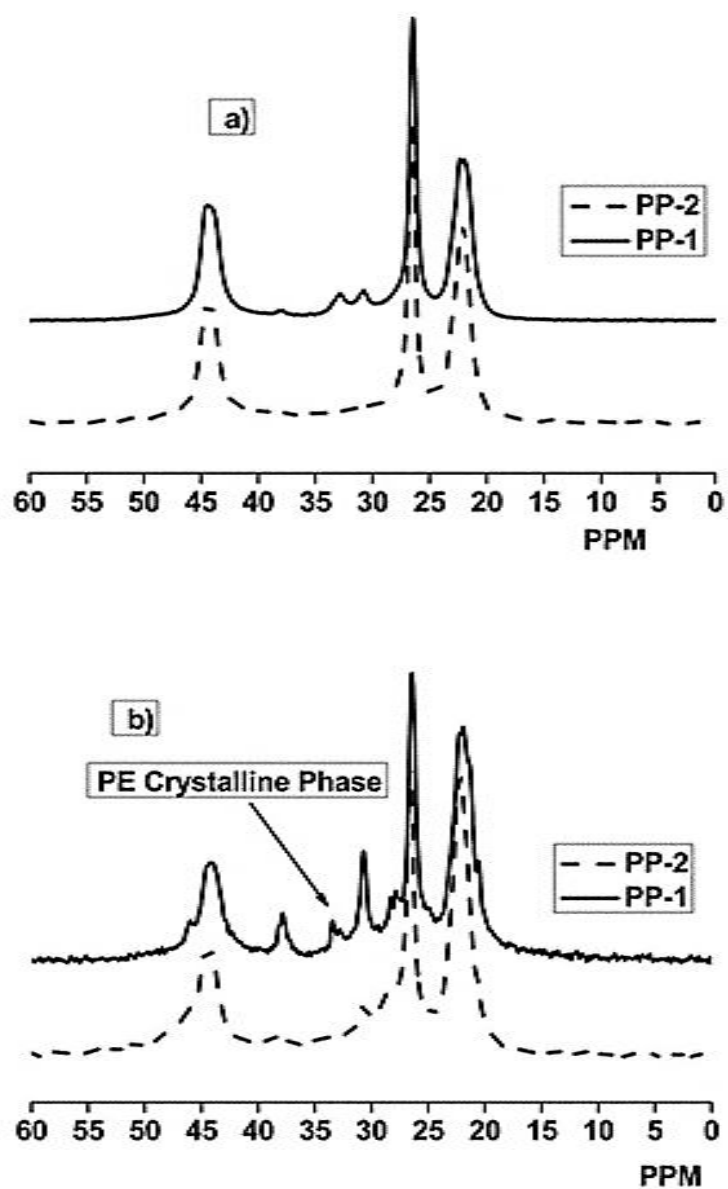

Figure 4.10 (a) 13C CP and (b) SPE MAS NMR spectrum of the PP-1 and PP-2 samples performed at room temperature. A recycle delay of 60 s was applied for SPE spectra.

From the CP/MAS (cross polarisation/magic angle spinning) spectra (Figure 4.10-a), signals at 44 and 22 PPM in the methylene (-CH$_2$-) and methyl region are observed, confirming that these PP materials are isotactic PP (Comotti, A. et al., 2001). The methane (-CH-) carbon shows a peak at 26.5 PPM for both PP materials, this represents the crystalline phase. Other signals are also found at 31 and 33 PPM for PP-1which are not observed for PP-2 in CP/MAS spectra. Peaks at 31 and 33 PPM represent the amorphous and crystalline PE phase in the PP matrix respectively (Botha, L. et al., 2014).SPE (Figure 4.10-b) is used to provide quantitative information for all regions. For PP-1, peaks at 31 and 33 PPM are identified whereas the peak at 33 PPM is not observed for PP-2. Prasad et al. (Prasad, J., 1992) identified a signal at 33 PPM for the block copolymers of propylene with ethylene which was not observed for random propylene-ethylene copolymers. Botha et al. (Botha, L. et al., 2014) also observed a peak at 33 PPM for block propylene ethylene copolymers. In the SPE spectra a signal at 38 PPM is also observed for both PP-1 and PP-2, this is reported as the best resonance for the quantification of the ethylene phase or defects in the propylene- ethylene copolymers (Alamo, R. G. et al., 2005; Botha, L. et al., 2014).The ethylene content is quantified from the de-convolution of the SPE spectra as per Table 3.2. From these results, it can be said that PP-1 and PP- 2 are propylene-ethylene block and random copolymers with 13.4 % and 7.3 % PE content respectively.

4.2.2 Dynamic mechanical thermal analysis (DMTA) of PP

In the storage modulus curve (Figure **4.11**), PP-2 shows higher storage modulus in lower temperature and with the increase of temperature it shows lower storage modulus compared to PP-1 particularly after 0 ℃. Lower storage modulus in the higher temperature is expected for PP-2 samples, since it has lower crystal thickness compared to PP-1. In the loss modulus graph (Figure **4.12**) PP-2 shows the α peak at lower temperature and at lower modulus which indicates the lower thickness of the crystal of PP-2 compared to PP-1. The major transitions, the β peaks are observed at 6℃ and -23 ℃ for PP-1 and PP-2 respectively. The intensity of the β peak for PP-2 is much higher than PE-1. In the tanδ curves (Figure **4.13**), different peaks are obvious for PP-1 and PP-2 samples. PP-2 samples

shows the higher dissipation energy or damping factor compared to PP-1 due to the higher loss modulus.
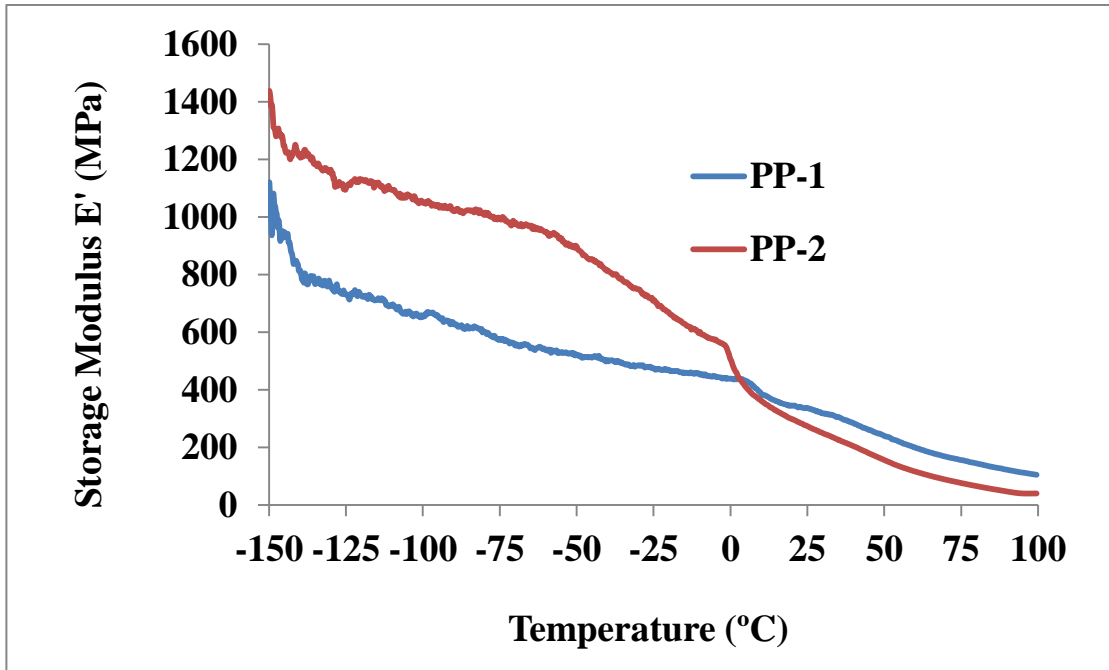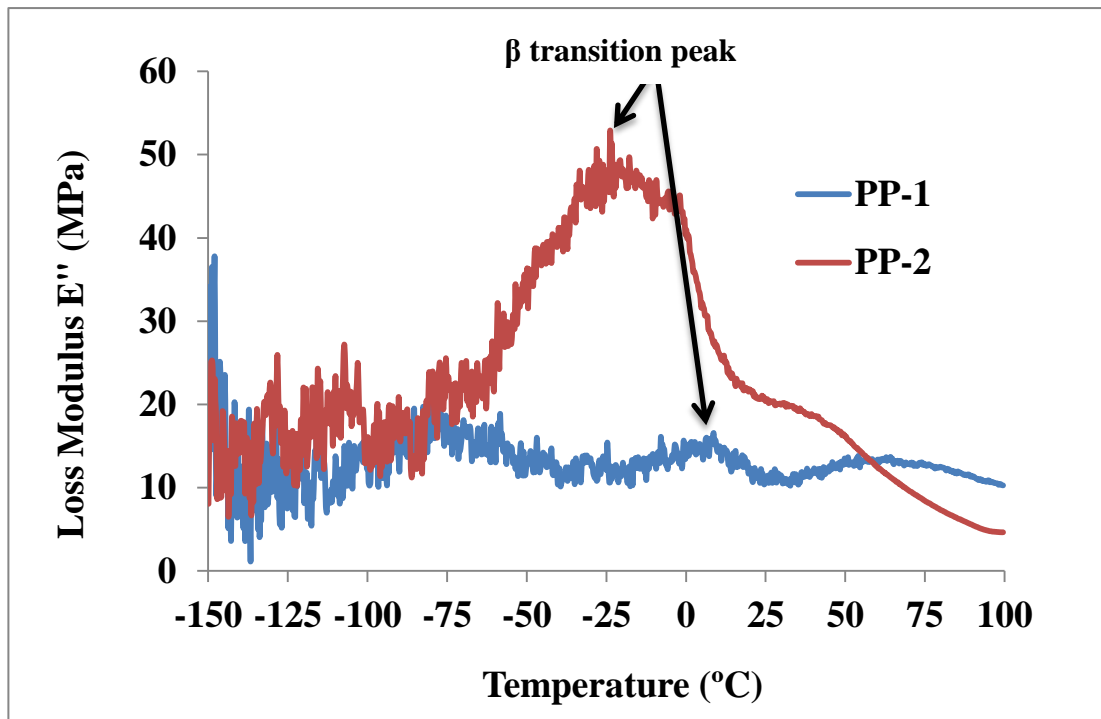

Figure 4.11 Storage modulus of PP-1 and PP-2.

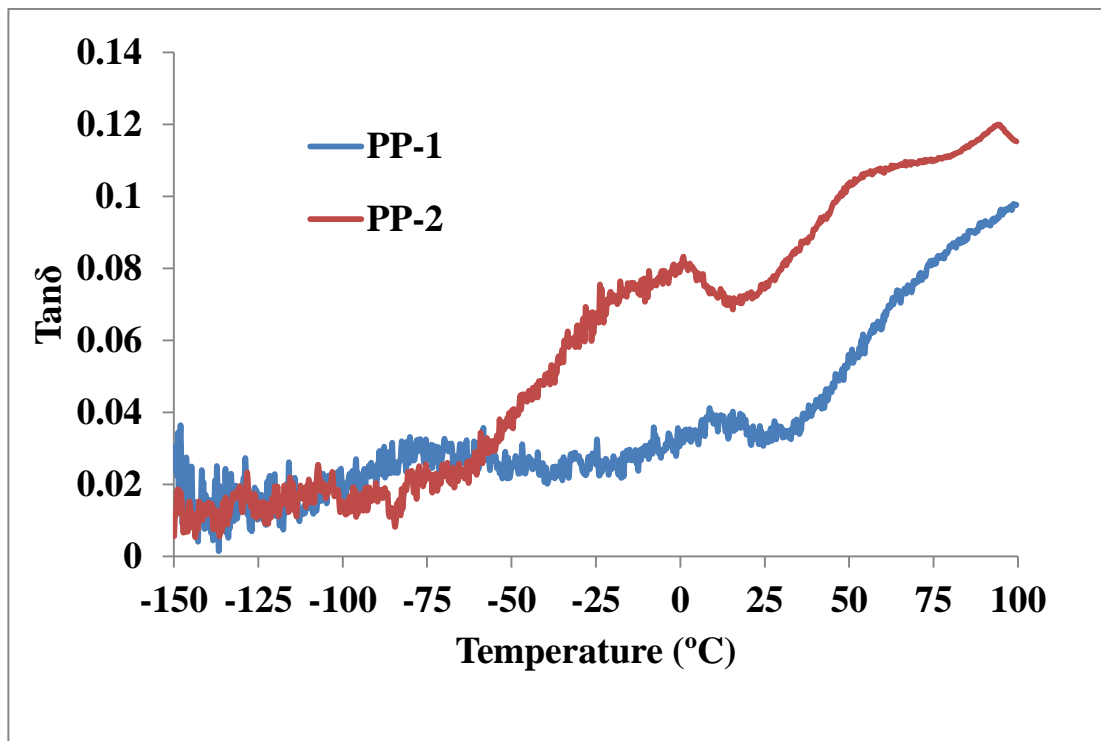Figure 4.12 Loss modulus of PP-1 and PP-2.

Figure 4.13 Damping factor tanδ curves of PP-1 and PP-2.

4.3 Discussion

In this work, orthorhombic crystal structure is found for both of the PE plastics. Higher melting point is observed for PE-2 because of its higher density. SAXS analysis provides information of thicker amorphous and crystal region thickness for PE-2 compared to PE-1. Higher melting point of PE-2 also supports its higher crystal region thickness. Lower crystallinity of PE-2 is observed both in DSC and WAXS analysis. From crystal structure analysis in WAXS and side chain analysis in solid-state NMR it is confirmed that the rotational mould grade PE-1 and PE-2 materials tested are ethylene-1-octene copolymers. Higher storage modulus curve for PE-2 in DMTA analysis is noticed because of the higher density and crystal thickness of PE-2. PE-2 also exhibits higher loss modulus and the β relaxation peak compared to PE-1. Generally higher density reduces the β relaxation peak height because of the higher crystal thickness which is not found for PE-2 samples. Therefore it can be said that larger amorphous thickness are responsible for the higher loss modulus curves and the β relaxation peak of PE-2 both in ambient and sub-ambient temperatures.

From the WAXS analysis, it is found that in the crystalline region PP-1 has α crystal structure whereas PP-2 contains both α and γ polymorph in its crystal structure. DSC analysis also supports this observation. In DSC curves, PP-2 shows doubling melting peak for the α and γ polymorph whereas PP-1 contains only one peak for the α crystal structure. Solid state NMR analysis confirms PP-1 and PP-2 as propylene-ethylene block and random copolymers respectively. SAXS analysis reveals larger amorphous and lower crystal region thickness which also supports the lower crystallinity of PP-2 compared to PP-1. In DMTA analysis, higher loss modulus, the β relaxation peak, dissipation energy and storage modulus at higher temperature are also observed due to the larger amorphous thickness and lower crystallinity of PP-2 than that of PP-1.

4.4 Conclusion from microstructural analysis of the plastics

The conclusions from this work are as follows-

- PE-1 and PE-2 are identified as ethylene-1-octene copolymers from NMR analysis in this work. WAXS and DSC analysis confirms orthorhombic crystal structure for both of the PE plastics. Larger amorphous and crystal thicknesses are found for PE-2 in SAXS analysis which are behind for its higher β relaxation peak and storage modulus than PE-1 respectively.

- PP-1 and PP-2 are confirmed as propylene-ethylene block and random copolymers respectively. PP-2 contains both of the α and γ crystal structure. Larger amorphous thickness and lower crystallinity of PP-2 contributes to the observed higher loss modulus, the β relaxation peak in dynamic mechanical analysis.

Chapter 5. Fracture toughness and impact properties analysis of rotationally moulded plastics

Fracture toughness of rotationally moulded PE and PP was measured for the first time and presented in this chapter. As detailed in the literature review section 2.3.2, all of the current research in the literature relating to fracture toughness measurement and behaviour analysis was done for injection or other moulded PP and PE but notably not for rotationally moulded samples. By developing a better understanding of rotationally moulded PE and PP it is hoped that the potential applications for this manufacturing method can be expanded. Two different commercially available rotational moulding grades of materials for each category (PE and PP, see the Table 3.1) were investigated using the elastic plastic fracture mechanics J integral method at static loading conditions (1mm/min) at room temperature.

At the end of this chapter, impact properties of rotationally moulded PE and PP samples were also investigated at a range of temperature from -40 to 30 ºC. Peak impact strength, crack initiation and crack propagation energies were calculated for all of the samples from the impact properties to get the understanding of the fracture behaviour at different temperature under impact loading condition. Microstructural details described in Chapter 4 were used to analyse the fracture toughness and impact properties of the materials tested here.

5.1   Fracture Toughness Analysis

Fracture toughness was measured for rotationally moulded PP and PE using elastic-plastic fracture mechanics J-integral method under static loading condition at room temperature. Fracture surfaces were examined with a digital microscope and also scanning electron microscope.
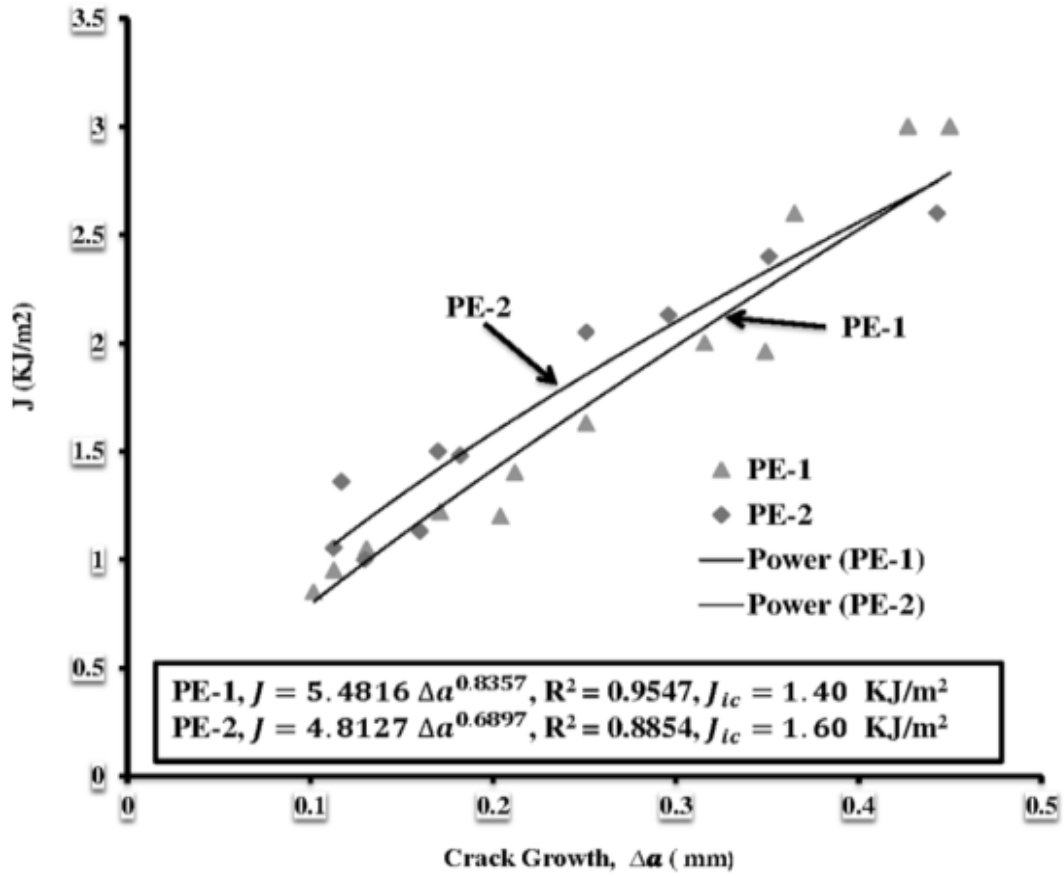
Figure 5.1 J-R curve of PE-1 and PE-2.

5.1.1   Fracture Toughness and Fractography of PE

Fracture toughness ($J_{0.2}$) values are calculated from the J-R curves for PE-1, PE-2 (see Figure **5.1**) and shown below in Figure **5.2**. The J-R curve is found to follow the power law relation $J = A\,(\Delta a)^N$, N≤1 and confirms the plane strain state fracture condition according to equation no. 2.7. PE-2 is seen to have higher fracture toughness values than that of PE-1, though they are close to each other.
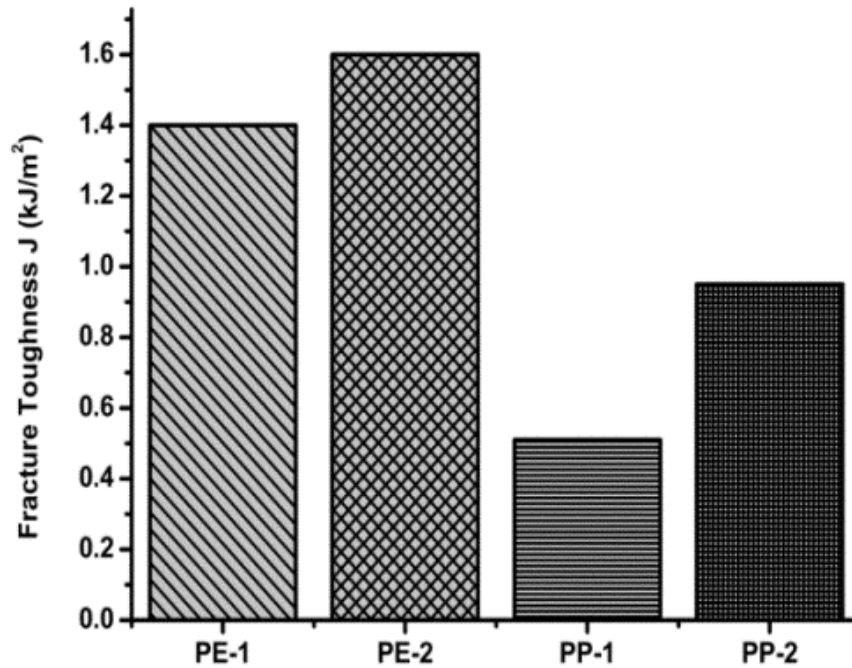
Figure 5.2 Fracture Toughness values of PP and PE samples at $J_{0.2}$ in J-R curve.

Figure 5.3 shows the low magnification images (a, b) and the scanning electron microscope images (c, d) of the fracture surfaces of PE-1 and PE-2 and confirms the differences in fracture toughness values between PE-1 and PE-2. Three distinct zones are clearly identified on the surfaces (Figure 5.3- a, b), the stress whitened slow stable crack growth zone (Z-1), the diffuse and smooth stress whitened zone for plastic deformation (Z-2) and the brittle fracture zone (Z-3). Higher magnification SEM images (Figure 5.3 - c, d) of Z-1 for all the PE's tested reveal microfibrillar morphology during loading which is seen to be more extensive for PE-2. In PE, voids are observed to form next to the notch region under load. These voids create crazes as they coalesce leading to fibril formation and subsequent rapid crack propagation (Li, Z.-M. et al., 2005; Swei, H. et al., 1991). This more extensive microfibrillar morphology leads to more plastic deformation and higher fracture toughness in PE-2 over PE-1 tested here. This is because more energy is needed to break these fibrils in order to start the rapid crack propagation. In Z-3, stick-slip lines were seen under the optical microscope for both of the PE materials tested, these are characterised by
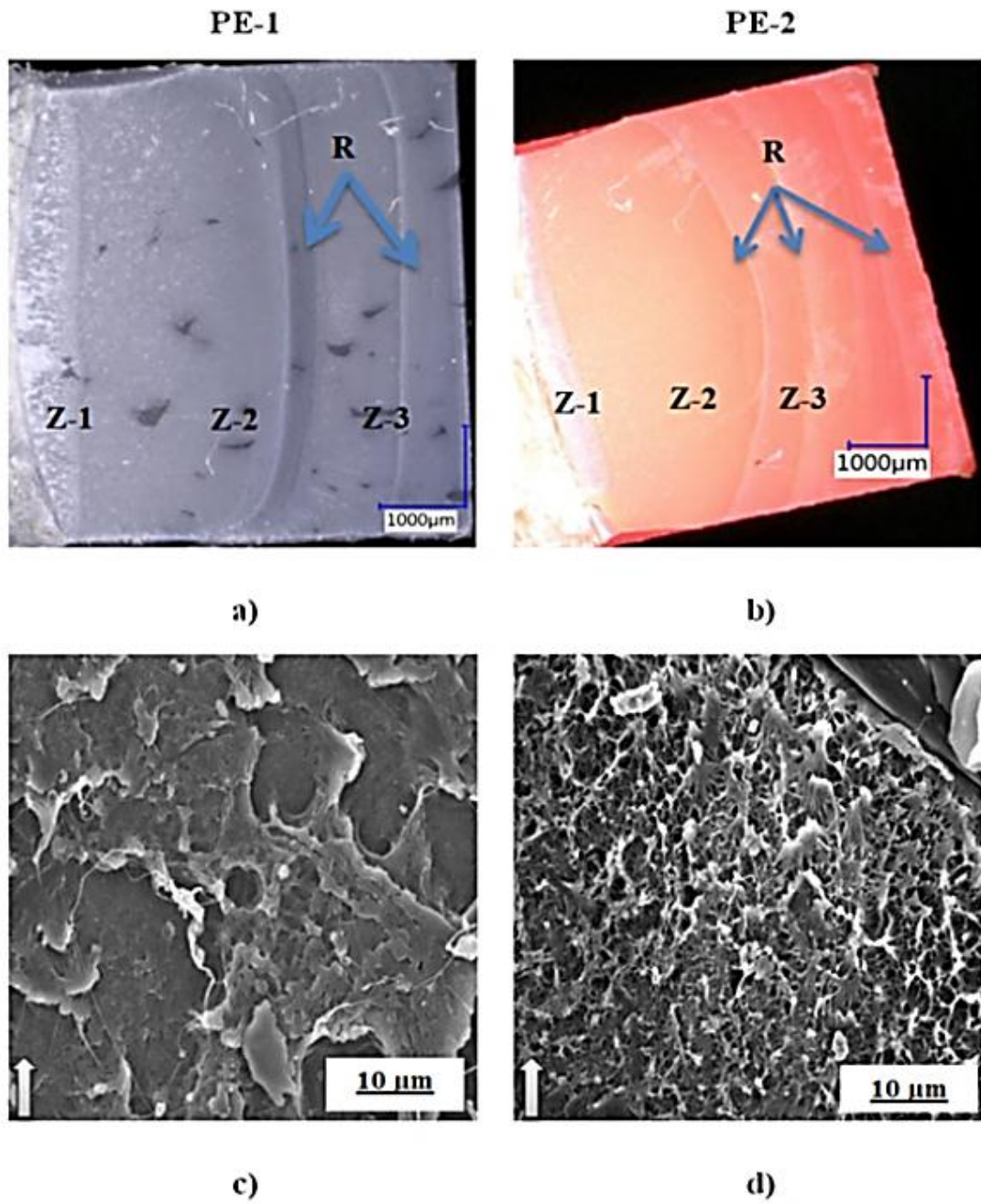
Figure 5.3 Fracture surfaces under optical microscope of (a) PE-1, (b) PE-2 and SEM images (c) PE-1 (d) PE-2 taken at Zone-1 (z-1).The arrow indicates the crack growth direction.

protuberant ridges (R). These ridges slow down the crack growth in the rapid crack growth region (Chan, M. and Williams, J., 1983; Li, Z.-M. et al., 2005). Three ridges are observed in PE-2, with two ridges seen for PE-1.

For PE, different fracture toughness values are found in the published research works for other moulding processes depending on their composition and toughness grade. Swei et al. (Swei, H. et al., 1991) tested different grades of PE at room temperature and reported 1.7 kJ/m2 and 8.2 kJ/m2 as J_{IC} values for HDPE and gas pipe grade tough PE co-polymer respectively. Microfibrillar tufts and dimple-like characteristics were identified in the slow crack growth region which is also found in this work. For conventional HDPE a 1 kJ/m2 J_{IC} value was reported (Chan, M. and Williams, J., 1981). Several extrusion moulded pipe grade HDPEs were found to have J_{IC} values in the range of 0.2 kJ/m^2 to 20 kJ/m^2 at room temperature depending on their strain rate in the testing process (Barry, D. and Delatycki, O., 1992). For high toughness grade compression moulded HDPE, and pressurised HDPE pipe using in gas or water distribution 28 kJ/m^2 and 31 kJ/m^2 fracture toughness values were measured at 23 °C respectively (Chan, M. and Williams, J., 1993; Salazar, A. et al., 2015).

In this work fracture toughness values for rotationally moulded PE are lower particularly compared to high toughness grade extruded or compression moulded PE, though there are differences between the PE materials as these are different blends with different additives. Also, differences in the various moulding processes, particularly in the heating/cooling cycles could be another reason for this observed difference in fracture toughness that needs to be confirmed by future investigation.
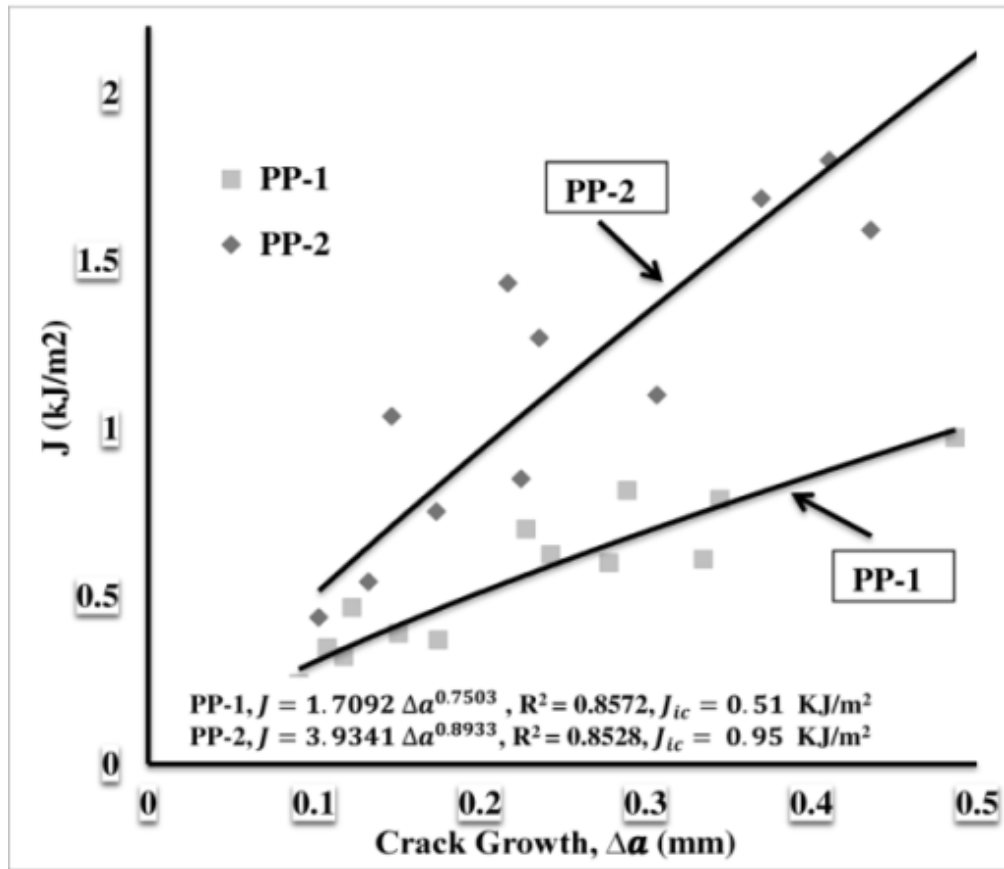
5.1.2   Fracture Toughness and Fractography of PP

Figure 5.4 J-R crack growth resistance curve for PP-1 and PP-2.

Figure 5.4 provides the J-crack growth resistance curve (J-R curve) of PP-1 and PP-2. This plot also includes the fit of the J-R curve to the power law $J = A\,(\Delta a)^{N}$, N≤1. Fracture toughness $J_{0.2}$ values of PP-1 and PP-2 are presented in Figure **5.2**. It was found that PP-2 has almost double the fracture toughness as the PP-1 material. These fracture toughness values followed the plane strain state, confirmed from equation 2.7. The fracture toughness values measured in this work for PP-1 and PP-2 are very low compared to those published in literature for other manufacturing methods such as injection moulding process. In injection moulding process 19 kJ/m^2 and 9 kJ/m^2 were reported for the PP random and

block co-polymers respectively as fracture toughness values (Salazar, A. et al., 2014). It must be noted that the materials tested in injection moulding process differ in composition
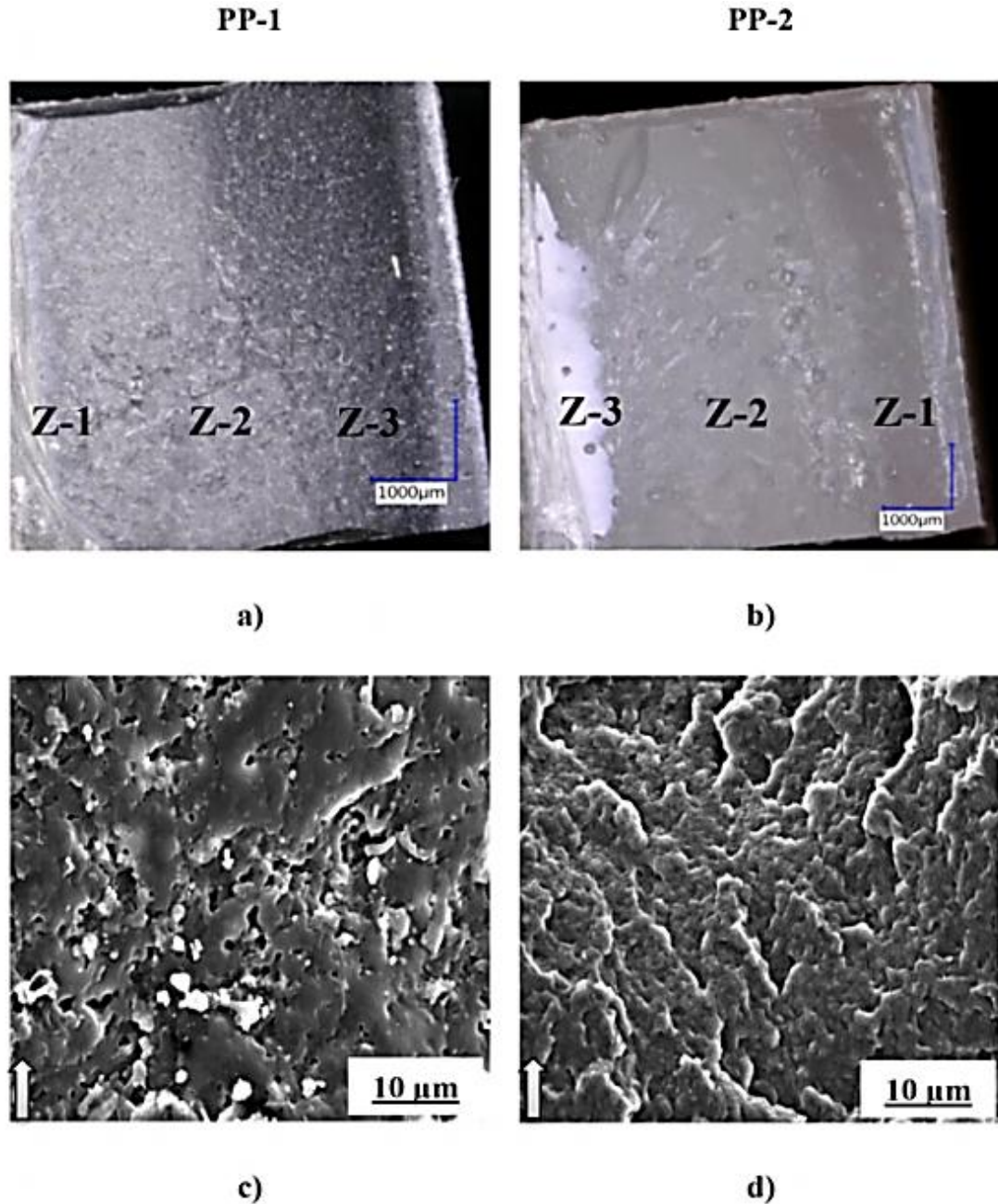

Figure 5.5 **Fracture surface (a, b) under optical microscope and SEM images (c, d) of Zone -1 and Zone-3 of PP-1 and PP-2 respectively. The arrow points out the crack growth direction.**

from the PP random and block co-polymer (PP-1 and PP-2 respectively) tested in this work. Different moulding processes require different grades of materials and the plastics are manufactured under different processing conditions, hence we would expect to see mechanical properties are changed in the plastics. The rapid cooling rates with injection moulding processes induce lower crystallinity and smaller spherulites that increase the toughness properties. In rotational moulding the absence of shear, and the low cooling rates favour the coarse, larger and brittle spherulitic morphology in PP that reduces the impact toughness found in previous research work (Cramez, M. et al., 2001). This could be a reason for the observed lower fracture toughness of rotationally moulded PP materials tested in this work.

Three different zones were observed on the fracture surfaces (Figure **5.5**) for both of the PP materials using the optical microscope. In PP-2, a deep stress whitened area is situated next to the notch (Z-1), after that a large, diffuse, smoother stress whitened area is noted as Zone-2 (Z-2) and finally, an un-whitened and plain area is found as Zone-3 (Z-3). PP-1 also shows these different regions, however there is less depth of stress whitened area in Zone-1. These three zones were also observed in previous studies by various researchers for PP. Here, Zones 1, 2 and 3 were described as an outcome of slow stable crack growth , plastic deformation and brittle fracture respectively (Salazar, A. et al., 2014). In general, crazing is the main deformation process for PP, crazes appear and develop around the crack tip and proceed up to a certain point beyond which they can't go further and this finally leads to rapid brittle fracture. No shear lip is found in any of the materials tested. Some deflected crack paths are observed in PP-2, which could be due to small voids generated during the manufacturing process in the fracture surfaces or due to shear yielding, which was also reported in previous research work (Gensler, R. et al., 2000; Salazar, A. et al., 2014). Under the SEM, Figure **5.5** (c, d), PP-1 shows the flat and smooth surfaces that are related to brittle fracture with lower plastic deformation, whereas for PP-2 the surfaces are wavy and patchy, with micro-voiding due to the de-bonding between the PP matrix and PE phases. For PP-2 micro-voiding, wavy or patchy-like structures that act to increase plastic deformation with increasing ductility and fracture toughness values (Shao, Y. et al., 2015) are observed.

5.2   Impact properties

Rotationally moulded PE and PP samples were conditioned at every 10ºC from -40 to 30 ºC in an environmental chamber and then tested with an instrumented falling weight impact testing machine according to section 3.5 of this thesis. A force – displacement curve was derived for each of the samples. Peak impact strength or crack initiation energy was calculated from data recorded by the impact dart load cell using the area under the curve up-to highest point in the force-displacement curve shown in Figure 3.8. Total impact strength or energy absorbed was found from the area under the whole curve. Crack initiation energy is deducted from the total energy absorbed for calculating the crack propagation energy.

5.2.1   Impact properties analysis of PE

Figure 5.6 shows an example of the force-displacement curve of PE-1 and PE-2 observed in impact testing. Both of the PE samples exhibit ductile failure at every temperature tested here.
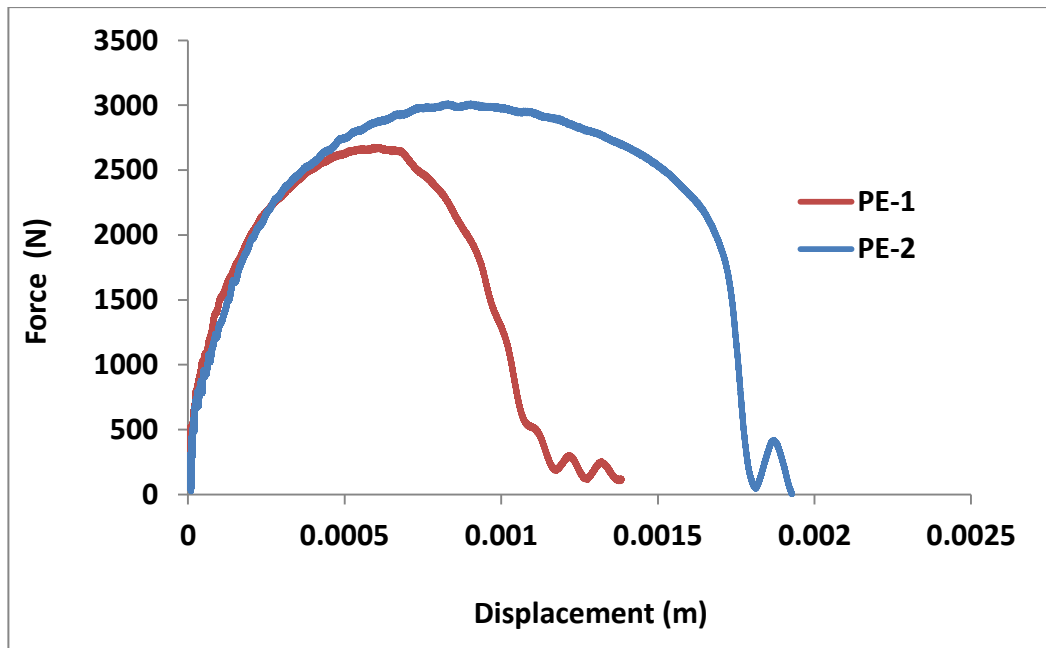

Figure 5.6 Force-displacement curves of PE-1 and PE-2 at -10 ºC.

One of the images of the ductile failure is given in

Figure 5.7. From the force – displacement curve it can be seen the total energy can be divided into two parts – crack initiation and crack propagation energy.
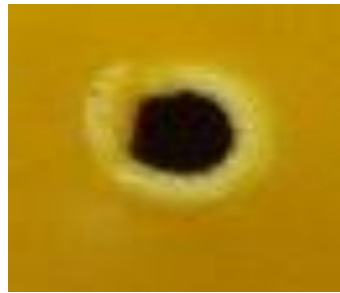

Figure 5.7 Typical ductile failure of PE-1 at drop weight impact testing.

Table 5.1 Average peak impact energies of PE-1 and PE-2 at a range of temperatures.

Temp-erature (ºC)	PE-1		PE-2	
	Energy (J/mm)	**Standard Deviation (±)**	**Energy (J/mm)**	**Standard Deviation (±)**
-40	1.953	0.174	2.150	0.180
-30	1.500	0.200	2.155	0.237
-20	1.400	0.167	2.350	0.240
-10	1.143	0.135	1.940	0.165
0	1.473	0.140	1.443	0.156
10	0.903	0.123	1.670	0.115
20	0.735	0.100	1.190	0.105
30	0.750	0.173	1.310	0.110

Table 5.1 and 5.2 present the peak impact energies or the crack initiation energies and crack propagation energies of PE-1 and PE-2 samples. Peak impact energies are also presented in Figure **5.8**. From the Figure **5.8** and table 5.1, it is found that PE-2 has better impact properties than PE-1. It also can be seen that the peak impact strength of both PE

reduces with temperature from -40 to 30 ºC. PE-2 varies less only 0.84 J/mm between   -40 to 30 ºC whereas PE-1 shows more than 1 J/mm in the same temperature range. The peak impact strength is found at -20 ºC for PE-2 and PE-1 shows the peak impact strength at -40 ºC. In table-5.2, generally PE-2 shows the better crack propagation energies compared to PE-1 except at -40 ºC. For both of the PE samples show the reduction in crack propagation energies with temperature from -40 ºC to 30 ºC. PE-1 and PE-2 show their peak crack propagation energies at -40 ºC and -20 ºC respectively as like as peak impact strength.

Table 5.2 Average crack propagation energies of PE-1 and PE-2 at a range of temperatures.

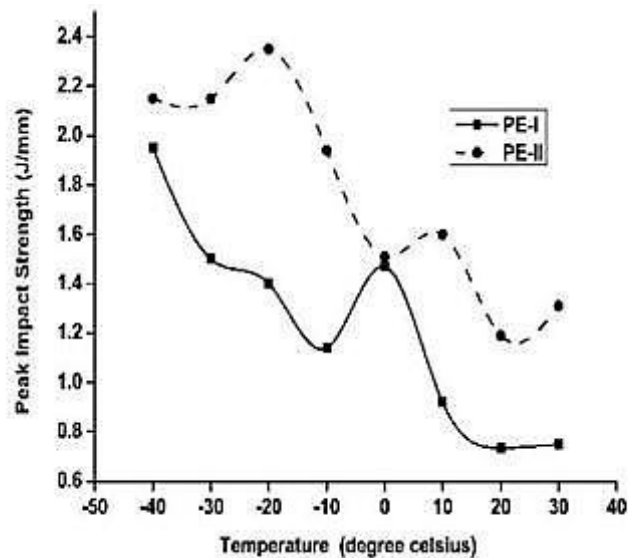| Temperature	PE-1		PE-2	
(ºC)	Energy (J/mm)	Standard Deviation (±)	Energy (J/mm)	Standard Deviation (±)
-40	1.78	0.24	1.69	0.44
-30	1.64	0.12	1.71	0.17
-20	1.13	0.22	2.81	1.85
-10	1.11	0.16	2.25	0.13
0	1.61	0.37	1.70	0.24
10	1.35	0.12	2.63	1.23
20	0.95	0.08	1.71	0.28
30	1.03	0.27	1.93	0.17

Figure 5.8 Peak impact strength of PE-1 and PE-2.

5.2.2   Impact properties of PP

An example of force-displacement curve of PP-1 and PP-2 samples is given in Figure 5.9. Impact force drops suddenly in the figure when it reaches the peak impact force point. This feature is also evident in fracture mode as all of the PP samples show the brittle fracture behaviour at every temperature. Figure **5**.**10** shows the brittle failure of PP samples. From the force-displacement curve the crack initiation or peak impact strength is measured. The crack propagation energy is not possible to be measured since the force –displacement curves drop suddenly at peak impact force and does not take any time for the propagation of failure or crack.
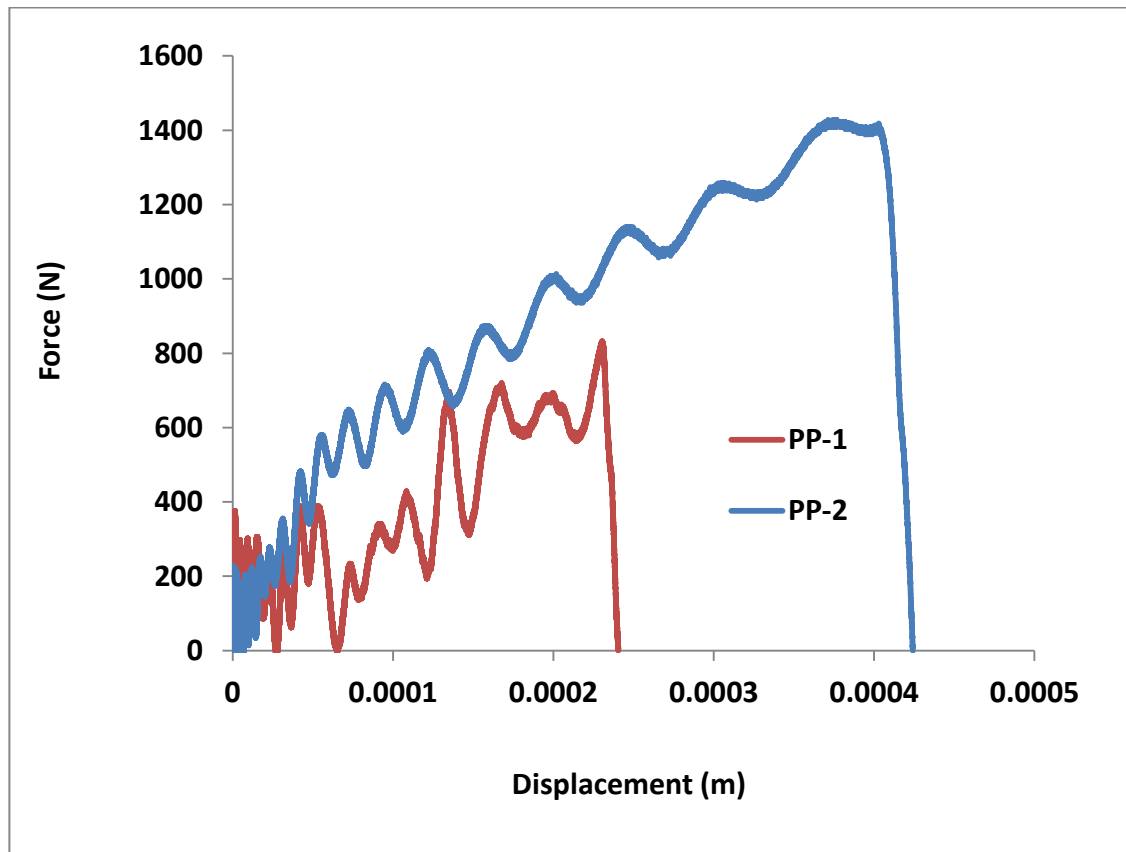

Figure 5.9 Force-displacement curves of PP-1 and PP-2 at 20º C.

Figure 5.10 Typical brittle failure of PP samples.

Table 5.3 Peak impact strength of PP-1 and PP-2 at a range of temperatures.

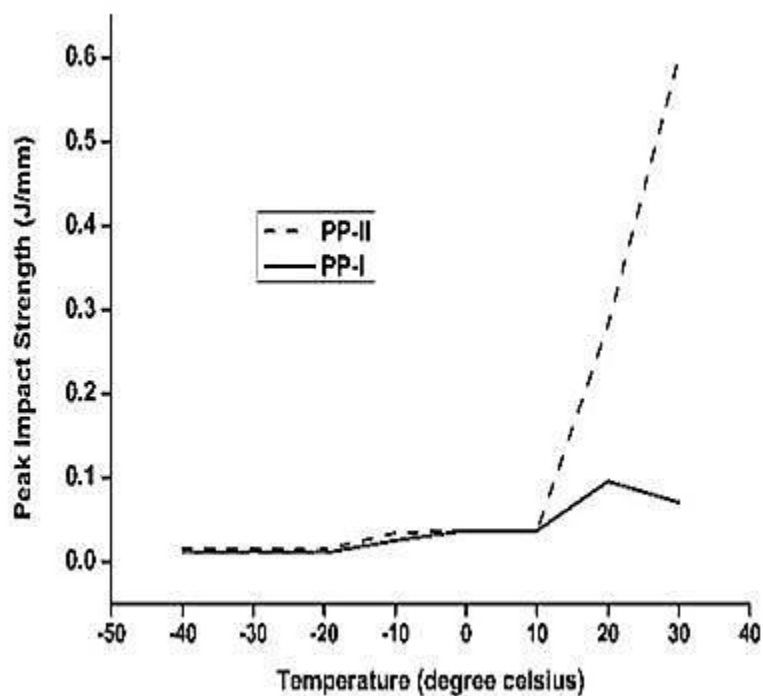| Temp-erature (ºC)	PP-I		PP-II	
	Energy (J/mm)	Standard Deviation (±)	Energy (J/mm)	Standard Deviation (±)
-40	0.010	0.008	0.015	0.007
-30	0.012	0.005	0.015	0.005
-20	0.010	0.004	0.014	0.004
-10	0.025	0.015	0.034	0.009
0	0.036	0.020	0.037	0.015
10	0.036	0.016	0.036	0.020
20	0.095	0.024	0.281	0.092
30	0.070	0.010	0.600	0.135

Figure 5.11 Peak impact strength of PP-1 and PP-2.

Table 5.3 presents the peak impact strength or crack initiation energies of PP-1 and PP-2 samples. Figure **5.11** also shows the peak impact strength of PP samples. From the Figure **5.11** and Table 5.3, it is seen that there is no difference in the impact strength between PP-1 and PP-2 samples and also constant up-to 10ºC for both of the PP materials. After 10 ºC, the impact strength is found to be increased rapidly for PP-2 compared to PP-1.

5.3   Discussion

5.3.1   Fracture toughness

In this work it is found that PE-2 has higher fracture toughness than that of PE-1. From the microstructural details in Chapter 4, SAXS analysis confirms that PE-2 contains higher amorphous and crystal thickness for the two PE materials tested. PE-2 also shows lower crystallinity than PE-1 both in DSC and WAXS analysis. For the fracture toughness analysis and slow crack growth process, crystallinity is not the main governing factor (Lu, X. et al., 1995) and toughness value was found to be decreased with the increase of

99

crystallinity as higher crystallinity induces comparatively more brittle behaviour, reduction in craze formation and amorphous region (Park, S. D. et al., 2006). This feature is also found for PE-2 here. Comparing PE-1 and PE-2 it is seen that the higher amorphous region and crystal thickness are responsible for the higher toughness value seen in PE-2. The toughening mechanism due to the higher amorphous thickness was described in recent research works (Bai, H. et al., 2011; Geng, C. et al., 2014). For higher amorphous region thickness in PE-2, more flexible chain structures are created in the amorphous phase. The flexible amorphous region makes the formation of the micro-voiding process easier which has a positive effect on fracture toughness. Easier formation of micro-voids that help to increase crazing leads to more fibril formation, and more energy absorbed (Figure **5.3**- c, d) for crack growth initiation and propagation which accounts for the higher fracture toughness of this material. The higher crystal thickness measured in PE-2 results in better crystal perfection (Li, Z.-M. et al., 2005). The perfection of the crystals increases the micro-voiding process in the amorphous region , enhances plastic deformation with more absorbed energy before crystallite shearing, resulting in higher toughness (Bai, H. et al., 2011).

PP-2 shows better fracture toughness with values recorded almost double that of PP-1 in this work. From Table 3.1, it is found that PP-2 has a higher MFI value compared to PP-1. A material with a high MFI value has a lower molecular weight and as molecular weight has a linear relationship with fracture energy, it would be expected that higher MFI materials would exhibit lower fracture toughness (Wang, M.-D. et al., 1993). This relationship is not observed for PP-2 in this work however. Salazer et al. (Salazar, A. et al., 2014) observed the linear relationship between fracture toughness and molecular weight for block propylene-ethylene copolymer whereas for homo-polymer and random co-polymer this linear relationship was not found. From microstructural analysis in Chapter 4 of this thesis, solid state NMR testing confirms PP-1 and PP-2 as propylene-ethylene block and random copolymers respectively and in SAXS analysis PP-2 is found to have higher amorphous region thickness compared to PP-1. A higher amorphous thickness absorbs more energy for crack initiation and propagation (Bai, H. et al., 2011; Geng, C. et al., 2014). Though PP-2 is seen to have a larger amorphous thickness and better fracture

toughness compared to PP-1, it is difficult to directly compare fracture toughness between PP-2 and PP-1 based on microstructural details as they have different chemical composition in their structure. From the WAXS analysis in microstructural details, it is found that in the crystalline region of PP-1 has α crystal structure whereas PP-2 contains both α and γ polymorph in its crystal structure. In PP-2, the γ crystal form increases the energy absorption and resistance to deformation (Lezak, E. and Bartczak, Z., 2007; Lezak, E. et al., 2006b). The γ crystal form only shows transverse slip in its chain arrangement instead of slip along the chain direction during the deformation or crack growth process as it does not contain any parallel chain arrangement. Transverse slip absorbs more energy and shows higher resistance to deformation. In this work, SEM images show brittle and plastic deformation for PP-1 and PP-2 in the fracture surfaces respectively. Plastic deformation absorbs more energy and tends to increase toughness values (Shao, Y. et al., 2015) and this is observed for PP-2 in this work.

The fracture toughness values measured in this work for PE and PP materials are very low, notably lower for PP compared to those published in the literature for other plastics manufacturing processes, though it should be noted that the materials tested differ in composition from the PP and PE materials investigated in this study. While the resources are not available in this study, comparative analysis between rotational moulding and other moulding processes, e.g. injection moulding using the same PP and PE materials blends would give the relative differences in fracture toughness properties in different moulding processes and this is recommended for future work.

5.3.2   Impact properties

In this work, PE-2 shows better impact properties than that of PE-1 from -40 ℃ to 30 ℃. In previous research works, it is found that the dynamic mechanical thermal analysis (DMTA) particularly loss modulus curve and the β relaxation peak have a direct relation with the impact properties (Pick, L. and Harkin-Jones, E., 2005; Pick, L. T. and Harkin-Jones, E., 2003). The β relaxation peak in loss modulus curve is occurred due to the glass transition or the movements of side chains of polymers. Higher β relaxation peak in loss modulus curve indicates the dissipation of higher amount of energy during the glass

transition or the movement of side chains in polymers and influences on the impact properties by absorbing high amount of energy. For PE-2 samples, higher loss modulus and the β relaxation peak are found in DMTA analysis of microstructural details investigation in Chapter 4 of this thesis that are related to better impact properties compared to PE-1. PE-1 and PE-2 samples differ in density, crystallinity, crystal and amorphous thickness (see table 3.1, 3.2 and 4.1). Generally higher density reduces the β relaxation peak height because of the higher crystallinity and crystal thickness and ultimately reduces the impact strength. This was not found for PE-2 samples. Therefore it is clear that larger amorphous thickness is responsible for the higher loss modulus curves and the β relaxation peak that increases the impact properties of PE-2 at each temperature of this study.

For PP, the relationship between loss modulus and peak impact strength is very evident which was also observed in a previous work (Vincent, P., 1974). PP-2 has higher loss modulus curve and the β relaxation peak height (Figure 4.12, Chapter 4) and shows better impact properties especially at higher temperature. Brittle fracture with lower peak impact strength was found at temperatures lower than the β-transition (6 ℃ and -23 ℃ for PP-1 and PP-2 respectively, Figure 4.12, section 4.2.2 in Chapter 4 of this thesis) for both of the PP materials. After the β transition the peak impact strength increases which is prominent for PP-2 although no change in fracture mode is found. PP-1 has higher molecular weight compared to PP-2 since it has lower MFI value than PP-2 and showed the less impact strength particularly from 10 ℃ to 30 ℃. In this work, effect of molecular weight on loss modulus or impact properties is not observed for PP-1. PP-2 has α and γ crystal structure, larger amorphous region in its microstructure. The γ crystal structure offers greater resistance to the deformation and amorphous region absorbs more energy for its flexible chain structure. These might be responsible for the higher loss modulus curve and the β relaxation peak height that enhances the impact properties in PP-2 compared to PP-1.

5.4   Conclusion from fracture toughness and impact properties analysis

The following conclusions can be drawn from the fracture toughness measurement and impact properties analysis of rotationally moulded PP and PE, conducted in this work.

- Higher amorphous and crystal thicknesses in PE-2 are the reason for the better fracture toughness values in PE-2 over PE-1.

- The thicker amorphous region contains flexible chain structures which lead to easier micro-voids formation, absorbing more energy and resulting in increased toughness values. Greater perfection of the crystals within the higher crystal thickness also contributes to micro-voiding in the amorphous region before crystallite shearing occurs and enhances toughness.

- PP-1 and PP-2 are block and random propylene-ethylene copolymers. PP-2 contains a higher amorphous thickness, the α and γ crystal structure and better fracture toughness compared to PP-1.

- Greater plastic deformation is evident in the fracture surfaces for PP-2 and this is the reason for its higher toughness values. The more brittle failure seen in PP-1 is also reflected into less deformation ability with lower toughness values.

- Fracture toughness values measured in this work are lower than those recorded for other plastics moulding processes in the literature which could be due to the unique characteristics such as longer heating cycles and lower cooling rates of rotational moulding process.

- PE-2 has better impact properties than PE-1 for the temperature range tested here since higher loss modulus and the β relaxation peak are observed for PE-2 in DMTA analysis.

- Higher density of PE-2 is not found to reduce the β relaxation peak or loss modulus because larger amorphous thickness is considered to be responsible for the increase of the β relaxation peak that is related to better impact properties.

- Better impact properties are identified for PP-2 particularly at higher temperature, though it shows the similar impact behaviour as like as PP-1 at lower temperature. DMTA analysis also supports this observation.

- PP-2 has α and γ crystal structure while PP-1 shows only α crystal structure. It is believed that the γ crystal and larger amorphous thickness are behind the improved impact properties of PP-2 at higher temperatures.

Chapter 6. Low velocity impact properties of rotationally moulded sandwich structure

The low velocity impact behaviour of rotationally moulded sandwich composites is investigated here using a drop weight impact testing machine. The test methodology and test schedule are described in section 3.7 of Chapter 3 of this thesis. In this purpose, rotationally moulded sandwich composite were manufactured at four different thickness combinations and tested under low velocity drop weight impact condition. Polyethylene (PE) was used for skin and foamed core layer as well. Damages were identified at different layers of sandwich composites due to the impact testing. Force - time, force –displacement curves were analysed to understand the skin-core thickness effects on the low velocity impact response of rotationally moulded sandwich composites.

6.1   Low velocity impact test

Low velocity impact properties were tested with an instrumented impact testing machine according to section no. 3.7 at 20 J to 100 J energy levels. The diameter of the hemispherical impactor indenter was 12 mm and 9.1 kg was the total falling mass of the impactor in this test. The impact velocities were 2.10 , 2.56 , 2.96 , 3.31 , 3.92 , 4.2 and 4.68 m/s at 20 , 30 , 40 , 50 , 70, 80 and 100 J impact energy level.

Table 6.1 Skin-core-skin thickness combinations of rotationally moulded sandwich samples.

Sandwich Type	Thickness Combination (Skin + Core + Skin) (mm)
Sandwich-1	1+4+1
Sandwich-2	1+8+1
Sandwich-3	2+4+2
Sandwich-4	2+8+2

Four different skin-core thickness combinations of rotationally moulded sandwich composites were manufactured and named as sandwich-1, 2, 3, and 4, described in section

3.6. For the convenience, skin and core thickness combinations of four different sandwich samples are also given in Table **6.1**. Force-displacement curves are found in low velocity impact testing are shown in Figure 6.1, 6.2, 6.3, 6.4 and 6.5 for 20 J, 30 J, 40 J, 50 J and 70 J energy levels respectively.
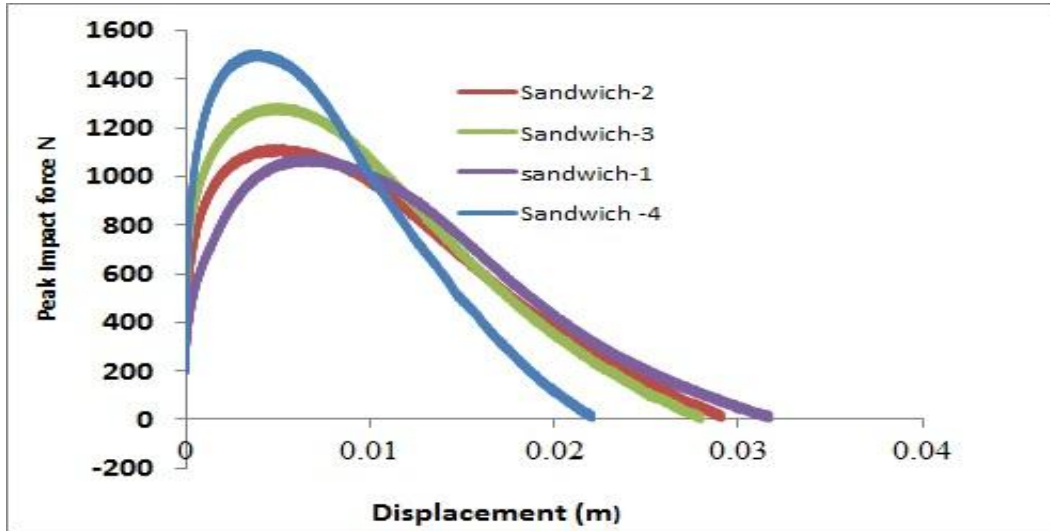
6.1.1   Force-displacement curves

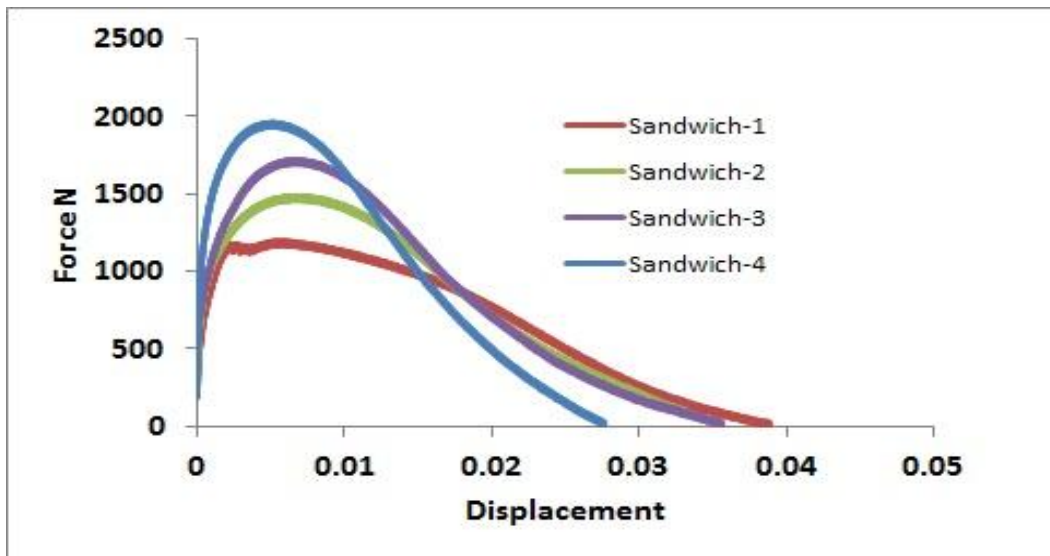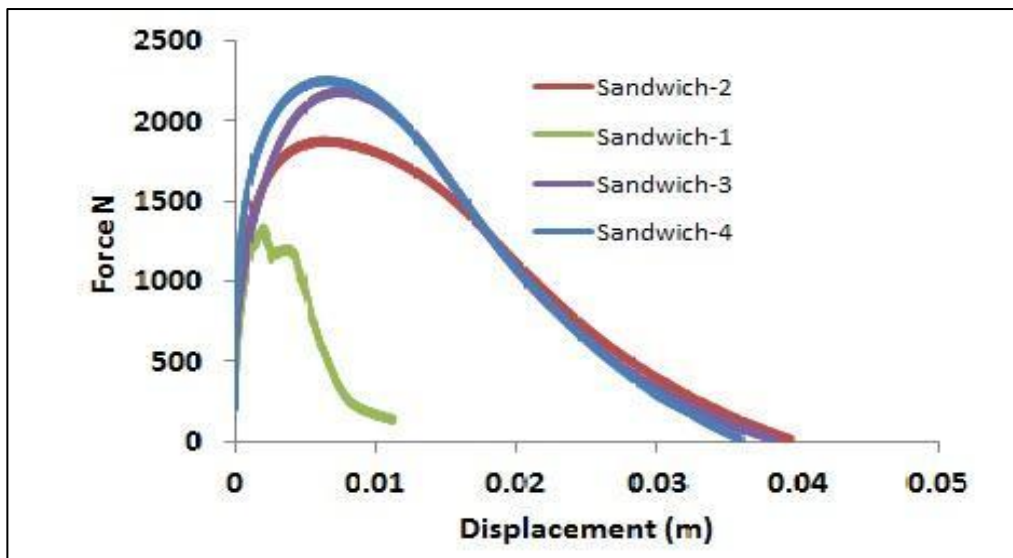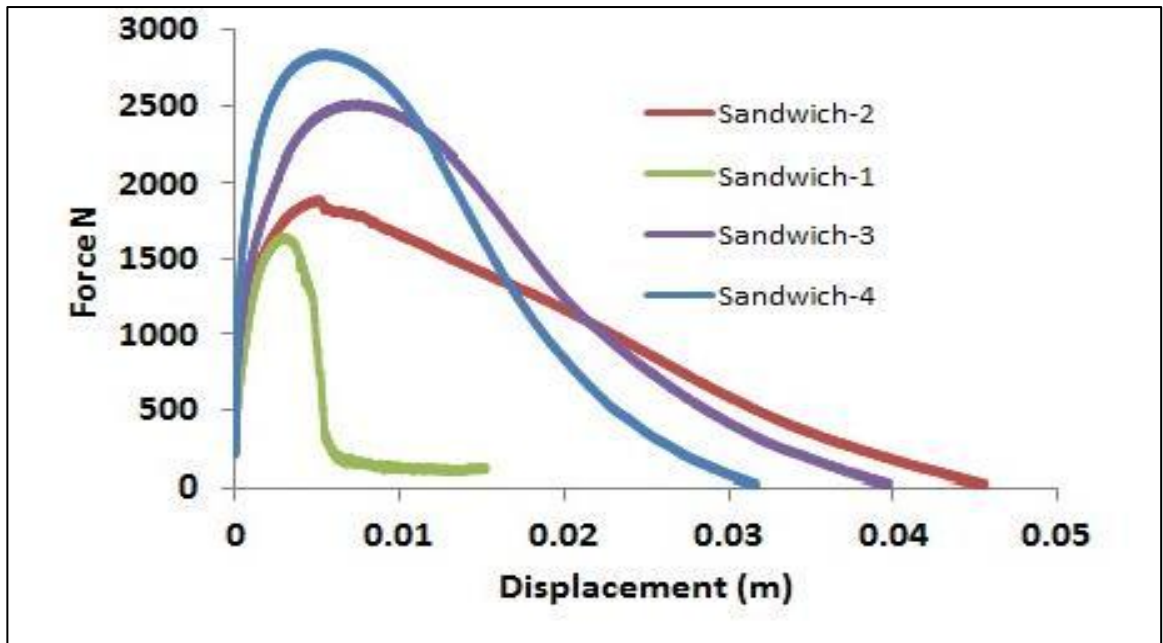Figure 6.1 Force displacement curves of sandwich samples for various thicknesses at 20 J.

Figure 6.2 Force displacement curves of sandwich samples for various thicknesses at 30 J.

From figure 6.1 to 6.5, generally it is seen that force values increase with the increase of the skin and core layer thickness. Displacement values are also found to be decreased with the increase of core and skin layer thickness. Therefore it can be said that bending stiffness of this sandwich structure increases with the increase of foamed core or skin layer thickness. Sandwich-4 has the highest thickness and exhibits the highest force and lowest displacement values at every energy level among all of the sandwich samples. Sandwich-1 shows the lowest force values at each energy level as it is the thinnest sandwich structure tested in this work. It has the greatest displacement at 20 J and 30 J before it gets the penetration at 40 J energy level. Penetration refers to the case where the dart fully passes through the sandwich samples. The foamed core thickness of sandwich-2 is twice of the sandwich-1 and for this sandwich-2 shows higher force and lower displacement compared to sandwich-1. Sandwich-3 has 2 mm skin thickness while sandwich-1 has 1mm skin thickness and both of them contain the similar foamed core thickness. Due to the 1 mm increase of the skin thickness, sandwich-3 shows the higher force and lower displacement than sandwich-1. It also shows the higher force and lower displacement than sandwich-2 though it has lower foamed core and overall thickness compared to sandwich-2. Sandwich-3 has 2 mm skin thickness and 4 mm core thickness

Figure 6.3 Force displacement curves of sandwich samples for various thicknesses at 40 J.

Figure 6.4 Force displacement curves of sandwich samples for various thicknesses at 50 J.
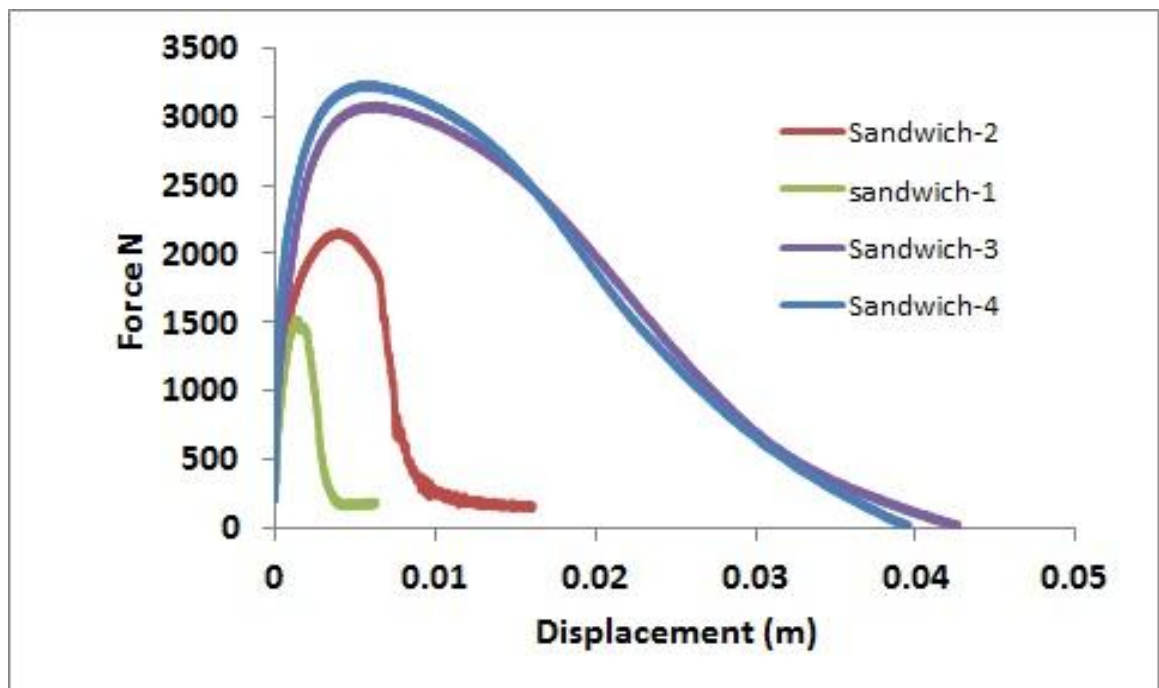

Figure 6.5 Force displacement curves of sandwich samples for various thicknesses at 70 J.

whereas sandwich-2 is manufactured of 1 mm skin and 8 mm core thickness respectively. From these results it can be said skin thickness is contributing more to the stiffness increase of this sandwich structure during the low velocity impact compared to foamed core thickness. Similar observation is also found when the comparisons are made among sandwich-4, sandwich-3 and sandwich-2.

Loading and unloading portion of the force –displacement curves provide information on damage mechanisms. The loading portion of the curves for all the thicknesses is almost same while unloading portion shows some differences. At 20 J impact energy level (figure 6.1) only one peak is observed for all of the samples. It expresses that 20 J is not enough to create fracture or fully penetrate the samples. At 30 J energy level (Figure 6.2) only one peak is also observed for all of the sandwich samples except sandwich-1. Sandwich-1 shows fracture at the bottom face sheet and shows a sudden decrease in the load-displacement curve.

Sandwich-1 shows two clear peaks and gets penetration at 40 J energy level. The first peak is for the failure of the bottom layer as the fracture starts from the bottom layer and the second peak is for the top skin layer. No extra peak is observed for the foam layer. The impactor does not return from the samples due to the penetration and for this the unloading portion of sandwich-1 is not observed to be reached at the X-axis. At this energy level all other samples show only one peak in their force-displacement curves. Sandwich-2 shows fracture in its bottom layer when tested at a 50 J energy level. It is clear from the force-displacement curve for this test that failure has occurred on the lower surface as a sudden drop is noticed in the peak force. The penetration occurs in sandwich-2 at 70 J impact energy. Sandwich-1 shows the penetration at both of the energy levels as it is expected. Sandwich-3 and sandwich -4 do not get any fracture or penetration at these energy levels and so testing is continued at higher energy levels for these samples as discussed below at the end of the section 6.1.4.

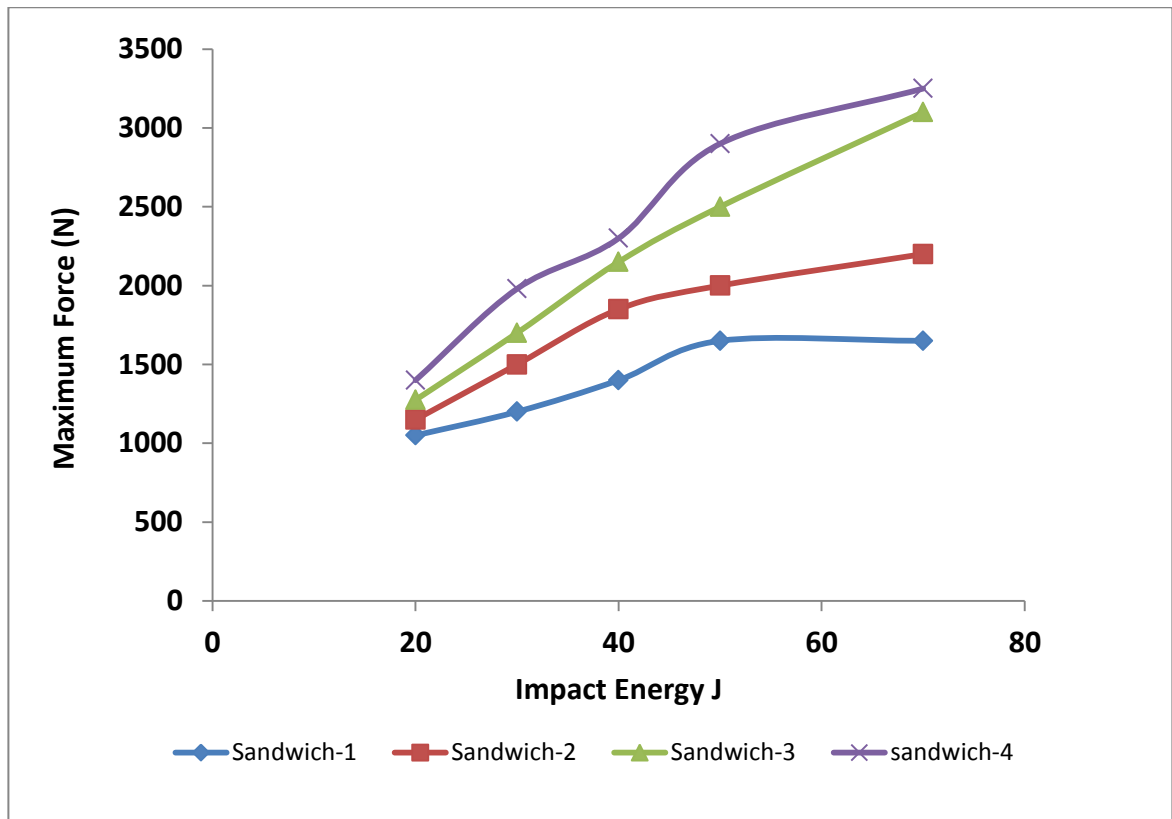### 6.1.2 Maximum Force - impact energy curves

Figure 6.6 Maximum force- impact energy graphs for all of the thicknesses.

Figure 6.6 shows the maximum force-impact energy curves of the samples for all of the thicknesses. It is clear from the graph that the maximum contact force increases with the increase of skin and core thickness of the samples and skin thickness contributes more to the increase of maximum contact force compared to core thickness. The maximum contact force of sandwich-3 and sandwich-4 increases very rapidly at every energy level as they don't get any fracture or penetration. For sandwich-1 the maximum contact force increases quickly up-to 40 J impact energy level. After that it increases slowly and from 50 J no significant changes are observed which corresponds to the penetration level. Similar trend is also noticed for sandwich-2 samples. Initially the maximum force increases rapidly up-to 50 J energy and then it slows down when fracture and penetration are occurred in the sandwich samples.

6.1.3   Contact time- impact energy curves

Contact time-impact energy graphs of the samples are shown in figure 6.7. From these results it is found that generally contact time decreases with the increase of skin and core layers thickness, and skin layer thickness is contributing more to the reduction of the contact time during the low velocity impact event at different energy levels. Sandwich-1 shows the highest contact time at 20 and 30 J energy levels. From 40 J it decreases suddenly because of the penetration and continues nearly linear for other energy levels. Sandwich-2 exhibits lower contact time than sandwich-1, though it shows higher contact time compared to sandwich-3. Contact time is also found to decrease from 50 J for sandwich-2 samples because of the observed penetration and fracture in the structure. The lowest contact time is noticed for sandwich-4 samples among all of the samples at each energy level.
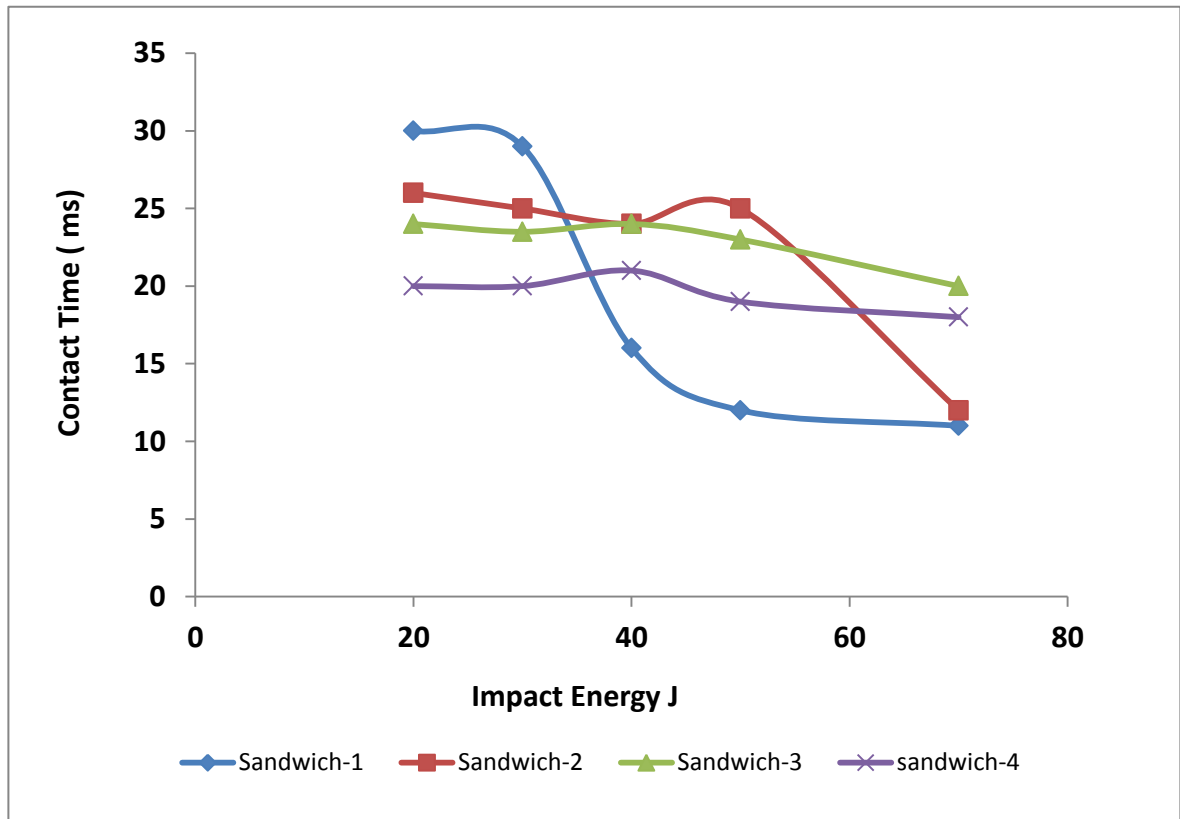
Figure 6.7 Contact time- impact energy curves for all of thicknesses.

6.1.4   Maximum displacement-impact energy curves
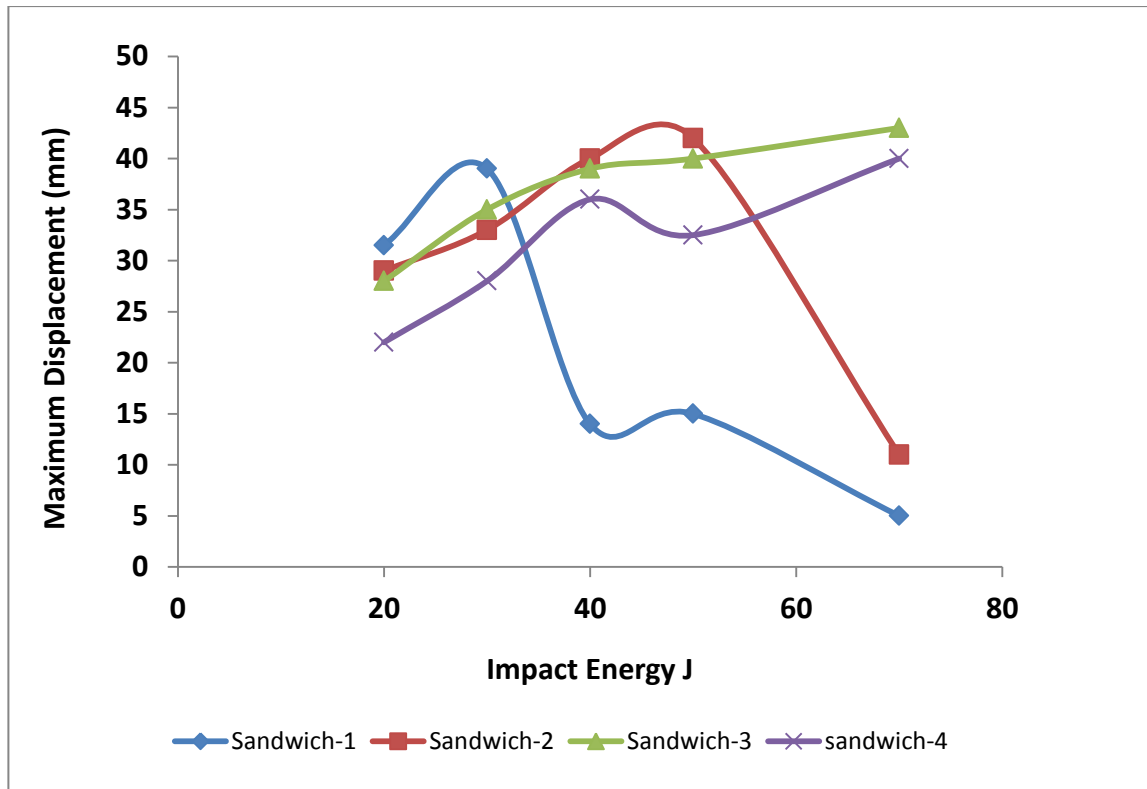
Figure 6.8 Displacement impact energy curves of the samples for various thicknesses.

The displacement-impact energy curves in figure 6.8 shows the expected behaviour. Displacement during the impact event at each energy level decreases with the increase of skin and core layer thicknesses because of the increase of the bending stiffness of the sandwich samples tested here. In this analysis skin layer thickness is also found to be more responsible for the decrease of displacement compared to core layer thickness as like as maximum contact force and contact time analysis. Sandwich -1 shows the highest displacement at 20 and 30 J among all of the samples and after 30 J the displacement reduced dramatically due to the penetration. Sandwich-2 has lower displacement than sandwich-1 and from 50 J the displacement is observed to be decrease suddenly for the fracture and penetration of the samples. Lower displacement is found for sandwich-3

113

compared to sandwich-2. The lowest displacement is noticed for sandwich-4 as it gets the highest thickness. In this work, 80 J and 100 J energy levels are also used for only sandwich-3 and sandwich-4 to investigate their penetration energy as these samples were found to not fail at lower impact energies. It is found that sandwich-3 gets full penetration at 80 J and for sandwich-4 it occurs at 100 J energy level.

6.2   Damages of the sandwich samples

Energy (J)	Sandwich-1 (1+4+1)	Sandwich-2 (1+8+1)	Sandwich-3 (2+4+2)	Sandwich-4 (2+8+2)
20				
30				
40				
50				
70				

Figure 6.9 Damages of top surface of the sandwich samples
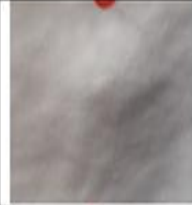
Energy (J)	Sandwich-1 (1+4+1)	Sandwich-2 (1+8+1)	Sandwich-3 (2+4+2)	Sandwich-4 (2+8+2)
20				
30				
40				
50				
70				

Figure 6.10 Damages of bottom surface of the sandwich samples.

To investigate the damage modes of the rotationally moulded sandwich samples in the low velocity impact event, the images of the top and bottom surfaces are presented in figure 6.9, 6.10 and 6.11. At 20 and 30 J impact energy levels no clear crack or fracture is observed in the top surface for all of the samples tested.

Energy (J)	Sandwich-3	Sandwich-4
Top Surface 80		
100		

Bottom Surface 80		
100		

Figure 6.11 Damages of top and bottom surface of sandwich-3 and sandwich-4 at 80 and 100 J.

The only visible damage is the local plastic deformation or indentation depth of the top surface. The depth of the plastic deformation increases with the increase of the energy level

until the sandwich samples gets any fracture in the upper skin. For sandwich-3 and sandwich-4, an increase of the depth of the plastic deformation is
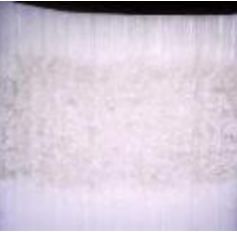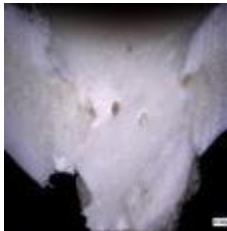
Energy J	Sandwich-1	Sandwich-2	Sandwich-3	Sandwich-4
30				
70				

Figure 6.12 Cross section of the impacted sandwich samples at 30 and 70 J for all of the thicknesses.

observed as they do not get any fracture up-to 70 J energy level. Sandwich -2 and sandwich-1 also exhibit the similar result up-to 50 and 40 J respectively. In the bottom surface generally a small protrusion is noticed following impact which increases with the increase of impact energy. At 20 J energy level, protrusion is seen clearly only in sandwich-1 samples compared to other samples and it gets cracks at 30 J impact energy which is not observed for the other samples. Sandwich -1 does not get any fracture or crack in the top surface at 30 J while it shows the penetration at 40 J. From this observation it can be said that the damage or crack starts in the bottom surface at first because of the bending during

the impact event. From the images the similar observation is also found for sandwich-2 samples. Sandwich-2 exhibits the cracks at 50 J in the bottom surface whereas no crack is observed in the top surface at this energy level. Penetration is occurred for sandwich-2 at 70 J impact energy. In the bottom surface of sandwich-3, protrusion size is found to be increased with the energy level and at 70 J impact energy some clear scratches are observed in the bottom surface. It gets the penetration at 80 J (Figure 6.11). For sandwich-4, protrusion is clearly seen at 70 J which gets some scratches or voids due to the displacements at 80 J (Figure 6.11) impact energy. No crack is observed at 70 or 80 J in the top surface for sandwich-4. Finally 100 J (Figure 6.11) impact energy penetrates the sandwich-4 samples.

Figure 6.12 presents the cross sections of the samples after impact. From these images it is found that plastic deformation (indentation depth) on the top surface, core crushing and protrusion (deformation in back surface) in the bottom surface are the main deformation modes for sandwich-3 and sandwich-4. No interfacial crack or delamination at the skin/core interface is observed. The amount of top surface indentation or plastic deformation, and the protrusion in the bottom surface are found to increase with increasing impact energy as expected. The amount of crushing of the core layer also increases with the increase in energy level and results in a reduction in the overall thickness of the sample. These deformations are permanent deformation and would represent permanent visible damage in a real world case. Sandwich-1 and sandwich-2 also exhibit similar damage modes until their penetration level. At 30 and 50 J fractures are found as fracture starting point from the bottom surfaces for sandwich-1 and sandwich-2 respectively leading to penetration at higher energy level. Sandwich -4 shows the lowest amount of core crushing and thickness reduction among all of the samples. The lower amount of damages in terms of top surface indentation depth, core crushing and bottom surface deformations are observed in sandwich-3 compared to sandwich-2. It proves that the skin thickness is playing more crucial role to the impact damage resistance than core layer thickness. Sandwich-2 shows better resistance compared to sandwich-1.

6.3   Discussion

From the results section it is found that the peak impact force increases while displacement and contact time decreases with the increase of core and skin layer thickness at each impact energy level. Therefore it can be said that the bending stiffness and resistance to impact load increases with the increase of both skin and core layer thickness for these rotationally moulded sandwich samples. Raju et al. (Raju, K. et al., 2008) also observed the higher peak force and reduced impact duration for an increase of the skin thickness of honeycomb sandwich composite. A thicker core also exhibited the higher impact force and resistance to impact force in previous work (Sawal, N. and Hazizan, M. A., 2011). Peak impact force, contact time and displacement analysis prove that an increase in skin layer thickness offers better stiffness and more resistance to impact load compared to an increase in core layer thickness. From the comparison of all of the thicknesses it is observed that doubling the skin thickness enhances the fracture initiation or penetration energy level more than twice while for the foam core less than two times resistances are found.

Cross sections of the impacted samples, top and bottom surfaces show that the damage starts from the bottom surface of the sandwich samples which also becomes clear from the observed drop in force-displacement curves of the samples. Damage analysis identifies the plastic deformation or indentation depth in the top surface, protrusion in the back surface, core crushing as the main damage modes. During the impact event the impactor touches the top surface, transfers energy to the sandwich samples and creates the indentation depth, core crushing and protrusion in the top skin, core layer and bottom surfaces respectively. At higher energy level indentation depth and protrusion in the bottom surface increases. Core layers get more crushing and consolidation. For the further increase in energy level, due to the increasing bending or displacement bottom layer gets fracture which continues to grow through the crushed and consolidated core layer and reaches to the top skin and finally the top skin gets penetration. An increase in core layer thickness accommodates more crushing and consolidation that helps to prevent the start of fracture in the bottom layer. Skin thickness increase enhances bending or displacement capability, better resistance to impact force and an accommodation for more crushing and consolidation compared to an increase

in core layer thickness that ultimately prevents the penetration at higher impact energy level. For all of the samples tested here delamination at skin/core interface or core cracking is not observed here. Delamination at core and skin interfaces reduces the load bearing capacity of a sandwich structure drastically. For these tested sandwich structures the skin and core layers are manufactured of same material (PE) and therefore the bonding between the skin and core is strong enough to resist the sudden impact load from 20 J to 100 J impact energy level. In the impact event all the deformations are found as permanent deformation. Skin and core layers exhibit the ductile deformations and removes the problem in detection of barely visible impact damage in sandwich structure which shows elastic behaviour (Compston, P. et al., 2006). Moreover, in this work no catastrophic or localised failure is not observed in the core or skin layer that is also considered helpful for the improvement of the mechanical performance.

6.4   Conclusion from low velocity impact properties analysis

In this study, rotationally moulded skin-foam-skin sandwich structures are manufactured at various skin and core layer thickness combinations and tested under low velocity impact conditions. Impact properties such as peak impact force, displacement, contact time and damages at skin and core layers are obtained and compared for each of thickness combination. The main conclusions are presented here from this analysis-

- Bending stiffness during the impact event and resistance to impact force of the rotationally moulded sandwich samples increase with the increase of both skin and core layer thickness since the peak impact force is found to be increased while displacement and contact time are observed to be reduced at each energy level.
- Between skin and core layer, skin layer thickness is more responsible for enhancing the impact resistance of the sandwich samples.
- Indentation depth in top surface, protrusion in bottom surface, crushing and consolidation in core layer are identified as the damage modes which are noticed to be increased with the increase of the energy level for all of the thicknesses.
- No delamination at core/skin interface is observed.

- Fracture starts from the bottom surface, continues to grow in the core layer and finally the top surface gets the penetration.

- Thicker skin layer increases impact resistance by providing a better accommodation for more crushing and consolidation in core layer and enhances bending or displacement capability compared to thicker core layer that ultimately prevents fracture initiation or penetration at higher impact energy level.

- Ductile deformations in core and skin layers create visible impact damage in sandwich structure which is easy to find out. No catastrophic or localised failure is observed here for core or skin layer which is considered to be advantageous for the improvement of mechanical performance.

- Developing a mathematical model for low velocity impact properties of sandwich structures from the experimental investigation and material properties analysis such as compression properties of foamed core and skin layer could be done in future which are not conducted in this work.

Chapter 7. Low velocity repeated impact test of rotationally moulded sandwich samples

Low velocity repeated impact behaviour of the rotationally moulded sandwich structure was investigated in this chapter. This analysis was only carried out for sandwich-3 (skin + core + skin -- 2+4+2 thickness combination) sample which has 2 mm thickness for top and bottom layer and 4 mm thickness for the foamed core layer as this sandwich structure is mostly used in various applications such as marine leisure craft and automotive applications. The samples were subjected to impact event repeatedly up-to penetration at each energy level. The impact force, time and displacement were obtained for each of the repeated impact event. Damages at top and bottom surfaces and impact energy-impact number curves were also identified to get the understanding on effect of repeated impact event on the lifetime of the sandwich structure.

7.1   Low velocity repeated impact event

Repeated impact test were conducted according to the section no. 3.8. From the impact properties analysis in Chapter 6 it was observed the sandwich-3 gets only indentation depth at 20 J, prominent scratches in bottom surface at 70 J and penetration at 80 J. Therefore it was decided to choose the energy range of repeated impact test between 20 J and 70 J. The impact energies were chosen as 20 J, 30 J, 40 J and 50 J. During this experiment the sandwich samples were inserted in the sample holder and impacted repeatedly up-to penetration of the sample at each energy level. A secondary impact was observed at each repeated impact event after rebound of the impactor. From the initial screening test it was found that the secondary impact only creates five percent energy of the primary impact at each repeated impact event and so we have focussed on the initial impact for our testing and calculations. Here, force-displacement curves represent only the primary impact of each repeated impact event. Development of an anti-rebound system would be a useful development for more detailed future work on this topic

Force-displacement curves are found in repeated impact testing are presented here in Figure 7.1 to Figure 7.4 for 20 J, 30 J, 40 J and 50 J energy levels respectively. The maximum number of repeated impact is found for the minimum energy level at 20 J whereas it decreases with the increase of energy level as expected. The sandwich samples are found to

be penetrated after 273rd repeated impacts at 20 J (Figure 7.1). The minimum impact number is found as 4 at 50 J impact energy (Figure 7.4). At 30 and 40 impact energy it is counted as 48 (Figure 7.2) and 11 (Figure 7.3) repeated impacts.

It is observed in Figure 7.1-7.4 that the maximum impact force and displacement in the first impact are found to be increased for the increase in impact energy level of these sandwich samples. Similar observation is also found in impact properties analysis of sandwich samples in Chapter 6.
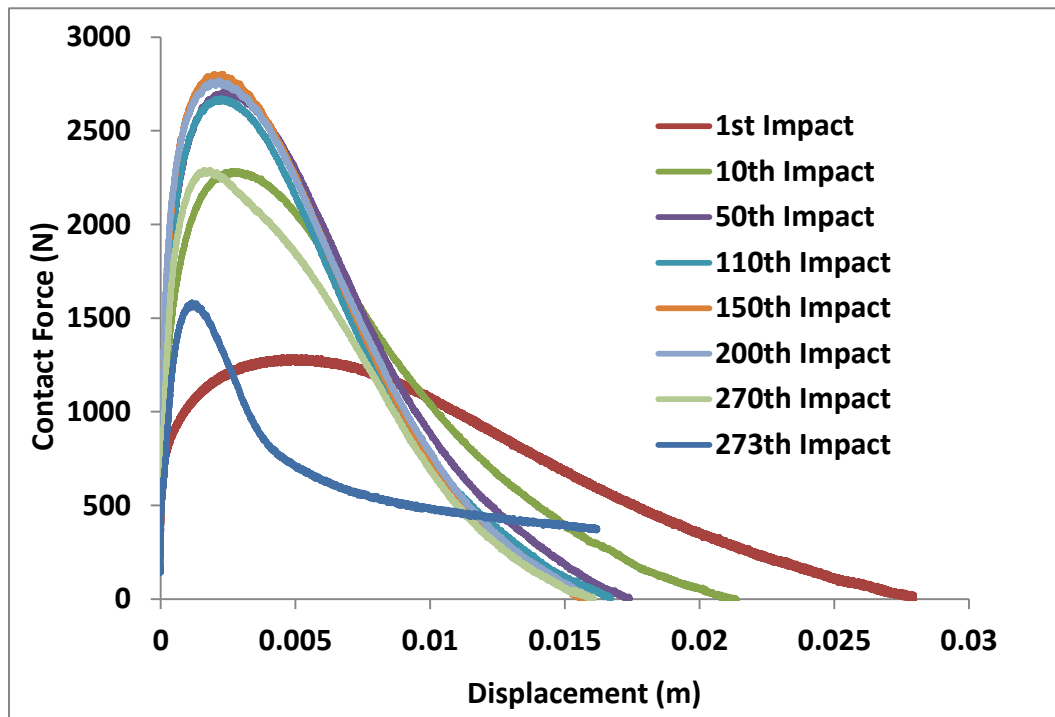
Figure 7.1 Force-displacement curves of repeated impact events at 20 J of sandwich-3 samples.
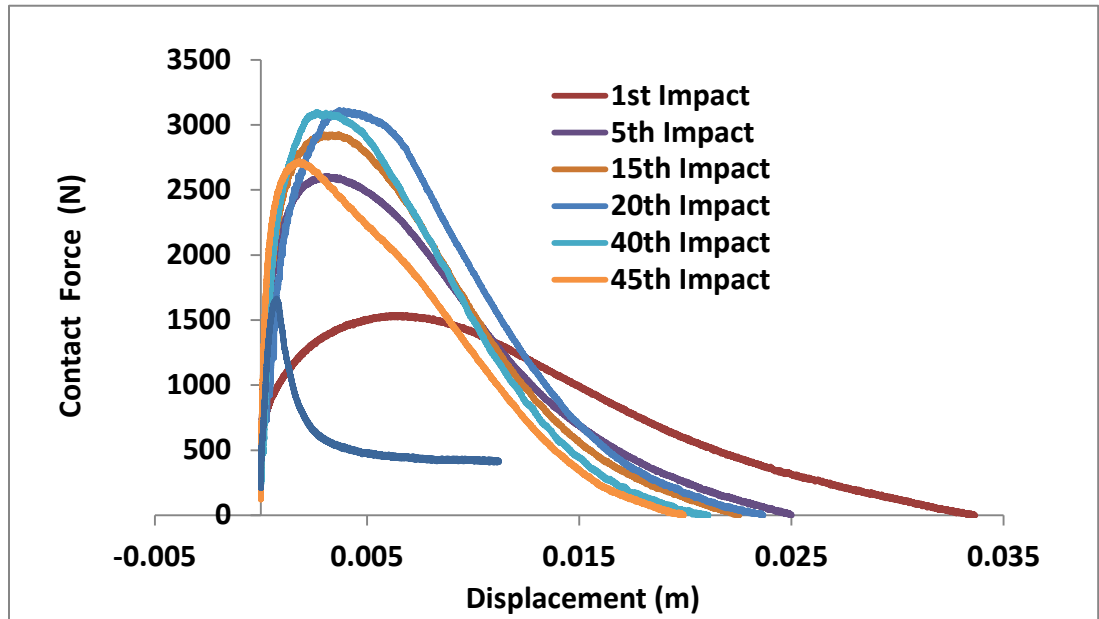
Figure 7.2 Force-displacement curves of repeated impact experiment at 30 J of sandwich-3 samples.
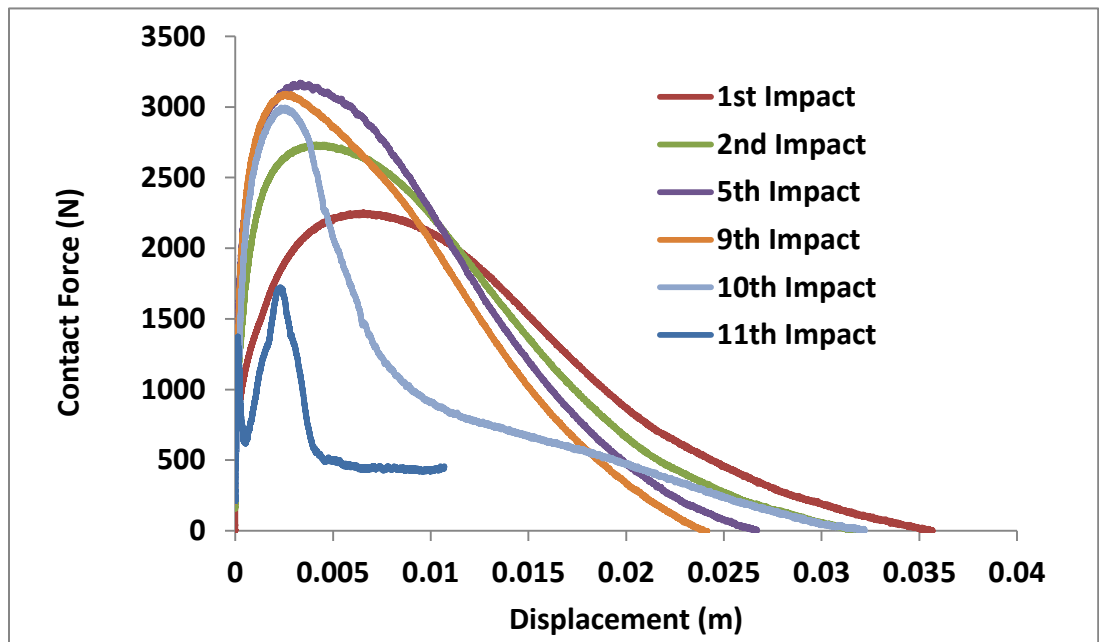
Figure 7.3 Force-displacement curves of repeated impact experiment at 40 J of sandwich-3 samples.

.
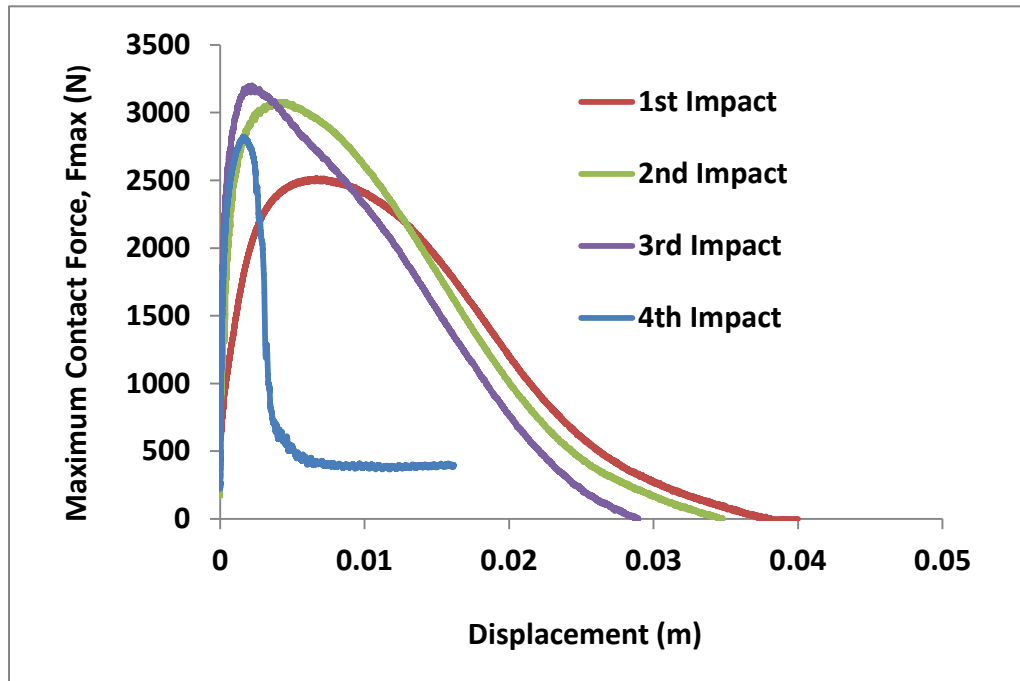
Figure 7.4 Force-displacement curves of repeated impact test at 50 J of sandwich-3 samples.

After the first impact at each energy level displacement reduces with the increase of impact number. At 20 J energy level (Figure 7.1), displacement reduces from 35 mm to less than 5 mm and at 50 J (Figure 7.4) it reduces from 40 mm to less than 5 mm.

During the repeated impact test at every energy level, maximum impact force (Fmax) values are increased quickly with the impact number up-to certain impact numbers. After that they are reduced until the samples are penetrated. At 20 J (Figure 7.1), the peak impact force is identified as 1250 N in the first impact, it is increased to 2750 N in the 150th impact and then it is reduced to 1500 N in the 273rd impact where the sample fails. In the first impact peak impact force is also found as 2500 N at 50 J energy level (Figure 7.4), increased to 3200 N in the 3rd impact and in 4th impact the impact force is reduced and the sandwich sample gets penetrated. Similar trends are also found for the peak impact force at 30 J (Figure 7.2) and 40 J (Figure 7.3) energy levels.
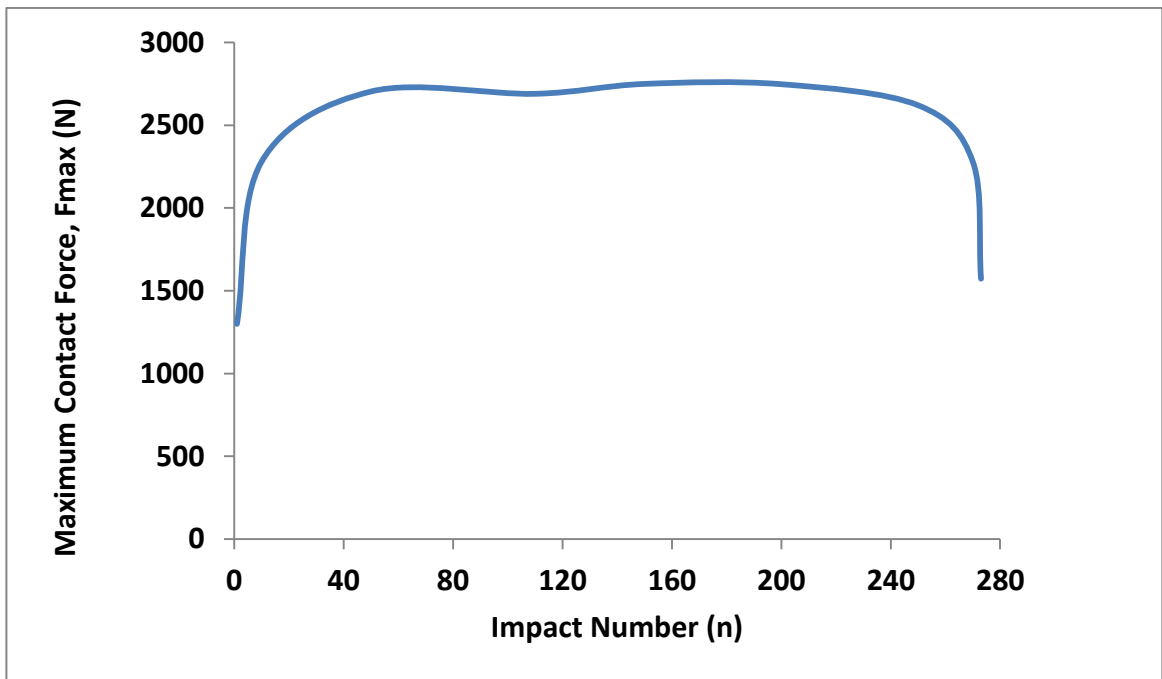
Figure 7.5 Changes of peak impact force (Fmax) values during the repeated impact test at 20 J.
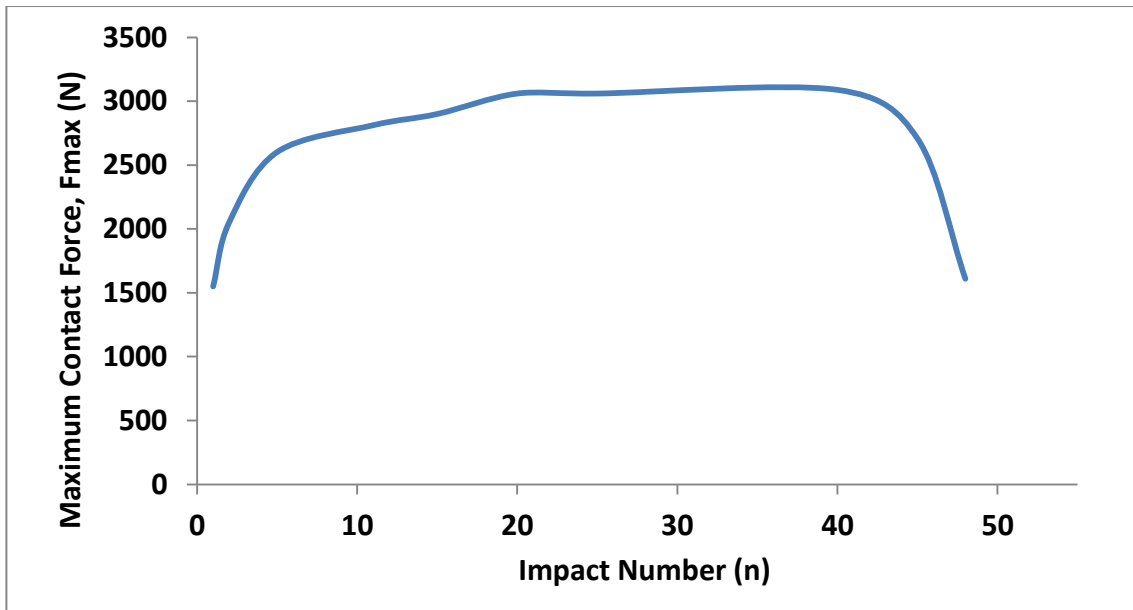
Figure 7.6 Changes of peak impact force (Fmax) values during the repeated impact test at 30 J.
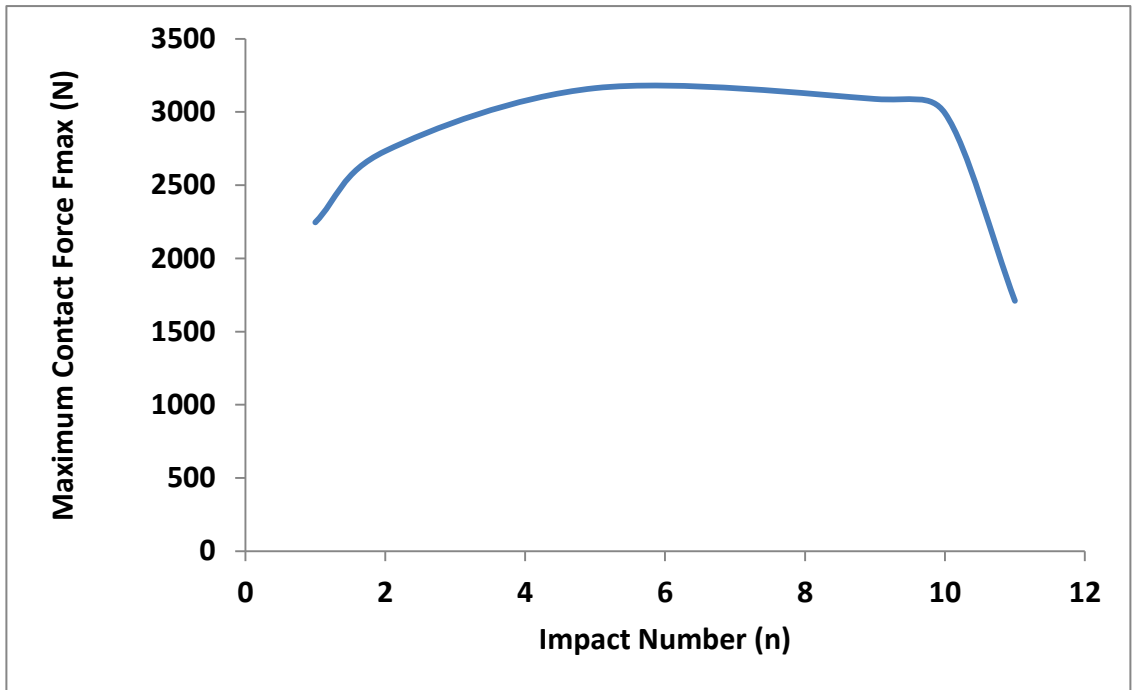
Figure 7.7 Changes of peak impact force (Fmax) values during the repeated impact test at 40 J.
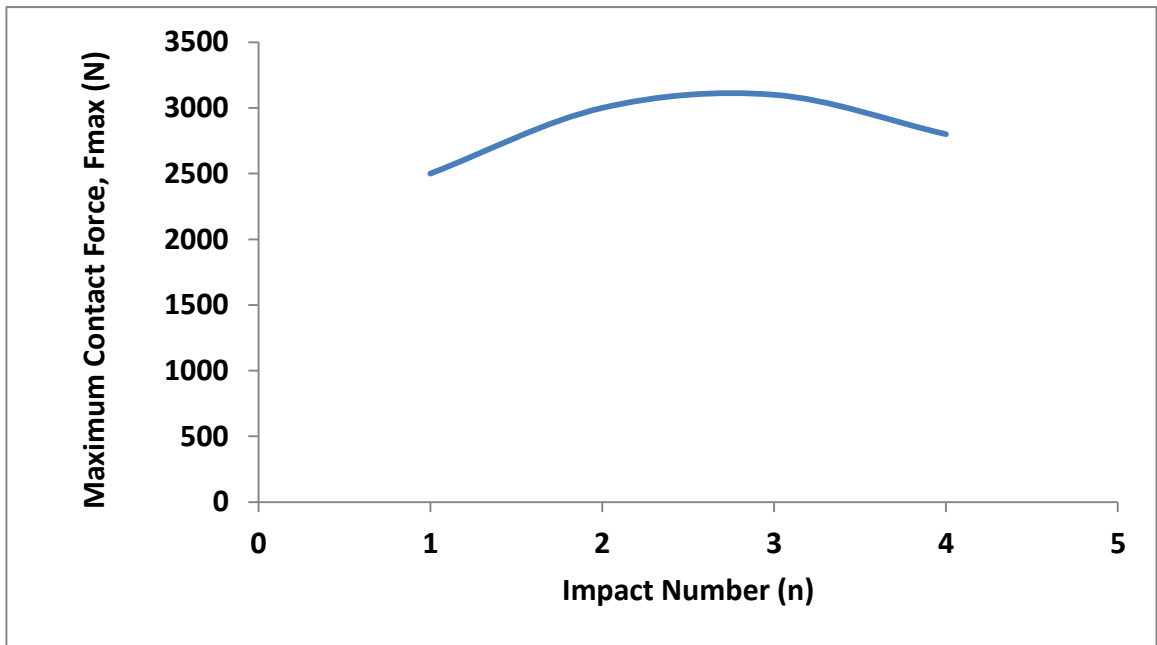
Figure 7.8 Changes of peak impact force (Fmax) values during the repeated impact test at 50 J.

The changes in peak impact force (Fmax) are illustrated in figure 7.5 to figure 7.8 during the repeated impact event for 20 J, 30 J, 40 J and 50 J respectively. It is clearly seen that there are three regions in Fmax changes curves at each energy level. At first region, Fmax values are increased sharply. It could be due to the compression behaviour and densification of the foamed core layer of the sandwich sample. The peak impact force values are found almost same around a certain value in the second region. The second region can be termed as plateau region. In this region, the increase of consolidation and thickness reduction in foamed core layer, initiation and propagation of cracks in bottom layer are observed. Scratches are also observed in the indentation depth of the top surface in this region. At the end of this region the bottom layer loses its load carrying capacity and the foamed core layer also gets the highest thickness reduction and cracks. As a result in the third region the impact dart penetrated the top surface and the penetration is happened in the whole sample which becomes clear from the sudden decrease of peak impact force in the curves. An increase in peak impact force with the impact number and reduction of its values for the fracture and penetration after a certain impact number in the repeated impact test are also observed in low velocity impact analysis of honeycomb sandwich structures and PVC foam sandwich composites (Atas, C. and Sevim, C., 2010). On the other hand Bora et al. (Bora, M. Ö. et al., 2009) observed the reduction in peak impact force with the impact number for the impacted thermoplastic matrix composites. They concluded this behaviour because of the compression behaviour of the composite, fibre fracture in the compression zone and multiplication of delamination of the composite structure. Analysis of the compression behaviour of the foamed core used in this work will give better understanding of the increase of the peak force with impact number which is not covered in this thesis.
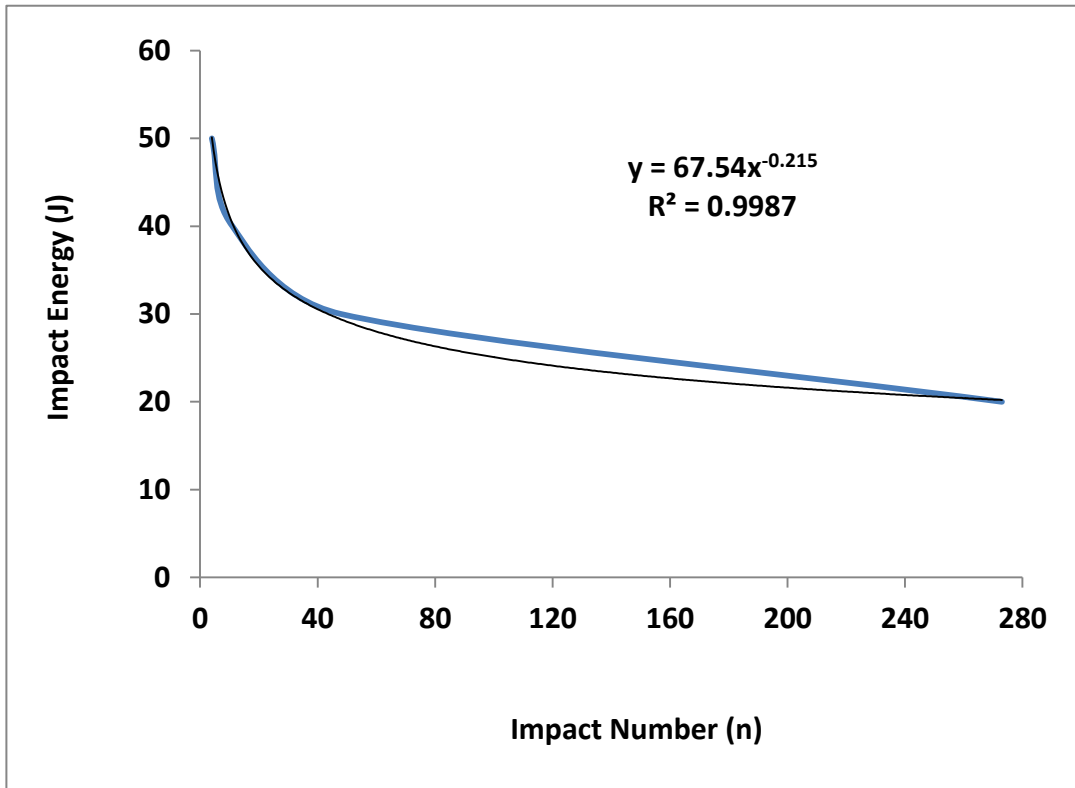
Figure 7.9 Impact energy- impact number curve of sandwich - samples.

In order to see the relationship between the impact energy and impact number, the impact number for all of the energies are plotted in figure 7.9. This figure gives the information on low energy impact-fatigue life of rotationally moulded sandwich sample. It is seen that lower than 30 J impact energy, the impact number up-to penetration increased sharply and suddenly. The opposite trend is found for the higher impact energy than 30 J. The equation of this curve is also given with this figure.

7.2   Damages occurred in repeated impact test

The digital images of low velocity repeated impacted top and bottom surfaces of sandwich-3 samples at 20, 30 , 40 and 50 J energy levels are given in Figure 7.10 to 7.13 respectively. Images at 20 and 50 J show the damage modes at the lowest and highest energy level used in this study. With 20 J impact energy, in the first impact only a small amount of
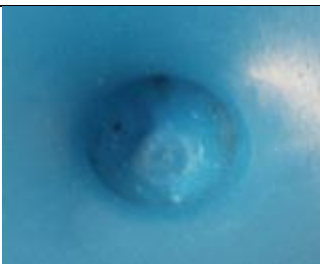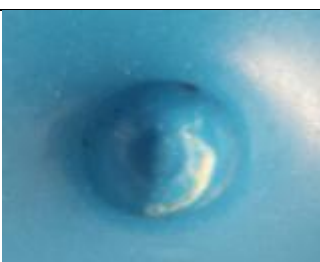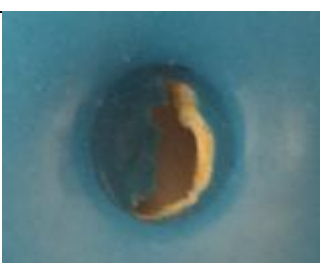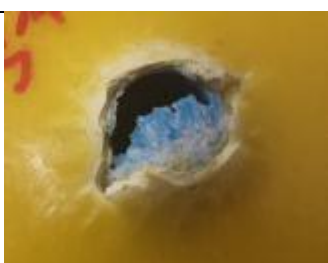
Impact No.	Top Surface	Bottom Surface
1st		
100th		
160th		
270th		
273rd		

Figure 7.10 Damages at top and bottom surface during repeated impact test at 20 J of sandwich-3 samples.
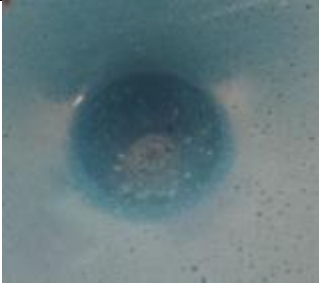
Impact No.	Top Surface	Bottom Surface
1st		
10th		
35th		
45th		
48th		

Figure 7.11 Damages at top and bottom surface during repeated impact test at 30 J of sandwich-3 samples.

Impact No.	Top Surface	Bottom Surface
1st		
5th		
9th		
11th		
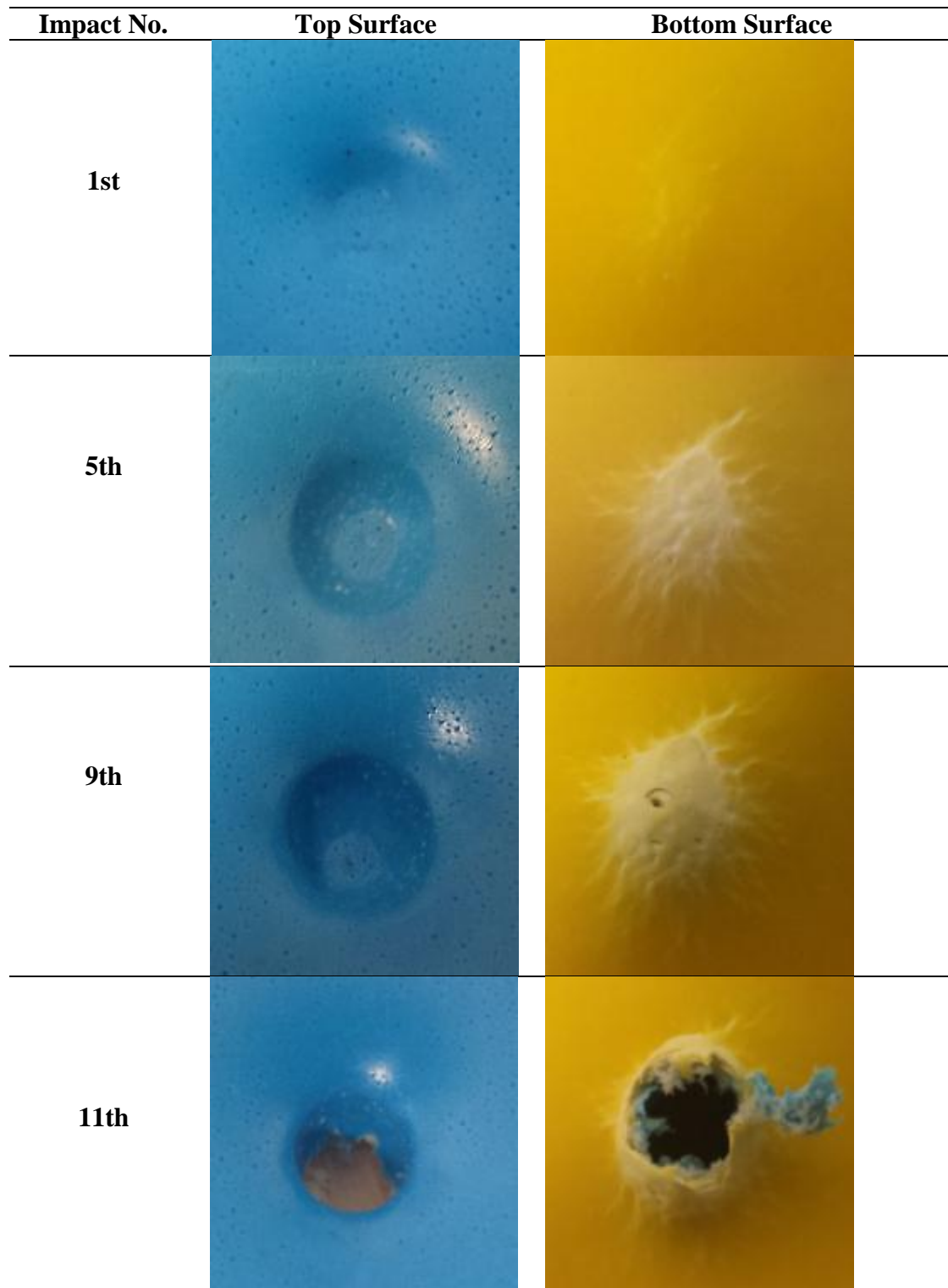
Figure 7.12 Damages at top and bottom surface during repeated impact test at 40 J of sandwich-3 samples.

Impact No.	Top Surface	Bottom Surface
1st		
3rd		
4th		
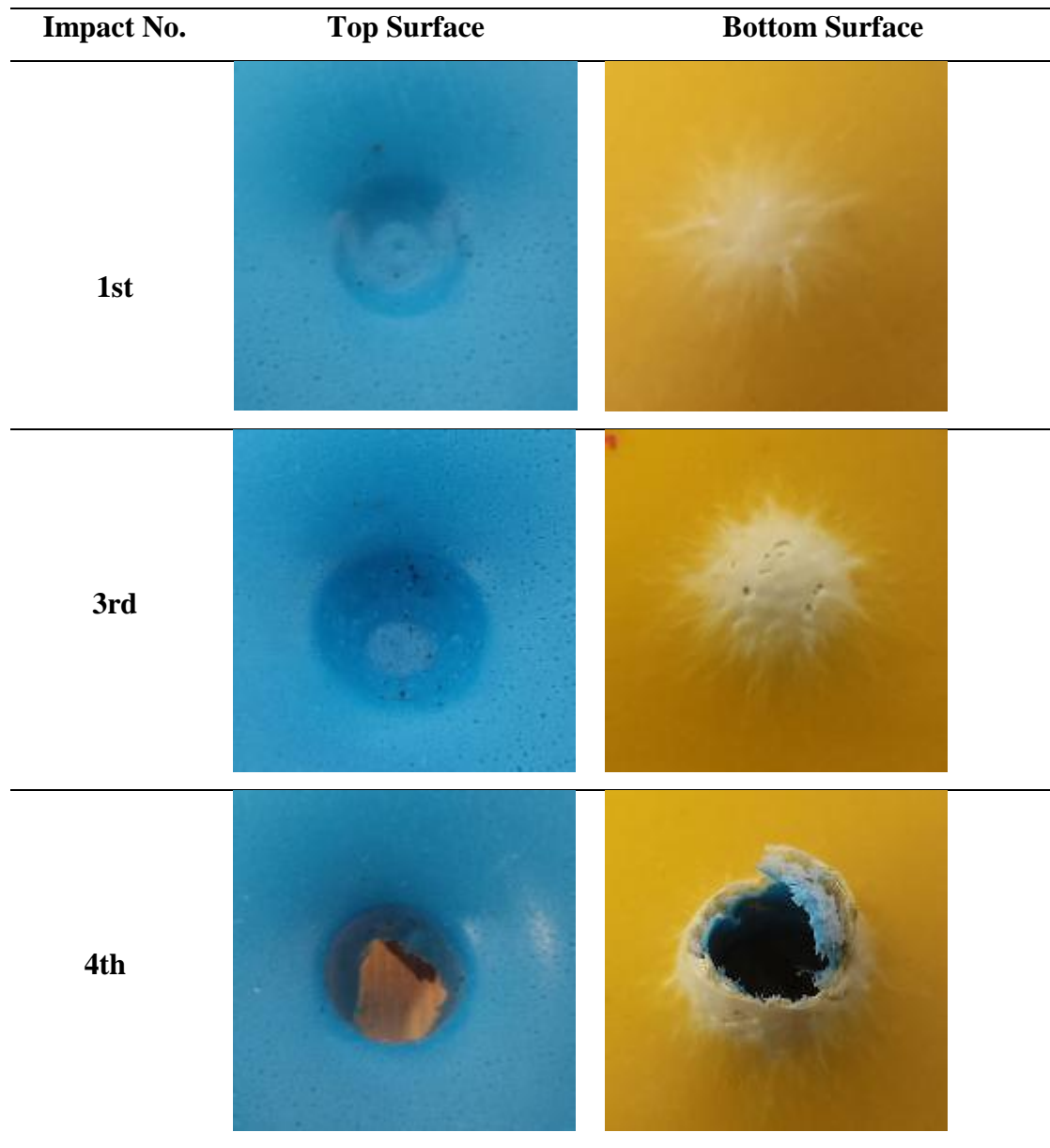
Figure 7.13 Damages at top and bottom surface during repeated impact test at 50 J of sandwich-3 samples.

indentation depth is clearly seen without any deformation visible in the bottom surface. With the increase in impact number, the indentation depth in the top skin is increased. Therefore crushing and consolidation of the core layer with corresponding overall local thickness reduction of the sandwich section is observed. Deformation in the bottom surface

is also observed to increase with impact number once crushing of the core layer has taken place. In the 100th impact these damage modes are noticed clearly. Due to the plastic and ductile deformation, white stretches are found in the bottom surface. In core layer thickness reduction is observed and in the top surface an increase in indentation depth occurred. White stretches in bottom surface continues to grow with the further increase of impact number and create open point or cracks or fractures in the bottom surface. In the impacted zone the core layer also get stretched with the creation of cracks or fractures because of the growing indentation depth in the top skin. Images of top and bottom surfaces at the 160th impact (Figure 7.10) reveal this feature. After the initial cracks appear in the bottom layer these increase slowly with the impact number and at this stage most of the impact load is carried by the top skin layer leading creation of crack in the top skin and subsequent penetration of the whole structure. These incidents are clearly seen in 220th and 273rd impact. At 30, 40 and 50 J energy level similar mechanism for damage initiation and propagation is also observed.

7.3   Conclusion from low velocity repeated impact properties analysis

In this study repeated impact behaviour of the rotationally moulded sandwich samples with 2 mm thickness for outer and inner layer and 4 mm thickness for core layer were studied. The findings are stated as follows-

- It is observed that impact number is increased for the penetration of sandwich sample with the decrease of the impact energy. Here at 20 J the highest number of impact events is found for the sandwich samples while the lowest impact number is counted for the 50 J impact energy.
- In the peak impact force-impact number curve three regions are identified. An equation is also developed from the impact energy-impact number curve for prediction of the total number of repeated impact for penetration of the sandwich samples at various energy levels.

- Indentation depth in the first impact event is found to be increased with the impact number and creates core crushing, consolidation, densification in the core layer with plastic deformation in the bottom surface. For further increase of impact number, open points or cracks are developed in the bottom surface, stretching and cracking in the impact zone of the core layer leading to crack initiation and propagation in the top surface and thus full penetration of the sample is happened.

- Sandwich samples with various skin and core thickness combination could be tested in future for developing appropriate mathematical model of the impact energy-impact number relation that will predict the number of repeated impact events to penetrate the sandwich samples at various sandwich thickness combinations and impact energy levels as well.

Chapter 8. Conclusion and Future work

This chapter summarises the major findings of the research carried out in this work. In addition some recommendations for further work are also suggested.

8.1 Microstructural analysis of rotationally moulded plastics

Crystal structure, amorphous and crystal thickness, thermal behaviour and melting point, degree of crystallinity, polymer structures and side chain quantity, storage and loss modulus and damping factor were investigated for rotationally moulded PE and PP plastics with X-ray scattering, DSC, solid-state NMR and DMTA analysis. The following conclusions are drawn from this study-

- Only orthorhombic crystal structure is found in both PE plastics in WAXS and DSC analysis. Solid-state NMR testing observes hexyl side branches in PE plastics microstructure and confirms PE-1 and PE-2 as ethylene-1-octene copolymers. Larger amorphous and crystal thicknesses are found for PE-2 in SAXS analysis.

- In DMTA analysis, better storage and loss modulus curves are found for PE-2. Higher α and β relaxation peak of PE-2 at higher temperature compared to PE-1 are noticed for the   larger crystal and amorphous thicknesses of PE-2 than that of PE-1.

- PP-1 has only α crystal in its structure while PP-2 contains both of the α and γ crystal structure, observed in WAXS analysis. DSC analysis also confirms the α and γ crystal structure in PP-2. PP-1and PP-2 are identified as propylene-ethylene block and random copolymers respectively in NMR investigation.

- PP-1 has higher molecular weight compared to PP-2 as MFI values for PP-1 is lower than PP-2. In this work, molecular weight effect on higher loss modulus and β relaxation peak is not found for PP-1 since DMTA analysis proves higher loss modulus and the β relaxation peak for PP-2 compared to PP-1. Therefore it is concluded; thicker amorphous region found in SAXS analysis for PP-2 is responsible for better loss modulus curve in DMTA analysis.

8.2 Fracture toughness and impact properties analysis of the rotationally moulded PE and PP plastics

Fracture toughness of rotationally moulded plastics particularly for PE and PP is investigated in this study for the first time. For this single edge notched samples are developed and tested according to the guidelines of the elastic plastic fracture mechanics at static loading rate (1 mm/min) at room temperature. In this study, impact properties and fracture behaviour are also investigated at drop weight impact testing condition of rotationally moulded PE and PP from -40ºC to 30ºC temperature . Microstructural details investigated in Chapter 4 are used here to analyse the measured fracture toughness and impact properties of the plastics. The following conclusions can be drawn-

8.2.1 Fracture toughness

- PE-2 shows better fracture toughness than that of PE-1. Higher amorphous and crystal thicknesses are found for PE-2 compared to PE-1 in WAXS and SAXS analysis which are related to toughness property.

- The thicker amorphous region in PE-2 contains flexible chain structures which lead to easier micro-voids formation, absorbing more energy and resulting in increased toughness values. Greater perfection of the crystals within the higher crystal thickness also contributes to micro-voiding in the amorphous region before crystallite shearing occurs and enhances toughness.

- PP-2 exhibits the higher toughness compared to PP-1. The γ crystal structure increases the resistance to the deformation and greater plastic deformation is observed in the fracture surface for PP-2 which is behind for the observed higher fracture toughness.

- Lower fracture toughness values are measured for rotationally moulded PE and PP compared to those published in the literature for other moulding processes such as injection moulding process. This might be due to the unique characteristics such as longer heating and lower rate of cooling cycle of rotational moulding process.

8.2.2 Impact properties

- Better impact properties are found for PE-2 compared to PE-1. In the dynamic mechanical analysis three transitions are clearly observed for both of PE materials. Loss modulus and the β relaxation peak show a clear relation with the impact properties for PE-2. Higher values of these two factors are found to increase the impact properties in PE-2. Higher density in PE-2 is supposed to reduce the β relaxation peak and impact property which is not observed in this work. Therefore it is concluded that the larger amorphous thickness are considered to be responsible for the increase of the β relaxation peak and loss modulus that is related to better impact properties.

- PP-2 and PP-1 show the constant and similar impact properties from -40ºC to 10ºC. After this a sudden increase in impact properties is noticed only for PP-2 which is clearly related to the higher β relaxation peak the loss modulus curve. It is believed that the γ crystal is also responsible for the improved impact properties of PP-2 at higher temperatures.

The findings of this work provide a better understanding about the suitability and fracture behaviour of these tested materials subjected to real-world external static and dynamic loads and it is hoped this increased understanding will widen the range of potential applications for rotationally moulded components.

8.3 Low velocity impact properties analysis of rotationally moulded skin-foam-skin sandwich structure

Rotationally moulded sandwich composites are manufactured at four different skin-core thickness combinations and tested under low velocity impact condition. Force – displacement curves, peak impact force, contact time and deflections are found from the test and damages are also analysed. Following conclusions are found from this work-

- An increase in both skin and core layer thickness is found to able to increase the bending stiffness and resistance of the sandwich structure during the low velocity

impact events. Between them, skin thickness is contributing more to enhance the impact resistance of the sandwich samples.

- It is observed that increasing the skin thickness double enhances the fracture starts or penetration energy level more than two times while for the foam core less than two times resistances are found.

- Indentation depth in top surface, protrusion in bottom surface, crushing and consolidation in core layer are identified as the damage modes. These damage modes are noticed to be increased with the increase of the energy level for all of the thicknesses.

- No delamination at core/skin interface is observed.

- Due to the bending in impact loading, fracture or crack starts from the bottom surface, continues to grow in the core layer, reaches at the top skin and finally the top surface gets the penetration.

- Thicker skin layer increases impact resistance by providing a better accommodation for more crushing and consolidation in core layer and enhances bending or displacement capability of the sandwich structure compared to thicker core layer that ultimately prevents fracture initiation or penetration at higher impact energy level.

- No catastrophic or localised failure is observed here for core or skin layer which is considered to be advantageous for the improvement of mechanical performance.

8.4 Low velocity repeated impact event of rotationally moulded sandwich structure

In this study repeated impact behaviour of the rotationally moulded sandwich samples were studied. For this only sandwich -3 samples are tested. The samples are subjected to impact event repeatedly up-to penetration at each energy level. The findings are listed below-

- Higher impact number is needed for the penetration at lower energy level as expected and lower impact number is found for higher energy level. At 20 J impact energy, after 273 repeated impacts sandwich samples are penetrated while for 50 J only four repeated impacts are found for the penetration of the samples.

- In peak impact force-impact number curve three regions are identified. An equation is also developed from the impact energy-impact number curve for prediction of the impact-fatigue of these samples.

- Indentation depth in the first impact event is found to be increased with the impact number and creates core crushing, consolidation, densification in the core layer with plastic deformation in the bottom surface. For further increase of impact number, open points or cracks are developed in the bottom surface; stretching and cracking in the impact zone of the core layer leading to crack initiation, propagation in the top surface and full penetration of the sample are identified.

8.5 Recommendations for future work

Based on the research works carried out here and conclusions made above, the following recommendations are drawn-

- Analysis and comparison of fracture toughness of the plastics made of rotational moulding and other moulding processes such as injection , compression moulding process would be interesting and will provide the better insight for the observed lower fracture toughness in rotational moulding process in this work.

- Investigation of fracture toughness of rotationally moulded plastics at various temperatures at static and dynamic loading rate.

- It would be interesting to study the low velocity impact properties of the rotationally moulded sandwich samples made of different core density.

- Analysis of mechanical properties particularly the compression properties of rotationally moulded polyethylene plastics and foam materials for getting more insight about the damage mechanism during low velocity impact event of rotationally moulded sandwich structures.

- Analysis of damages during the impact event by using non-destructive methods such as C-scan and X-ray imaging will provide more understanding in damage initiation and progression mechanisms during impact event.

- Development of a mathematical model to analyse the low velocity impact properties of rotationally moulded sandwich samples.

- It would be interesting to analyse the high velocity impact properties of these samples.

- Experimental investigation of repeated impact properties of sandwich samples at various skin-core thickness combinations for developing an appropriate mathematical model of the impact energy-impact number relation that will predict the number of repeated impact events to penetrate the sandwich samples at various thickness and impact energy levels.

References

Abrate, S., 1997. Localized impact on sandwich structures with laminated facings. *Applied Mechanics Reviews,* 50 (2), 69-82.

Abrate, S., 2005. *Impact on composite structures.* Cambridge university press.

Akatay, A., Bora, M. Ö., Çoban, O., Fidan, S., and Tuna, V., 2015. The influence of low velocity repeated impacts on residual compressive properties of honeycomb sandwich structures. *Composite Structures,* 125, 425-433.

Akay, M., and Hanna, R., 1990. A comparison of honeycomb-core and foam-core carbon-fibre/epoxy sandwich panels. *Composites,* 21 (4), 325-331.

Alamo, R. G., Ghosal, A., Chatterjee, J., and Thompson, K. L., 2005. Linear growth rates of random propylene ethylene copolymers. The changeover from γ dominated growth to mixed (α+ γ) polymorphic growth. *Polymer,* 46 (20), 8774-8789.

Archer, E., Harkin-Jones, E., Kearns, M., and Fatnes, A.-M., 2007. The rotational molding characteristics of metallocene polyethylene skin/foam structures. *Journal of Cellular Plastics,* 43 (6), 491-504.

Archer, E., Harkin-Jonesy, E., Kearns, M., and Fatnes, A., 2003. Investigation of the processing characteristics and mechanical properties of metallocenecatalysed polyethylene foams for rotational moulding. *Journal of cellular plastics,* 39 (6), 487-497.

Astm-D3763-02. Astm d3763-02 standard test method for high speed puncture properties of plastics using load and displacement sensors.

Astm-D6068-96. 2002. Astm : D6068-96 (reapproved 2002) standard test method for determining j-r curve of plastic materials.

Atas, C., and Sevim, C., 2010. On the impact response of sandwich composites with cores of balsa wood and pvc foam. *Composite Structures,* 93 (1), 40-48.

Bai, H., Luo, F., Zhou, T., Deng, H., Wang, K., and Fu, Q., 2011. New insight on the annealing induced microstructural changes and their roles in the toughening of β-form polypropylene. *Polymer,* 52 (10), 2351-2360.

Bárány, T., Czigány, T., and Karger-Kocsis, J., 2010. Application of the essential work of fracture (ewf) concept for polymers, related blends and composites: A review. *Progress in Polymer Science,* 35 (10), 1257-1287.

Barry, D., and Delatycki, O., 1992. The effect of molecular structure and polymer morphology on the fracture resistance of high-density polyethylene. *Polymer,* 33 (6), 1261-1265.

Benhamena, A., Aminallah, L., Bouiadjra, B. B., Benguediab, M., Amrouche, A., and Benseddiq, N., 2011. J integral solution for semi-elliptical surface crack in high density poly-ethylene pipe under bending. *Materials & Design,* 32 (5), 2561-2569.

Bernard, M. L., and Lagace, P. A., 1989. Impact resistance of composite sandwich plates. *Journal of Reinforced Plastics and Composites,* 8 (5), 432-445.

Bland, P., and Pitakthapanaphong, S., 2005. *A discussion on the role played by velocity in impact mechanics.* Paper presented at the 19th Conference of Mechanical Engineering Network of Thailand, Phuket, Thailand.

Boccaccio, A., Casavola, C., Lamberti, L., and Pappalettere, C., 2013. Structural response of polyethylene foam-based sandwich panels subjected to edgewise compression. *Materials,* 6 (10), 4545-4564.

Bora, M. Ö., Çoban, O., Sinmazçelik, T., Cürgül, İ., and Günay, V., 2009. On the life time prediction of repeatedly impacted thermoplastic matrix composites. *Materials & Design,* 30 (1), 145-153.

Botha, L., Sinha, P., Joubert, S., Duveskog, H., and Van Reenen, A., 2014. Solution and solid-state nmr characterization of heterophasic propylene–ethylene copolymers (hepc) with increasing ethylene content. *European Polymer Journal,* 59, 94-104.

Cantwell, W., and Morton, J., 1989. Comparison of the low and high velocity impact response of cfrp. *Composites,* 20 (6), 545-551.

Cantwell, W., and Morton, J., 1991. The impact resistance of composite materials—a review. *composites,* 22 (5), 347-362.

Casavola, C., Moramarco, V., and Pappalettere, C., 2014. Impact response of polyethylene sandwich panel obtained by rotational moulding. *Fatigue & Fracture of Engineering Materials & Structures,* 37 (12), 1377-1385.

Cerrada, M. L., Pérez, E., Benavente, R., Ressia, J., Sarmoria, C., and Vallés, E. M., 2010. Gamma polymorph and branching formation as inductors of resistance to electron beam irradiation in metallocene isotactic polypropylene. *Polymer Degradation and Stability,* 95 (4), 462-469.

Chai, G. B., and Zhu, S., 2011. A review of low-velocity impact on sandwich structures. *Proceedings of the Institution of Mechanical Engineers, Part L: Journal of Materials Design and Applications,* 225 (4), 207-230.

Chan, M., and Williams, J., 1981. Plane strain fracture toughness testing of high density polyethylene. *Polymer Engineering & Science,* 21 (15), 1019-1026.

Chan, M., and Williams, J., 1983. Slow stable crack growth in high density polyethylenes. *Polymer,* 24 (2), 234-244.

Chan, M., and Williams, J., 1993. J-integral studies of crack initiation of a tough high density polyethylene. *International Journal of Fracture,* 23 (2), 145-159.

Chen, H., Karger-Kocsis, J., Wu, J., and Varga, J., 2002. Fracture toughness of α-and β-phase polypropylene homopolymers and random-and block-copolymers. *Polymer,* 43 (24), 6505-6514.

Çoban, O., Bora, M. Ö., Sinmazçelik, T., Cürgül, I., and Günay, V., 2009. Fracture morphology and deformation characteristics of repeatedly impacted thermoplastic matrix composites. *Materials & Design,* 30 (3), 628-634.

Comotti, A., Simonutti, R., Bracco, S., Castellani, L., and Sozzani, P., 2001. Simultaneous crystallization of isotactic and syndiotactic sequences of polypropylene. *Macromolecules,* 34 (14), 4879-4885.

Compston, P., Styles, M., and Kalyanasundaram, S., 2006. Low energy impact damage modes in aluminum foam and polymer foam sandwich structures. *Journal of sandwich structures and materials,* 8 (5), 365-379.

Cramez, M., Oliveira, M., and Crawford, R., 2001. Effect of nucleating agents and cooling rate on the microstructure and properties of a rotational moulding grade of polypropylene. *Journal of materials science,* 36 (9), 2151-2161.

Cramez, M., Oliveira, M., and Crawford, R., 2002. Optimisation of rotational moulding of polyethylene by predicting antioxidant consumption. *Polymer Degradation and Stability,* 75 (2), 321-327.

Crawfoard, R. J. K., M.P. 2003. *Introduction to the rotational moulding process. In:Practical guide to rotary moulding.* Shrewsbury: GBR: Smithers Rapra.

Crawford, R., 1996. Recent advances in the manufacture of plastic products by rotomoulding. *Journal of materials processing technology,* 56 (1), 263-271.

Crawford, R., and Nugent, P., 1992. Impact strength of rotationally moulded polyethylene articles. *Plastics rubber and composites processing and applications,* 17 (1), 33-41.

Crist, B., Fisher, C. J., and Howard, P. R., 1989. Mechanical properties of model polyethylenes: Tensile elastic modulus and yield stress. *Macromolecules,* 22 (4), 1709-1718.

Cucinotta, F., Guglielmino, E., Risitano, G., and Sfravara, F., 2016. Assessment of damage evolution in sandwich composite material subjected to repeated impacts by means optical measurements. *Procedia Structural Integrity,* 2, 3660-3667.

Daniel, I. M., 2009. Impact response and damage tolerance of composite sandwich structures. *In: Dynamic failure of materials and structures*: Springer, 191-233.

Doshev, P., Lach, R., Lohse, G., Heuvelsland, A., Grellmann, W., and Radusch, H.-J., 2005. Fracture characteristics and deformation behavior of heterophasic ethylene–propylene copolymers as a function of the dispersed phase composition. *Polymer,* 46 (22), 9411-9422.

Du H, Z. Y., Liu H, Liu K, Jin M, Li X, Zhang J. 2014. Influence of phase morphology and crystal structure on the toughness of rubber-toughened isotatic polypropylene blends,

this. *Polymer (2014)*, doi: 10.1016/j.polymer.2014.1008.1012.

.

Duffy, K. 1990. Method for forming expanded foam rotomolded products: Google Patents.

El-Bagory, T. M., Sallam, H. E., and Younan, M. Y., 2014. Effect of strain rate, thickness, welding on the j–r curve for polyethylene pipe materials. *Theoretical and Applied Fracture Mechanics,* 74, 164-180.

Fasce, L., Pettarín, V., Bernal, C., and Frontini, P., 1999. Mechanical evaluation of propylene polymers under static and dynamic loading conditions. *Journal of applied polymer science,* 74 (11), 2681-2693.

Fasce, L. A., Frontini, P. M., Wong, S. C., and Mai, Y. W., 2004. Polypropylene modified with elastomeric metallocene-catalyzed polyolefin blends: Fracture behavior and development of damage mechanisms. *Journal of Polymer Science Part B: Polymer Physics,* 42 (6), 1075-1089.

Feng, Y., Jin, X., and Hay, J., 1998. Dynamic mechanical behavior analysis for low ethylene content polypropylene copolymers. *Journal of applied polymer science,* 68 (3), 395-401.

Fernando, P., and Williams, J., 1980. Plane stress and plane strain fractures in polypropylene. *Polymer Engineering & Science,* 20 (3), 215-220.

Ferrer-Balas, D., Maspoch, M. L. S., and Mai, Y.-W., 2002. Fracture behaviour of polypropylene films at different temperatures: Fractography and deformation mechanisms studied by sem. *Polymer,* 43 (10), 3083-3091.

Friedrich, K., 1979. Effect of morphology on the strength and fracture processes of polypropylene. *Kunststoffe-German Plastics,* 69 (11), 796-801.

Gao, X., Wang, L., Luo, H., Zou, Q., Feng, N., and Feng, J., 2010. Crystalline phases in ethylene copolymers studied by solid-state nmr and dsc. *Macromolecules,* 43 (13), 5713-5722.

Geng, C., Yang, G., Bai, H., Li, Y., Fu, Q., and Deng, H., 2014. Towards high-performance polypropylene and its random copolymer: Insight into toughening mechanism of supercritical carbon dioxide assisted annealing. *The Journal of Supercritical Fluids,* 87, 83-92.

Gensler, R., Plummer, C., Grein, C., and Kausch, H.-H., 2000. Influence of the loading rate on the fracture resistance of isotactic polypropylene and impact modified isotactic polypropylene. *Polymer,* 41 (10), 3809-3819.

Godinho, J., Cunha, A., and Crawford, R., 2002. Prediction of the mechanical properties of polyethylene parts produced by different moulding methods. *Proceedings of the Institution of Mechanical Engineers, Part L: Journal of Materials Design and Applications,* 216 (3), 179-191.

Gupta, P., Wilkes, G. L., Sukhadia, A. M., Krishnaswamy, R. K., Lamborn, M. J., Wharry, S. M., Tso, C. C., Deslauriers, P. J., Mansfield, T., and Beyer, F. L., 2005. Does the length of the short chain branch affect the mechanical properties of linear low density polyethylenes? An investigation based on films of copolymers of ethylene/1-butene, ethylene/1-hexene and ethylene/1-octene synthesized by a single site metallocene catalyst. *Polymer,* 46 (20), 8819-8837.

Hale, G. E., and Ramsteiner, F., 2001. J-fracture toughness of polymers at slow speed. *Fracture mechanics testing methods for polymers, adhesives and composites,* 28, 123.

Hamad, K., Kaseem, M., and Deri, F., 2013. Recycling of waste from polymer materials: An overview of the recent works. *Polymer degradation and stability,* 98 (12), 2801-2812.

Hashemi, S., and Williams, J., 1986. A fracture toughness study on low density and linear low density polyethylenes. *Polymer,* 27 (3), 384-392.

Heeley, E. L., Hughes, D. J., El Aziz, Y., Taylor, P. G., and Bassindale, A. R., 2014. Morphology and crystallization kinetics of polyethylene/long alkyl-chain substituted polyhedral oligomeric silsesquioxanes (poss) nanocomposite blends: A saxs/waxs study. *European Polymer Journal,* 51, 45-56.

Isasi, J. R., Mandelkern, L., Galante, M. J., and Alamo, R. G., 1999. The degree of crystallinity of monoclinic isotactic poly (propylene). *Journal of Polymer Science Part B: Polymer Physics,* 37 (4), 323-334.

Ismail, Y., Richardson, M., and Olley, R., 2001. Optimizing impact properties of pp composites by control of spherulitic morphology. *Journal of applied polymer science,* 79 (9), 1704-1715.

Iso, B., 2000. British standards, bs iso 13586:2000, plastics- determination of fracture toughness (g_{ic} and k_{ic})- linear elastic fracture mechanics approach (lefm).

Jancar, J., Dianselmo, A., Dibenedetto, A., and Kucera, J., 1993. Failure mechanics in elastomer toughened polypropylene. *Polymer,* 34 (8), 1684-1694.

Jemian, J. I. a. P. R., 2009. Irena: Tool suite for modeling and analysis of small-angle scattering. *J. Appl. Cryst,* 42 (2), 347-353.

Kalyon, D. M., and Moy, F. H., 1988. Ultimate properties of blown films of linear low density polyethylene resins as affected by alpha-olefin comonomers. *Polymer Engineering & Science,* 28 (23), 1551-1558.

Kawaguchi, T., Nishimura, H., Ito, K., Sorimachi, H., Kuriyama, T., and Narisawa, I., 2004. Impact fatigue properties of glass fiber-reinforced thermoplastics. *Composites science and technology,* 64 (7), 1057-1067.

Kelly, P., 1981. A microscopic examination of rotomoulded polyethylene. *Du Pont Canada, undated, vol. n pp.*

Khanna, Y. P., Turi, E. A., Taylor, T. J., Vickroy, V. V., and Abbott, R. F., 1985. Dynamic mechanical relaxations in polyethylene. *Macromolecules,* 18 (6), 1302-1309.

Kodjie, S. L., Li, L., Li, B., Cai, W., Li, C. Y., and Keating, M., 2006. Morphology and crystallization behavior of hdpe/cnt nanocomposite. *Journal of Macromolecular Science, Part B: Physics,* 45 (2), 231-245.

Kontopoulou, M., and Vlachopoulos, J., 1999. Bubble dissolution in molten polymers and its role in rotational molding. *Polymer Engineering & Science,* 39 (7), 1189-1198.

Kyu, T. a. N., Domasius. 2008. Overview of polyolefin blends , polyolefin blends.

Lezak, E., and Bartczak, Z., 2007. Plastic deformation of the γ phase isotactic polypropylene in plane-strain compression at elevated temperatures. *Macromolecules,* 40 (14), 4933-4941.

Lezak, E., Bartczak, Z., and Galeski, A., 2006a. Plastic deformation behavior of β-phase isotactic polypropylene in plane-strain compression at room temperature. *Polymer,* 47 (26), 8562-8574.

Lezak, E., Bartczak, Z., and Galeski, A., 2006b. Plastic deformation of the γ phase in isotactic polypropylene in plane-strain compression. *Macromolecules,* 39 (14), 4811-4819.

Li, Z.-M., Qian, Z.-Q., Yang, M.-B., Yang, W., Xie, B.-H., and Huang, R., 2005. Anisotropic microstructure-impact fracture behavior relationship of polycarbonate/polyethylene blends injection-molded at different temperatures. *Polymer,* 46 (23), 10466-10477.

Lim, T. S., and Lee, C. S., 2004. Failure modes of foam core sandwich beams under static and impact loads. *Journal of Composite Materials,* 38 (18), 1639-1662.

Liu, D., and Malvern, L. E., 1987. Matrix cracking in impacted glass/epoxy plates. *Journal of Composite Materials,* 21 (7), 594-609.

Liu, S. J., and Tsai, C. H., 1999. An experimental study of foamed polyethylene in rotational molding. *Polymer Engineering & Science,* 39 (9), 1776-1786.

Lu, X., Qian, R., and Brown, N., 1995. The effect of crystallinity on fracture and yielding of polyethylenes. *Polymer,* 36 (22), 4239-4244.

Mai, Y.-W., and Cotterell, B., 1986. On the essential work of ductile fracture in polymers. *International Journal of Fracture,* 32 (2), 105-125.

Mohan, K., Yip, T.-H., Sridhar, I., and Seow, H., 2007. Effect of face sheet material on the indentation response of metallic foams. *Journal of materials science,* 42 (11), 3714-3723.

Morhain, C., and Velasco, J., 2001. Determination of jr curve of polypropylene copolymers using the normalization method. *Journal of materials science,* 36 (6), 1487-1499.

Nedkov, E., and Dobreva, T., 2004. Wide and small-angle x-ray scattering study of isotactic polypropylene gamma irradiated in bulk. *European polymer journal,* 40 (11), 2573-2582.

Oliveira, M., and Cramez, M., 2001. Rotational molding of polyolefins: Processing, morphology, and properties. *Journal of Macromolecular Science, Part B,* 40 (3-4), 457-471.

Oliveira, M., Cramez, M., and Crawford, R., 1996. Structure-properties relationships in rotationally moulded polyethylene. *Journal of materials science,* 31 (9), 2227-2240.

Olsson, R., 2000. Mass criterion for wave controlled impact response of composite plates. *Composites Part A: Applied Science and Manufacturing,* 31 (8), 879-887.

Olsson, R., 2003. Closed form prediction of peak load and delamination onset under small mass impact. *Composite Structures,* 59 (3), 341-349.

Ozdemir, O., Karakuzu, R., and Al-Shamary, A. K. J., 2015. Core-thickness effect on the impact response of sandwich composites with poly (vinyl chloride) and poly (ethylene terephthalate) foam cores. *Journal of Composite Materials,* 49 (11), 1315-1329.

Park, S. D., Todo, M., Arakawa, K., and Koganemaru, M., 2006. Effect of crystallinity and loading-rate on mode i fracture behavior of poly (lactic acid). *Polymer,* 47 (4), 1357-1363.

Pegoretti, A., Castellani, L., Franchini, L., Mariani, P., and Penati, A., 2009. On the essential work of fracture of linear low-density-polyethylene. I. Precision of the testing method. *Engineering Fracture Mechanics,* 76 (18), 2788-2798.

Pereira, R., Mano, E., and Dias, M., 1998. Waxs study on orthorhombic crystalline phases in hot-drawn high density polyethylene: Polymer characterisation. *Polymer Testing,* 16 (6), 589-601.

Pérez, E., Zucchi, D., Sacchi, M. C., Forlini, F., and Bello, A., 1999. Obtaining the γ phase in isotactic polypropylene: Effect of catalyst system and crystallization conditions. *Polymer,* 40 (3), 675-681.

Pick, L., and Harkin-Jones, E., 2005. An investigation of the relationship between thermal relaxations and the impact performance of rotationally moulded linear low density polyethylenes. *Proceedings of the Institution of Mechanical Engineers, Part L: Journal of Materials Design and Applications,* 219 (1), 1-10.

Pick, L. T., and Harkin-Jones, E., 2003. An investigation into the relationship between the impact performance of rotationally molded polyethylene products and their dynamic mechanical properties. *Polymer engineering and science,* 43 (4), 905.

Pick, L. T., and Harkin-Jones, E., 2003. An investigation into the relationship between the impact performance of rotationally molded polyethylene products and their dynamic mechanical properties. *Polymer Engineering & Science,* 43 (4), 905-918.

Pollard, M., Klimke, K., Graf, R., Spiess, H. W., Wilhelm, M., Sperber, O., Piel, C., and Kaminsky, W., 2004. Observation of chain branching in polyethylene in the solid state and melt via 13c nmr spectroscopy and melt nmr relaxation time measurements. *Macromolecules,* 37 (3), 813-825.

Pop-Iliev, R., Lee, K.-H., and Park, C. B., 2006. Manufacture of integral skin pp foam composites in rotational molding. *Journal of cellular plastics,* 42 (2), 139-152.

Prasad, J., 1992. Characterization of propylene-ethylene block copolymers using solid state 13c-nmr spectroscopy. *Journal of Polymer Science Part A: Polymer Chemistry,* 30 (9), 2033-2036.

Raju, K., Smith, B., Tomblin, J., Liew, K., and Guarddon, J., 2008. Impact damage resistance and tolerance of honeycomb core sandwich panels. *Journal of composite materials,* 42 (4), 385-412.

Raju, K., and Tomblin, J., 2001. Damage characteristics in sandwich panels subjected to static indentation using spherical indentors. *AIAA Paper,* 1189, 2001.

Richardson, M., and Wisheart, M., 1996. Review of low-velocity impact properties of composite materials. *Composites Part A: Applied Science and Manufacturing,* 27 (12), 1123-1131.

Robinson, P., and Davies, G., 1992. Impactor mass and specimen geometry effects in low velocity impact of laminated composites. *International Journal of Impact Engineering,* 12 (2), 189-207.

Salazar, A., Frontini, P., and Rodríguez, J., 2014. Determination of fracture toughness of propylene polymers at different operating temperatures. *Engineering Fracture Mechanics,* 126, 87-107.

Salazar, A., Rodríguez, J., Arbeiter, F., Pinter, G., and Martínez, A., 2015. Fracture toughness of high density polyethylene: Fatigue pre-cracking versus femtolaser, razor sharpening and broaching. *Engineering Fracture Mechanics,* 149, 199-213.

Salazar, A., Rodríguez, J., and Martínez, A., 2013. The role of notch sharpening on the j-fracture toughness of thermoplastic polymers. *Engineering Fracture Mechanics,* 101, 10-22.

Santarelli, E., and Frontini, P., 2001. The effects of specimen size and testing conditions on fracture toughness evaluation of polypropylene homopolymer. *Polymer Engineering & Science,* 41 (10), 1803-1814.

Sawal, N., and Hazizan, M. A., 2011. *Effect of core thicknesses on impact performance of thermoplastic honeycomb core sandwich structure under low-velocity impact loading.* Paper presented at the Key Engineering Materials.

Schrauwen, B. A., Janssen, R. P., Govaert, L. E., and Meijer, H. E., 2004. Intrinsic deformation behavior of semicrystalline polymers. *Macromolecules,* 37 (16), 6069-6078.

Shao-Yun Fu, B. L., Yiu-Wing Mai. 2009. Fracture mechanics. *In: Science & engineering of short fibre reinforced polymer composites*. USA: Woodhead Publishing Limited and CRC press LLC, 231-323.

Shao, Y., Wu, C., Cheng, S., Zhou, F., and Yan, H., 2015. Effects of toughening propylene/ethylene graft copolymer on the crystallization behavior and mechanical properties of polypropylene random-copolymerized with a small amount of ethylene. *Polymer Testing,* 41, 252-263.

Shih, W., and Jang, B., 1989. Instrumented impact testing of composite sandwich panels. *Journal of reinforced plastics and composites,* 8 (3), 270-298.

Shuaeib, F., and Soden, P., 1997. Indentation failure of composite sandwich beams. *Composites science and Technology,* 57 (9), 1249-1259.

Sınmazçelik, T., Arıcı, A. A., and Günay, V., 2006. Impact–fatigue behaviour of unidirectional carbon fibre reinforced polyetherimide (pei) composites. *Journal of materials science,* 41 (19), 6237-6244.

Sirotkin, R., and Brooks, N., 2001. The dynamic mechanical relaxation behaviour of polyethylene copolymers cast from solution. *Polymer,* 42 (24), 9801-9808.

Sjoblom, P. O., Hartness, J. T., and Cordell, T. M., 1988. On low-velocity impact testing of composite materials. *Journal of composite materials,* 22 (1), 30-52.

Spence, A., and Crawford, R., 1996. Removal of pinholes and bubbles from rotationally moulded products. *Proceedings of the Institution of Mechanical Engineers, Part B: Journal of Engineering Manufacture,* 210 (6), 521-533.

Stehling, F. C., and Mandelkern, L., 1970. The glass temperature of linear polyethylene. *Macromolecules,* 3 (2), 242-252.

Sun, Z., and Yu, F., 1991. Sem study on fracture behavior of ethylene/propylene block copolymers and their blends. *Die Makromolekulare Chemie,* 192 (6), 1439-1445.

Swei, H., Crist, B., and Carr, S., 1991. The j integral fracture toughness and damage zone morphology in polyethylenes. *Polymer,* 32 (8), 1440-1446.

T, P. L., 2004. An investigation of the impact performance of rotationally moulded plastics, thesis. *Queen's University Belfast,* Belfast.

Torres, F., and Aragon, C., 2006. Final product testing of rotational moulded natural fibre-reinforced polyethylene. *Polymer testing,* 25 (4), 568-577.

Tripathi, D., 2002. Introduction. *In: Practical guide to polypropylene*: In Rapra Practical Guide Series.Shrewsbury : RAPRA Technology. 2002, 1-8.

Varga, J., 2002. B-modification of isotactic polypropylene: Preparation, structure, processing, properties, and application. *Journal of Macromolecular Science, Part B,* 41 (4-6), 1121-1171.

Vasile, C., and Pascu, M., 2005. Basic types. *In: Practical guide to polyethylene*: Shrewsbury : RAPRA Technology., 15-28.

Vázquez-Fletes, R. C., Rosales-Rivera, L. C., Moscoso-Sánchez, F. J., Mendizábal, E., Ortega-Gudiño, P., González-Núñez, R., and Rodrigue, D., 2016. Preparation and characterization of multilayer foamed composite by rotational molding. *Polymer Engineering & Science,* 56 (3), 278-286.

Vincent, P., 1974. Impact strength and mechanical losses in thermoplastics. *Polymer,* 15 (2), 111-116.

Waigaonkar, S., Babu, B., and Prabhakaran, R. D., 2008. A new approach for resin selection in rotational molding. *Journal of Reinforced Plastics and Composites*.

Wang, M.-D., Nakanishi, E., Hashizume, Y., and Hibi, S., 1992. Fracture energy analysis of single-edge-cracked isotropic ductile polyolefins. *Polymer,* 33 (16), 3408-3414.

Wang, M.-D., Nakanishi, E., and Hibi, S., 1993. Effect of molecular weight on rolled high density polyethylene: 2. Fracture. *Polymer,* 34 (13), 2792-2798.

Wang, M., Bernard, G. M., Wasylishen, R. E., and Choi, P., 2007. A solid-state 13c nmr investigation of the morphology of single-site and ziegler-natta linear low-density polyethylenes with varying branch contents. *Macromolecules,* 40 (18), 6594-6599.

Way, J., Atkinson, J., and Nutting, J., 1974. The effect of spherulite size on the fracture morphology of polypropylene. *Journal of Materials Science,* 9 (2), 293-299.

Weidinger, A., and Hermans, P., 1961. On the determination of the crystalline fraction of isotactic polypropylene from x-ray diffraction. *Die Makromolekulare Chemie,* 50 (1), 98-115.

Williams, J., and Rink, M., 2007. The standardisation of the ewf test. *Engineering fracture mechanics,* 74 (7), 1009-1017.

Williams, J. G., 1984. *Fracture mechanics of polymer.* Chichester, West Sussex, England: Ellis Horwood Limited.

Wolfe, A. R., 1998. Plastics pipes x: Plastics pipeline systems for the millennium, conference papers, goeteborg, . *Plastics pipes X: Plastics pipeline systems for the millennium, conference papers, Goeteborg*, pp. 95–102.

Yu, J., Wang, E., Li, J., and Zheng, Z., 2008. Static and low-velocity impact behavior of sandwich beams with closed-cell aluminum-foam core in three-point bending. *International Journal of Impact Engineering,* 35 (8), 885-894.
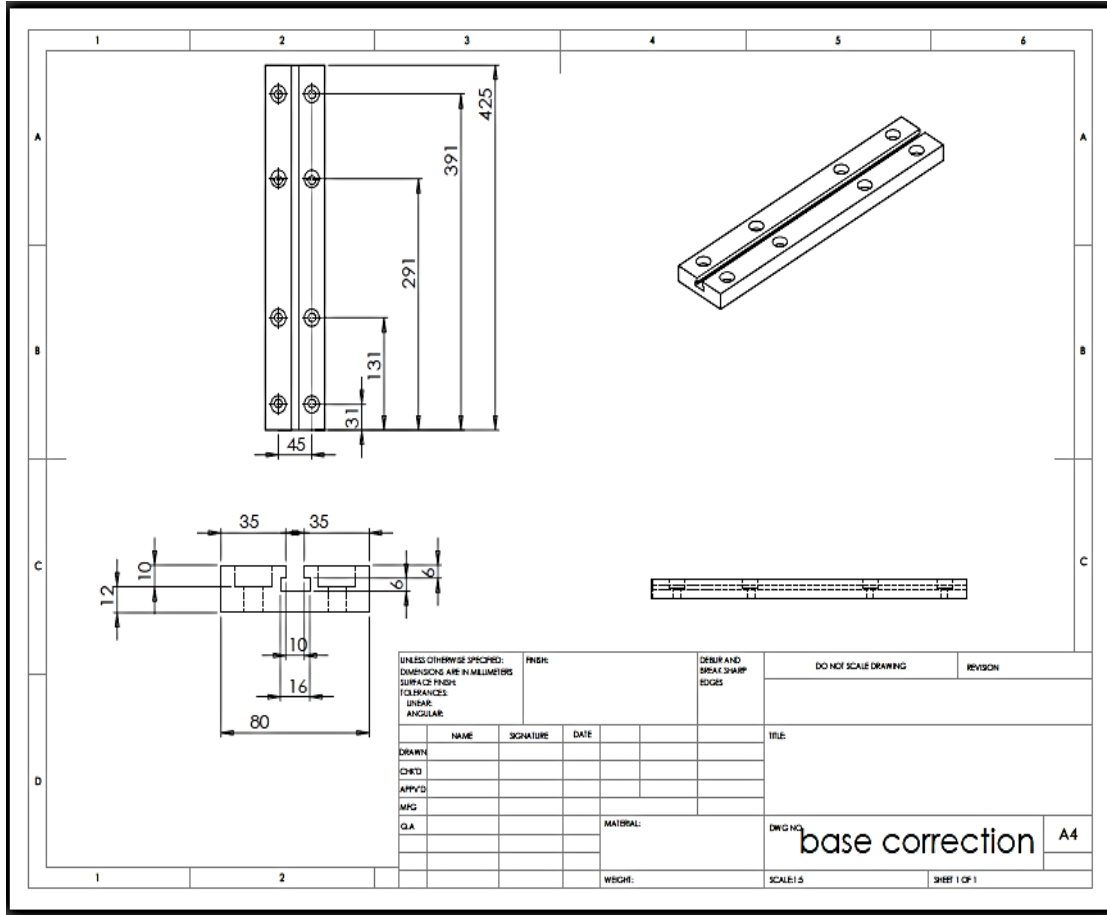
Zhou, G., Hill, M., and Hookham, N., 2007. Investigation of parameters governing the damage and energy absorption characteristics of honeycomb sandwich panels. *Journal of Sandwich Structures and Materials,* 9 (4), 309-342.

Zhou, G., Hill, M., Loughlan, J., and Hookham, N., 2006. Damage characteristics of composite honeycomb sandwich panels in bending under quasi-static loading. *Journal of Sandwich Structures and Materials,* 8 (1), 55-90.
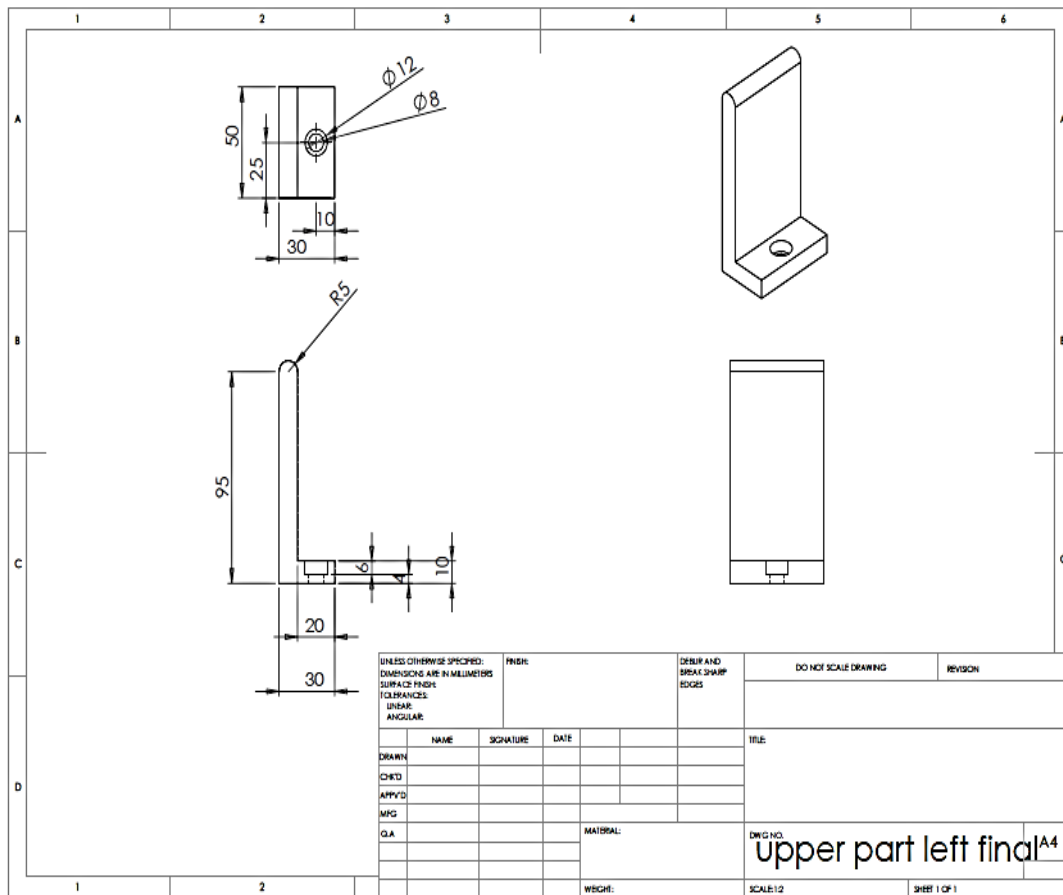
Appendix-A

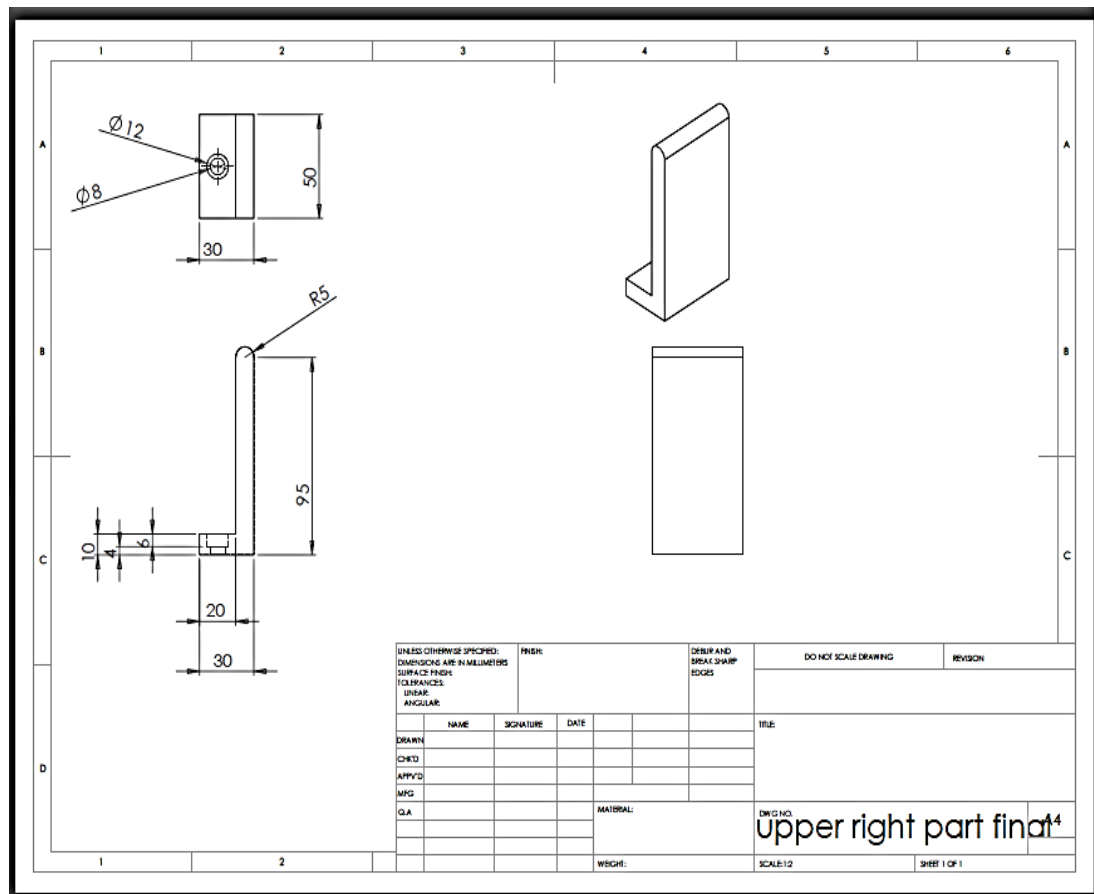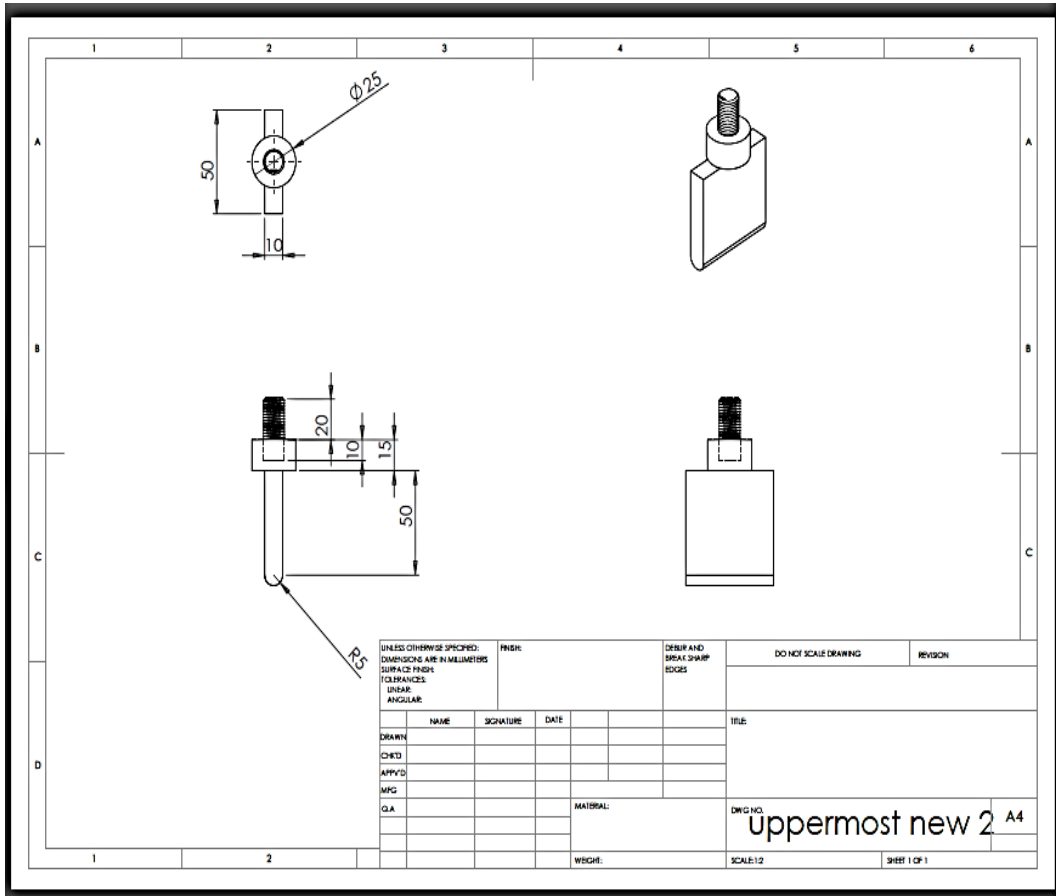**Three Point Bending Attachment Design**

Design of base-plate-

Drawing details:

	NAME	SIGNATURE	DATE			TITLE
DRAWN						
CHK'D						
APP'V'D						
MFG						
Q.A				MATERIAL:		DWG NO. base correction A4

UNLESS OTHERWISE SPECIFIED:
DIMENSIONS ARE IN MILLIMETERS
SURFACE FINISH:
TOLERANCES:
  LINEAR:
  ANGULAR:

FINISH:

DEBUR AND
BREAK SHARP
EDGES

DO NOT SCALE DRAWING   REVISION

WEIGHT: SCALE:1:5   SHEET 1 OF 1

Design of Left Roller

Technical drawing — Title block:

	NAME	SIGNATURE	DATE		TITLE:
DRAWN					
CHK'D					
APPV'D					
MFG					
Q.A			MATERIAL:		

UNLESS OTHERWISE SPECIFIED:
DIMENSIONS ARE IN MILLIMETERS
SURFACE FINISH:
TOLERANCES:
   LINEAR:
   ANGULAR:

FINISH:

DEBUR AND
BREAK SHARP
EDGES

DO NOT SCALE DRAWING   REVISION

DWG NO.
upper part left final A4

WEIGHT: SCALE:1:2   SHEET 1 OF 1

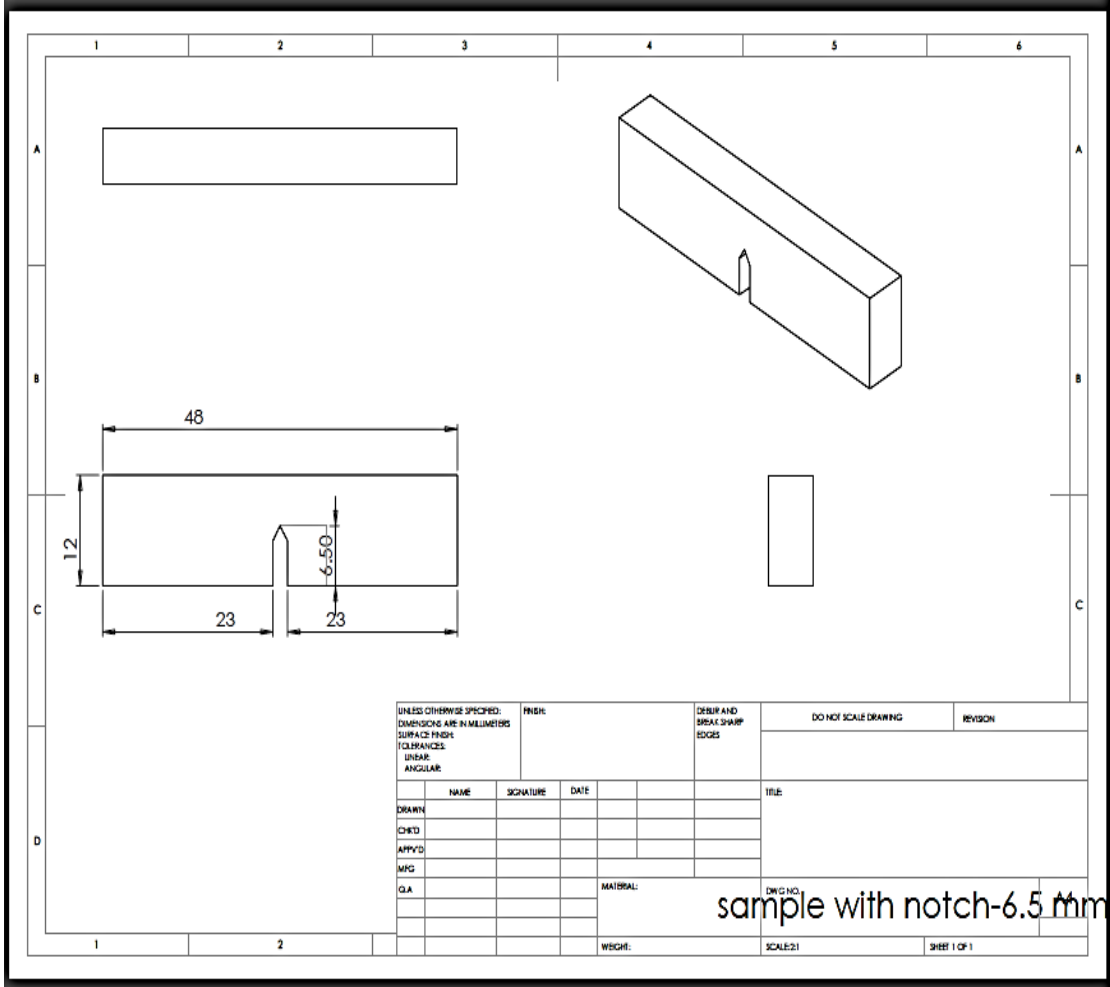**Design of Right Roller**

Design of Top Roller

Appendix-B

Test Sample Design Details-

Appendix-C

Test process for measuring fracture toughness and J-R curves for plastic materials

1. This test process describes the multiple specimen method for determining the fracture toughness and J-R curves of the polymeric materials in the elastic – plastic fracture mechanics approach based on the testing guidelines of ASTM:D6068-96 (Astm-D6068-96, 2002) and ESIS protocol (Hale, G. E. and Ramsteiner, F., 2001).

2. **Specimen configuration, size and preparation**

   Three point bend single edge notch specimens are used here. The specimen thickness (B) is 6 mm and the width (W) is the twice of the thickness, W=2B for obtaining plane strain conditions at the crack tip. The span, S, to width, W, ratio is 4. The crack should be sharp enough and pre-crack is produced by sliding a razor blade into the root of a machined notch. Here the tip radius of the pre-cracked machined notch, $\rho \leq 20\ \mu$m is maintained for all of the specimens. The original crack length, a, (machined notch plus crack) is greater than 0.5 W but less than 0.65 W. Specimens are also sidegrooved to promote the straight ductile crack front. Sidegrooves are equal in depth and have an included angle of 45º±5º with a root radius of 0.25±.05 mm. The total reduction of the thickness is not more than 0.20B.
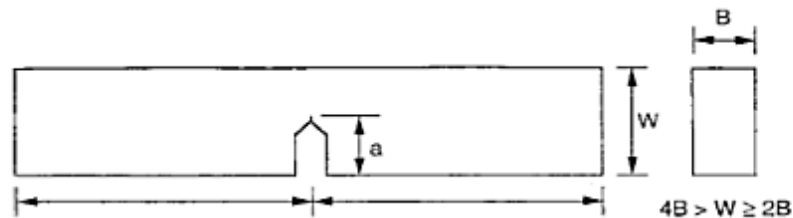

   Figure 1 Three point bend single edge notch samples (Astm-D6068-96, 2002).

3. **Loading rigs**

   For this test, a suggested test fixture is presented in Figure 2. According to this guideline a test fixture with stationary rollers of 10 mm diameter are developed here to minimize the excessive plastic deformation.
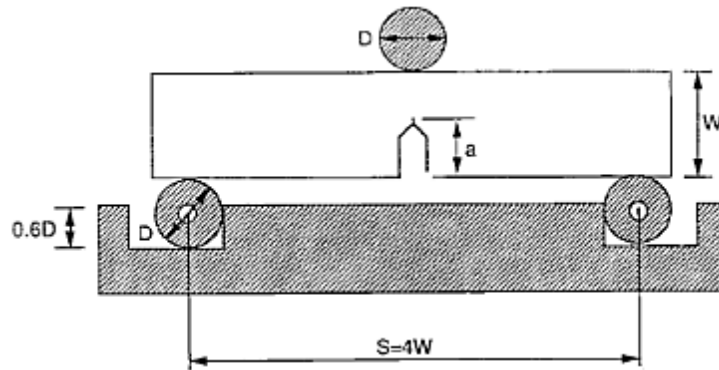
Figure 2 Suggested test fixture for single edge notch bend samples (Astm-D6068-96, 2002).

4. Displacement measurement

Displacements measurements are essential to calculate the J values from the area under the load-displacement curves. Displacement is measured from the machine crosshead displacement. Displacement data is corrected for the extraneous displacements due to the indentation effects, pin penetrations or machine compliance by conducting a separate indentation measurement. For indentation correction, an un-notched samples prepared identically is used according to the figure 3 to generate a load –displacement curve. This correction curve is then subtracted from the load-displacement curve obtained during the actual fracture test with notched samples.
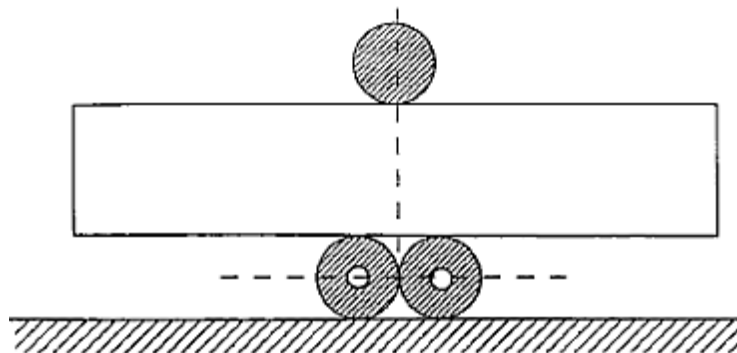

Figure 3 Arrangements for indentation correction test (Astm-D6068-96, 2002).

5. **Testing procedure**

   A series of specimens are loaded at 1mm/min loading rate to different displacements at 23º C using crosshead control of the testing machine. A minimum of seven samples are needed to generate the J-R curves mentioned in the testing guidelines. Generally the specimens are loaded to a selected displacement level that produces a crack growth at a desired level. After recording the load-displacement data, the specimen is unloaded and broken to measure the crack fronts. High speed impact is used for breaking operation of the tested specimens with 5-10 minutes prior cooling in liquid nitrogen in order to produce a brittle failure so that the amount of crack growth can be measured precisely. The J value is calculated from the recorded load-displacement curve. In this way each specimen provides a set of J, crack growth (Δa_P) values to construct the J-R curve.

6. **Crack length measurement**

   The original crack length (machined notch plus crack) is measured from the average of three measurements at distances of B/4, B/2, and 3B/4 according to the Figure 4.
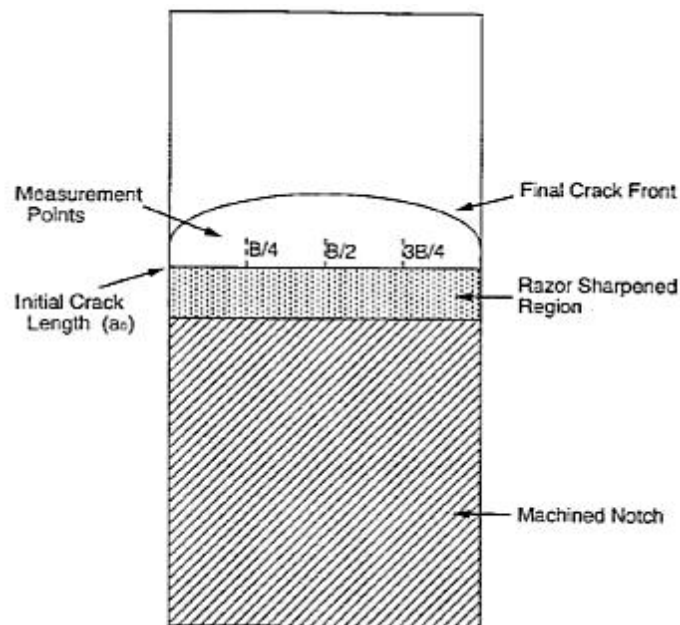

Figure 4 Measurement of initial crack length (a_0) (Astm-D6068-96, 2002).

The crack size is measured at five equally spaced points centred about the specimen centreline and extending to 0.005W from the surfaces of the specimens according to Figure 5. From the five measurements, average of the two near-surface measurement is combined with the rest of the three measurements and the average crack size, a_p is calculated from the average of these four measurements. The original crack length, a_0, is deducted from the average crack size, a_p, to calculate the average crack growth or extension, Δa_P.
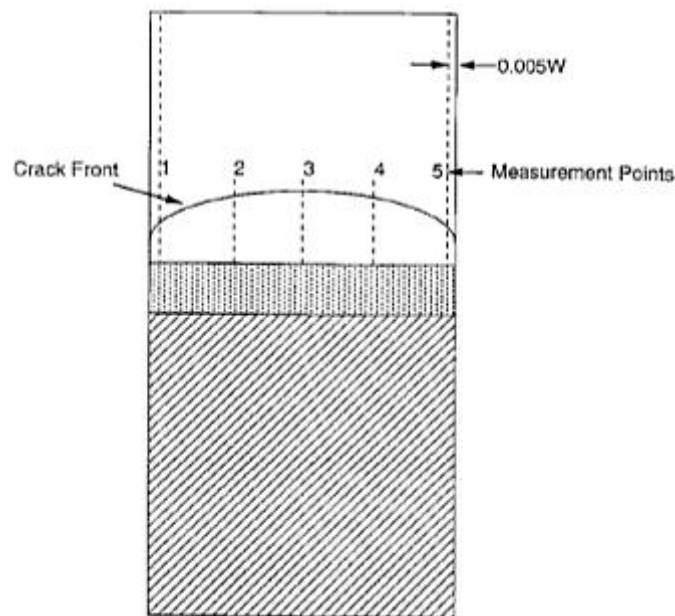

Figure 5 Measurement of crack growth Δa_P (Astm-D6068-96, 2002).

7. Calculation of J values and construction of J-R curve

Fracture resistance, J values are calculated from the following equation.

$$J = \frac{\eta U}{B(W - a_0)}$$

Where, $\eta = 2$ for single edge notch bend specimen, B is the thickness, W is the width of the samples and a_0 is the original crack length.
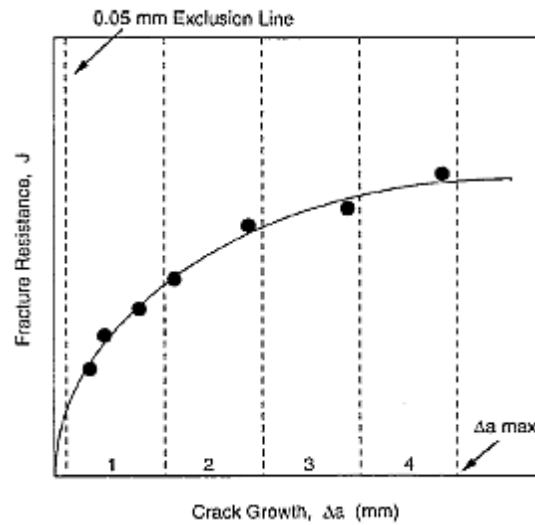
Figure 6 J-R curve (Astm-D6068-96, 2002).

A J-R curve is constructed from the sets of J and Δa_P data according to Figure 6. A minimum crack extension line is drawn at 0.05 mm of the crack extension. A maximum crack extension line is drawn at $\Delta a_P = 0.1\ b_0$, where $b_0 = (W - a_0)$, the initial un-cracked ligament. Data points are placed in the four equally spaced regions between the minimum and maximum crack extension line. Three data points are in the first interval, two data points are in the second interval and at least one data point in each of the two remaining regions. After that the data are fitted according to the power law relation as following form

$$J = A\Delta a^N$$

Where A and N are constants and $N \leq 1$. The initiation of toughness (J_{IC}) is measured at the 0.2 ($J_{0.2}$) mm extension of the total crack growth.

Appendix-D

Test process for measuring drop weight impact properties analysis of plastic materials using load and displacement sensors.

This test process describes the load versus displacement response of plastics under drop weight impact condition at different energy levels and impact velocities according to the guideline of ASTM D3763-02 (Astm-D3763-02) test standard.

1. **Test specimen**

   In this research work 125×125 and 110×110 mm squares specimens are cut from the rotationally moulded sheet for impact properties analysis of the plastics and low velocity impact properties analysis of skin-foam-skin sandwich structures respectively. The specimens are large enough to be adequately gripped in the clamp of the drop weight impact testing machine.

2. **Test procedure**

   A minimum of 3-5 specimens of each type of samples are tested at each energy level. The thickness of each specimen are measured and recorded before the testing. Specimens are placed in the clamp and gripped properly for preventing the slippage during testing. The desired energy and test speed are maintained by changing the impact height during the testing.

3. **Calculation of data**

   A piezoelectric impact force sensor of maximum loading capacity of 22.4 kN is attached with impact dart of the instrumented impact testing machine. A force-time curve is obtained from the voltage-time output of the impact force sensor for each impact test. Acceleration is calculated from the recorded force-time data. Displacement data for every test is determined from the double integration of the acceleration data and a force-displacement curve is built this way from the force-time curve during the test. Peak load, displacement and contact time are found from the force-displacement and force-time curves. Total absorbed energy is calculated from the area under the force-displacement curve by following trapezoidal method

and divided into two parts - peak impact strength or crack initiation energy and crack propagation energy. Peak impact strength or crack initiation energy is found from the area under the curve up-to peak impact force of a force-displacement curve. Crack propagation energy is defined as the difference between the total absorbed energy and the crack initiation energy.

Appendix-E

matrix polymers

REVOLVE® M-601

Rotational Moulding	**Super-Linear**	**M.F.I.**	**3.5**
		Density	**0.949**

Description

Revolve M-601 is a Super-Linear rotational moulding grade designed to provide high stiffness without compromising impact properties and toughness which makes the grade ideal for any leisure marine products like kayaks, canoes and boat. The grade is suitable for multi-layer application in combination with any Matrix foam.

Features & Benefits
Excellent impact properties
High toughness
Good mouldability
High stiffness

Available as
Natural powder
Black powder
Coloured powder

Physical Properties	**Test Method**	**Value**	**Units**
MFI	ISO 1133	3.5	g/10min
Density	ISO 1183	0.949	g/cm³
Tensile Strength @ Yield (50 mm/min)	ISO 527	21.4	MPa
Flexural Modulus (1.3 mm/min)	ISO 178	1304	MPa
HDT at 1.8 MPa	ISO 75-2	55	°C
ESCR at 100% Igepal	ASTM D1693	N/A*	hr
ESCR at 10% Igepal	ASTM D1693	N/A*	hr
ARM Impact (-40 °C, 3 mm thickness)	ARM-I Standard	118	J

Notes
* The grade is not suitable for ESCR applications

MEMBER

matrix polymers

REVOLVE® N-307
(5056)

Rotational	**M.F.I.** 3.5
Moulding	**Density** 0.939

Description

Revolve N-307 is a rotational moulding polyethylene hexene grade. It has been designed to provide an outstanding balance of properties such as stiffness, impact, mouldability, ESCR and creep. The grade carries a series of international approvals and certifications and complies with many international standards within the tank industry.

Features & Benefits	Available as
Good stiffness	Natural pellets & powder
Good mouldability	Black pellets & powder
Excellent impact strength	Coloured powder
TÜV approved resin	
UV10 stabilised	

Physical Properties**	Test Method	Value	Units
MFI	ISO 1133	3.5	g/10min
Density	ISO 1183	0.939	g/cm³
Tensile Strength @ Yield (50 mm/min)	ISO 527	17.7	MPa
Flexural Modulus (1.3 mm/min)	ISO 178	790	MPa
HDT at 1.8 MPa	ISO 75-2	50	°C
ESCR at 100% Igepal	ASTM D1693	>1000	hr
ESCR at 10% Igepal	ASTM D1693	400	hr
ARM Impact (-40 °C, 3 mm thickness)	ARM-I Standard	108	J

Notes

MEMBER

Issue number: 1
Issue Date: 21 May 2011

matrix
polymers

REVOLVE®
PP 25

Rotational
Moulding

M.F.I.   35[1]
Density   0.900

Description

Revolve PP 25 is a rotational moulding polypropylene grade designed to provide enhanced flow characteristics without compromising stiffness and high temperature resistance.
The grade is UV stabilised.

Features & Benefits
High stiffness and hardness
Good mouldability
High temperature resistance

Available as
Natural powder
Black powder
Coloured powder

Physical Properties**	Test Method	Value	Units
MFI	ISO 1133	35[1]	g/10min
Density	ISO 1183	0.900	g/cm³
Tensile Strength @ Yield (50 mm/min)	ISO 527	26	MPa
Flexural Modulus (1.3 mm/min)	ISO 178	1400	MPa
HDT at 0.45 MPa	ISO 75-2	89	°C
Vicat (A50 - 10N)	ISO 306	147	°C
Melting Temperature - DSC	Matrix method	160	°C
IZOD impact notched (23 °C)	ISO 180	7.0	kJ/m²

Notes
[1] MFI tested at 230°C and 2.16 kg

This information is to the best of our knowledge accurate. However, the circumstances and conditions in which it may be used are beyond our control and we do not accept liability for any loss or damage that may occur nor do we offer any warranty of immunity against patent infringement. The values indicated in the tables only describe typical properties. They do not constitute specification limits.

Issue number: 1
Issue Date: 17 Nov 2011

matrix polymers

REVOLVE®
S-TeQ PP 35

Rotational Moulding

| M.F.I. | 30[1] |
| Density | 0.900 |

Description

Revolve S-TeQ PP 35 is a rotational moulding polypropylene grade designed to provide enhanced impact properties without compromising stiffness and high temperature resistance. The grade is UV stabilised.

Features & Benefits
High stiffness and hardness
Good mouldability
High temperature resistance

Available as
Natural powder
Black powder
Coloured powder

Physical Properties**	Test Method	Value	Units
MFI	ISO 1133	30[1]	g/10min
Density	ISO 1183	0.900	g/cm³
Tensile Strength @ Yield (50 mm/min)	ISO 527	24	MPa
Flexural Modulus (1.3 mm/min)	ISO 178	1150	MPa
HDT at 0.45 MPa	ISO 75-2	90	°C
Vicat (A50 - 10N)	ISO 306	120	°C
Melting Temperature - DSC	Matrix method	160	°C
ARM Impact (23 °C, 3 mm thickness)	ARM-I Standard	45	J

Notes
[1] MFI tested at 230°C and 2.16 kg

This information is to the best of our knowledge accurate. However, the circumstances and conditions in which it may be used are beyond our control and we do not accept liability for any loss or damage that may occur nor do we offer and warranty of immunity against patent infringement. The values indicated in the tables only describe typical properties. They do not constitute specification limits.